

CHAPTER One

INTRODUCTION

The great development that has happened in the chemical and petroleum industries has led to the use of modern and complex equipment and devices. The chemical reactor of both types; fixed and fluidized bed is the most important part of the production process, in these days the chemical and petroleum industries use catalytic reactors over a wide range, the modern design of these reactors has led to some difficulties in control and make the process contains a large set of variables that must be tuned for a successful operation technically and economically, to reach this goal experiments have to be carried out to obtain the optimum values of these variables and the best way to do this is through mathematical models. Building a correct mathematical model with the help of simulation software will makes it easy to get a perfect process.

The objectives of this research work are to study the modeling, simulation, and optimization, of industrial fixed and fluidized bed reactors for gas phase solid catalytic reactions. In this regard two very important reaction systems, production of ammonia and methanol, are studied.

Ammonia is mainly used in the production of liquid fertilizer solutions which consist of ammonia, ammonium nitrate, and urea and aqua ammonia. It is also used in the manufacture of nitric acid, neutralizing the acid, several areas of water and wastewater treatment, stack emission control systems, industrial refrigeration systems, rubber industry, pulp and paper industry, food and beverage industry, leather industry, and other uses ¹.

The annual production of methanol exceeds 40 million tons and continues to grow by 4% per year ². Methanol has traditionally been used as feed for production of a range of chemicals including acetic acid and formaldehyde. In recent years methanol has also been used for other markets such as production of DME (Di-

methyl-ether) and olefins by the so-called methanol-to-olefins process (MTO) or as blend stock for motor fuels³.

The features of these processes reactions are:

- Reversible.
- Exothermic.
- Held in fixed bed reactors.

Fixed bed reactors provide effective gas-solid contacting but, they have some problems:

- Possibility of channeling that could lead to:
 - Poor heat transfer
 - Poor conversion
 - Harm to the catalyst because of hot spots
- sudden surges of flow may disturb the bed

Fluidized beds provide:

- Temperature uniformity
- Good heat transfer
- Transportability of rapidly decaying catalyst between reacting and regenerating sections.

As in any design, the fluidized bed reactor does have it draw-backs, which any reactor designer must take into consideration.⁶

- Increased Reactor Vessel Size: Because of the expansion of the bed materials.
- Pumping Requirements and Pressure Drop.
- Particle Entrainment: The high gas velocities present often result in fine particles becoming entrained in the fluid. These captured particles are then carried out of the reactor with the fluid, where they must be separated.
- Erosion of Internal Components: The fluid-like behavior of the fine solid particles within the bed eventually results in the wear of the reactor vessel.

1.1 Mathematical model building

Building a mathematical model for gas-solid reactive systems depends to large degree on the physical and chemical laws govern the processes taking place within the system boundaries⁴. For example the diffusion mechanism and rates of diffusion of reacting species to the neighborhood of active centers (or active sites) of reaction, and the chemi-sorption of the reacting species on these active sites for non-porous pellets, while for porous pellets it also includes the diffusion of reactants through the pores of the catalyst pellets, the mechanism and kinetic rates of the reaction of these species, the desorption of products and the diffusion of products away from the reaction center. It also includes the thermodynamic limitations, and also includes heat production and absorption as well as heat transfer rates⁵.

1.2 The advantages of mathematical models in design⁴

1. It gives more precise and optimal design of industrial units.
2. It allows the investigation of new more effective designs.
3. It can be used for simulation of the performance of existing units to ensure their smooth operation.
4. It is usable for the optimization of the performance of existing units and compensation for external disturbances in order to always keep the unit working at its optimum conditions.
5. Dynamic models are used in the design of control loops for different industrial units to compensate for the dynamic effects associated with external disturbances.
6. Dynamic models are also used for stabilization of the desirable unstable steady state by designing the necessary stabilizing control.
7. It is utilized in the organization and rationalization of safety considerations.
8. It is extremely useful for training purposes.

9. It provides an excellent guide regarding environmental impact and protection.

1.3 Steps of model building

The procedure for the development of a mathematical model can be summarized in the following steps⁴:

1. Identification of the system configuration, its environment and the manner of interaction between them.
2. Suggestion of the necessary justifiable simplifying assumptions.
3. Identification of the relevant state variables that describe the system.
4. Identification of the process happening within the boundaries of the system.
5. Determination of the laws governing the rates of the processes in terms of the state variables.
6. Identification of the input variables acting on the system.
7. Formulation of the model equations based on the principles of mass, energy, and momentum balances.
8. Development of the necessary algorithms for the solution of the model equations.
9. Validation of the model against experimental results to insure its reliability and to re-evaluate the simplifying assumptions which may result in imposing new simplifying assumptions or relaxing others.

1.4 Aims and Objectives

1. To build mathematical models describing the Ammonia and Methanol processes on both fixed and fluidized bed reactors.
2. To study the effect of the operation conditions on the performance according to the built models.

The organization of the dissertation is outlined below.

In chapter two literatures is reviewed for the different models of fixed and fluidized bed reactors, and the industrial fixed bed reactors used in producing ammonia and methanol which will be modeled and simulated in later chapters. Chapter three involve building the mathematical models of ammonia and methanol synthesis in industrial fixed bed reactor described in chapter two, also mathematical model in fluidized bed reactor are proposed. In chapter four the described models are solved and the results are listed and compared with the industrial data to validate the models, tests carried out to study the effect of different parameters on the performance of the reaction.

In chapter five the four models are simulated using HYSYS and compared with the results of the models, finally conclusions and recommendations are discussed in chapter six.

CHAPTER Two

LITERATURE REVIEW

2.1 Modeling of Fixed Bed Catalytic Reactor

Fixed bed catalytic reactors have a wide variety of configurations ranging from the single bed adiabatic configuration to the multi-tubular, non-adiabatic configurations with co-current or counter current cooling or heating ⁶. The configuration can sometimes be sophisticated where there are internal cooling tubes immersed into the catalyst bed as well as an external heat exchanger. In some cases the reactor may be quite simple with adiabatic single beds or multiple adiabatic beds in series.

The catalyst bed as a system can be looked upon from a topological point of view and be considered as formed of subsystems: the catalyst pellets which are stationary and distributed along the length of the catalyst tubes (which can be considered as the second subsystem), and the flowing gases through the packed bed ⁶.

In fixed bed catalytic reactors, the function of the system is to transform a raw material A to a product P. this transformation takes place according to a number of consecutive or parallel processes, these processes can be considered to be the elements (or subsystems) of the function of the catalyst bed system. This is equivalent to considering the function of transforming A to P to be an overall process and then distinguishing the steps which lead to the required transformation.

2.1.1 Types of Fixed Bed Reactor Models

Catalytic gas-phase chemical reactions play an important role in chemical industry. Such reactions are carried out in a multi-tubular reactor, in which each tube is packed with a catalyst. Some of the main fixed bed catalytic processes are listed in Table 2.1 ⁷.

Table 2.1 Main fixed bed catalytic processes

Basic Chemical industry	Petrochemical Industry	Petroleum Refining
Steam reforming	Ethylene oxide	Catalytic reforming
Carbon monoxide conversion	Carbon monoxide conversion	Catalytic reforming
Carbon monoxide methanation	Ethylene dichloride	Isomerization
Ammonia synthesis	Vinylacetate	Polymerization
Sulfuric acid synthesis	Maleic anhydride	Hydrodesulfurization
Methanol synthesis	Phthalic anhydride	Hydrocracking
Ox0 synthesis	Cyclohexane	Catalytic reforming
	Styrene	
	Hydrodealkylation	

Steady-State modeling and simulation studies of fixed bed reactors have been discussed in many researches. Froment proposed a general classification of fixed bed reactor¹⁵.

Table 2.2 Classification of Fixed Bed Reactor Models⁷

	Pseudo Homogeneous Models $T = T_s, C = C_s$	Heterogeneous Models $T \neq T_s, C \neq C_s$
One-dimensional	basic, ideal axial mixing	interfacial gradients intraparticle gradients
Two-dimensional	radial mixing	radial mixing

Where

C_s :Catalyst surface concentration,

C :Gas bulk concentration,

T_s :Surface temperature of the catalyst,

T :Bulk temperature of gas.

Pseudo-homogeneous models lump the gas and solid (catalyst) phases together in the reactor modeling mass and energy balance equations. When it is assumed that reactor temperature and composition only change in the axial direction of the reactor and do not change in the radial direction, it is referred to as a one-dimensional model. When it is assumed that the flow velocity is constant across the reactor and does not depend on the radial direction, the resulting model is called a one-dimensional plug-flow reactor model. In addition, very few data are available to date and no general correlation could be set up for the velocity profile⁷.

Sometimes in addition to plug flow, axial mixing is considered to account for non-ideal conditions in the reactor, and then the resulting reactor model is called the dispersed plug-flow model or simply the axial-dispersion model. The length of the industrial fixed bed reactors removes the need for reactor models with axial

diffusion. Hlavacek and Hofmann have shown that for ammonia, methanol, and oxo-synthesis and in ethylene, naphthalene, and o-xylene oxidation, there is no need to account for the effect of axial mixing. The overall model is still one-dimensional in nature.

For non-adiabatic reactors, there is a heat transfer across the wall of a tube, which generates radial temperature and concentration gradients. When these radial gradients are considered in the model, the model becomes two-dimensional.

For very rapid reactions with important heat effects, it may be necessary to distinguish between conditions in the fluid and on the catalyst surface or even inside the catalyst. In case of heterogeneous models, gas and solid phases are modeled as separate mass-balance and energy-balance equations by considering interfacial gradients of temperature and concentration. The heterogeneous model becomes more complicated when the temperature and concentration gradients inside the catalyst are accounted for⁸. Fortunately, even with strongly exothermic reactions, the catalyst is practically isothermal. The main resistance inside the catalyst is to mass transfer, and the main resistance in the film surrounding the catalyst is to heat transfer.

2.1.3 Solution Procedure

Both the homogeneous and heterogeneous dynamic fixed bed reactor models are described by a set of partial differential equations which may be solved using one of the several types of techniques: Crank-Nicolson, orthogonal collocation, and orthogonal collocation on finite elements. Froment integrated a two-dimensional homogeneous model using a Crank-Nicholson procedure to simulate a multi-tubular fixed bed reactor⁹.

However, orthogonal collocation has been the dominant method used for solving the fixed bed reactor model equations. The orthogonal collocation method proves to be faster and more accurate than the finite-difference method used. To this end,

various authors have applied collocation using two or three radial collocation points to the solution of the reactor model equations. Bonvinetal has applied collocation to non-adiabatic tabular reactors using quadratic radial profiles (i.e., two radial collocation points) ¹⁰. Jutan solved the steady-state reactor equations using two collocation points for temperature in radial direction and three collocation points for concentration in the radial direction. Ampaya and Rinker and Finlayson examined the convergence of collocation solutions to steady-state reactor equations as the number of radial collocation points is increased. Both of these papers show that collocation points placed at the roots of the Jacobi polynomials lead to faster convergence of the solutions as the number of collocation points is increased ¹⁰.

2.1.4 Optimization

The optimization of the fixed bed reactor over the length of catalyst life is important because the catalyst activity changes over the course of the operation. The operating temperature is increased over the life of the catalyst to compensate for the loss of catalyst activity. Taskar discussed the optimization of catalytic naphtha reformer, which is a fixed bed reactor, and described the formulation of the dynamic optimization problem. Orthogonal collocation and control vector parameterization can be used to solve a nonlinear dynamic optimization problem ⁵.

2.1.5 Mathematical model for the fixed bed reactor

It consists of the following aspects in its mass and energy balance equations:

Axial dispersion

Mixing of the components in the reactor in the axial direction is due to the turbulence and the presence of catalysts in the fixed bed reactor. It is accounted for by superimposing an effective transport mechanism on the overall transport by plug flow. The flux due to axial dispersion is described by a formula analogous to Fick's law for mass transfer or Fourier's law for heat transfer by conduction. The proportionality constants are effective diffusivity and conductivity in the axial direction¹¹.

Fick's law for mass transfer:

$$N_{ja} = -D_a \frac{\partial C_j}{\partial z} \quad (2.1)$$

Fourier's law for heat transfer:

$$N_{qa} = -\lambda_a \frac{\partial T}{\partial z} \quad (2.2)$$

Radial dispersion

Adiabatic commercial reactors exhibit no significant radial gradients since no heat transfer is involved across the wall of the tube. Non adiabatic fixed bed reactors can develop significant radial-temperature gradients because of the heat transfer at the wall. Temperature gradients will produce radial-concentration gradients as well. These gradients of temperature and concentration occur when large maxima (hot spots in exothermic reactions) or large minima (low temperatures in endothermic reactions) occur. To formulate the flux of heat or mass in the radial direction, it is superimposed on the transport by overall convection, which is the plug flow type¹².

Fick's law for mass transfer:

$$N_{jr} = -D_r \left(\frac{\partial C_j}{\partial r} \right) \quad (2.3)$$

Fourier's law for heat transfer:

$$N_{qr} = -\lambda_r \left(\frac{\partial T}{\partial r} \right) \quad (2.4)$$

Radial velocity gradients

The flow in a fixed bed reactor deviates from the ideal pattern (plug flow) because of radial variations in flow velocity and mixing effects due to the presence of catalyst.

Interphase mass and heat transfer resistance

Since the components (reactants, products) and energy must move from the catalyst interior, the exterior catalyst surface, and the bulk fluid phase, there exists a resistance to mass and heat transfer between the gas and solid phases. Since both heat and mass transfer coefficients are increased by increasing the mass velocities, it is possible and practical in most industrial reactors to avoid significant inter phase gradients⁹.

Intraparticle mass and heat transfer resistances

As the catalyst-pellet size increases, a significant concentration gradient between the surface and the interior can develop for all the components. Conversely, if the catalyst size is held constant and the temperature is increased, a similar gradient may occur due to more rapid consumption of the reactants because of the exponential rate increase caused by increased temperature. In both cases, the rate varies with position inside the catalyst. The effectiveness factor can be used to calculate the actual reaction rate that would be observed. The effectiveness factor is defined as follows⁹:

$$\eta = \frac{\text{rate of reaction with catalyst pore diffusion resistance}}{\text{rate of reaction with surface conditions}} \quad (2.5)$$

Pressure drop in fixed bed reactor

Pressure drop through a reactor is seldom more than 10% of the total pressure and thus is not a major factor in changing the chemical reaction rates in a gaseous reaction. The Ergun equation has been preferred for several years to calculate the pressure drop in the reactor¹³:

$$-\frac{dP}{dz} = \left[\alpha \frac{(1 - \varepsilon)^2}{\varepsilon^3} \frac{\mu}{D_p^2} \right] u + \left[\beta \frac{(1 - \varepsilon)^2}{\varepsilon^3} \frac{\rho_f}{D_p} \right] u^2 \quad (2.6)$$

2.1.6 The continuum models of fixed bed reactor

In the continuum models, the bulk fluid phase variables are described in terms of differential equations¹². Froment introduced the classification given in figure 2.1. The models are divided into six classes, three types of pseudo homogeneous models, and three types of heterogeneous models.

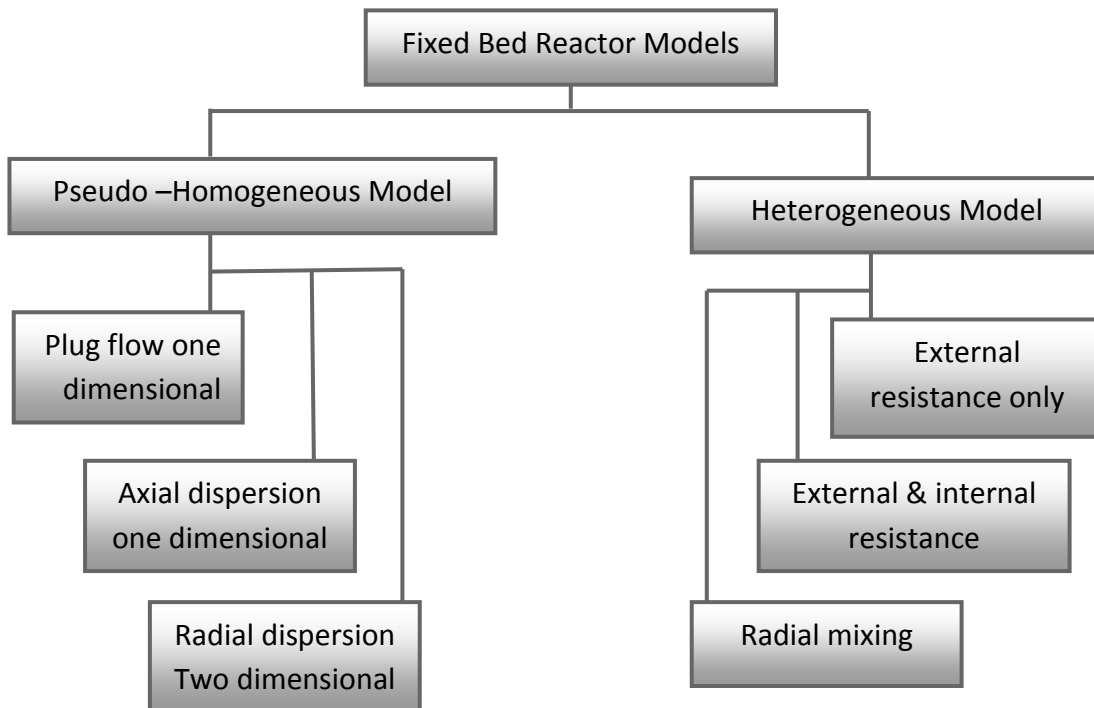


Figure 2.1 The continuum models of fixed bed reactor⁸

One-dimensional pseudo-homogeneous model

The simplest pseudo-homogeneous model describes only axial profiles of radially averaged temperatures and concentrations. Since the only transport mechanism taken into account is convection, the model is referred to as a plug-flow model¹³. Constant (averaged) physical properties of the fluid throughout the reactor are assumed, so that the conservation equations for the steady-state:

$$u_s \frac{dC_i}{dz} = -R_i(C, T) \quad (2.7)$$

$$u_s \rho_f c_P \frac{dT}{dz} = R_T(C, T) - \frac{4U_w}{d_t} (T - T_w) \quad (2.8)$$

One-dimensional heterogeneous model

The simplest one-dimensional heterogeneous model, taking into account temperature and concentration differences between the fluid bulk and catalyst surface⁹:

Fluid phase:

$$u_s \frac{dC_i}{dz} = k_f a_v (C_i^s - C_i) \quad (2.9)$$

$$u_s \rho_f c_P \frac{dT}{dz} = h_f a_v (T_s - T) - \frac{4U_w}{d_t} (T - T_w) \quad (2.10)$$

Solid phase:

$$k_f a_v (C_i^s - C_i) = -R_i(C^s, T^s) \quad (2.11)$$

$$h_f a_v (T_s - T) = R_T(C^s, T^s) \quad (2.12)$$

One-dimensional pseudo-homogeneous and heterogeneous models with axial dispersion

The plug flow model does not explicitly take into account vital characteristics of packed bed reactors such as non-uniform temperature and concentration distributions across the bed and mixing effects, caused by several mechanisms, including mixing due to presence of the packing, molecular diffusion, thermal conduction, radiation etc ¹⁴. The most common 1-D heterogeneous model taking dispersion in the fluid phase into account:

Fluid phase:

$$u_s \frac{dC_i}{dz} - D_{ez} \frac{d^2C_i}{dz^2} = k_f a_v (C_i^s - C_i) \quad (2.13)$$

$$u_s \rho_f c_p \frac{dT}{dz} - \lambda_{ez} \frac{d^2T}{dz^2} = h_f a_v (T^s - T) - \frac{4U_w}{d_t} (T - T_w) \quad (2.14)$$

Solid phase:

$$k_f a_v (C_i^s - C_i) = -R_i(C^s, T^s) \quad (2.15)$$

$$h_f a_v (T^s - T) = R_T(C^s, T^s) \quad (2.16)$$

Two-dimensional models

In the two-dimensional model the radial temperature and concentration profiles are accounted for. The most often used 2-D model is the pseudo-homogeneous model given by equations ¹⁵

$$u_s \frac{dC_i}{dz} - \frac{D_{er}}{r} \frac{\partial}{\partial r} \left(r \frac{\partial C_i}{\partial r} \right) = -R_i(C, T) \quad (2.17)$$

$$u_s \rho_f c_p \frac{\partial T}{\partial z} - \frac{\lambda_{er}}{r} \frac{\partial}{\partial r} \left(r \frac{\partial T}{\partial r} \right) = R_T(C, T) \quad (2.18)$$

and accompanied with boundary conditions:

$$z = 0: \quad C_i = C_0, T = T_0$$

$$r = 0: \quad \frac{\partial C_i}{\partial r} = 0, \frac{\partial T}{\partial r} = 0$$

$$r = \frac{d_t}{2}: \quad \frac{\partial C_i}{\partial r} = 0, \frac{\partial T}{\partial r} = -Bi(T - T_w)$$

Models accounting for intraparticle resistance. The effectiveness factor

All the models described above neglect the resistance to heat and mass transfer inside the catalyst particle. A one-dimensional pseudo-homogeneous plug flow model accounting for both interface and intraparticle resistances for simple shape particles reads ¹⁵:

$$u_s \frac{dC_i}{dz} = k_f a_v (C_i^{s,s} - C_i) \quad (2.19)$$

$$u_s \rho_f c_p \frac{dT}{dz} = h_{fs} a_v (T^{s,s} - T) - \frac{4U_w}{d_t} (T - T_w) \quad (2.20)$$

$$\frac{D_{ep}}{\xi^p} \frac{\partial}{\partial \xi} \left(\xi^p \frac{\partial C_i^s}{\partial \xi} \right) = -R_i(C^s, T^s) \quad (2.21)$$

$$\frac{\lambda_{ep}}{\xi^p} \frac{\partial}{\partial \xi} \left(\xi^p \frac{\partial T^s}{\partial \xi} \right) = R_T(C^s, T^s) \quad (2.22)$$

2.1.7 Dynamic models

Along with the steady state, the dynamic modeling of packed bed reactors has attracted considerable attention. Interest in dynamic modeling can be explained by the necessity to study important practical problems such as: 1) dynamically operating reactor, e.g. reverse flow reactors; 2) reactor start-up and shut down; 3) process stability, i.e. response of the reactor to disturbances in operation condition ¹⁶.

Equations of the dynamic models are typically the same as for steady state models, only additional terms describing the rates of temperature and concentrations change in time for example:

$$\frac{\partial T}{\partial t}, \frac{\partial C}{\partial t}, \frac{\partial C^s}{\partial t} \text{ and } \frac{\partial T^s}{\partial t} \text{ are added}$$

2.2 Modeling of Fluidized Bed Reactor

The fluidized-bed reactor has the ability to process large volumes of fluid. For the catalytic cracking of petroleum naphtha to form gasoline blends ¹⁷.

Their main characteristics are:

1. Negligible diffusion resistances within the catalyst particles.
2. High heat and mass transfer rates between gas and particles.
3. Low pressure drop.
4. Large capacity.
5. Isothermality due to mixing by bubbles.

Fluidization occurs when small solid particles are suspended in an upward flowing stream of fluid, as shown in Figure (2.2)

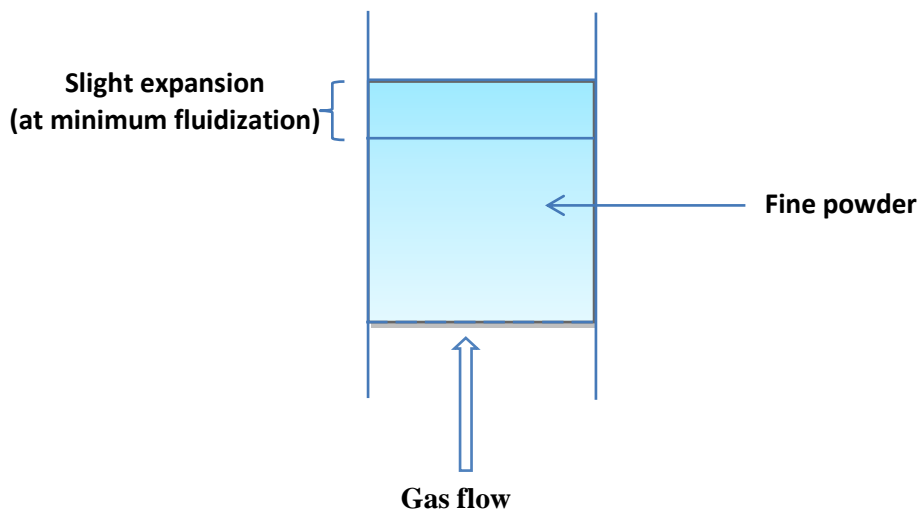


Figure 2.2 Fine powder inside a tube starting to fluidize due to gas flow rate ¹⁸

The fluid velocity is sufficient to suspend the particles, but it is not large enough to carry them out of the vessel. The solid particles swirl around the bed rapidly, creating excellent mixing among them. The material “fluidized” is almost always a solid and the “fluidizing medium” is either a liquid or gas. The characteristics and behavior of a fluidized bed are strongly dependent on both the solid and liquid or gas properties. Nearly all the significant commercial applications of fluidized-bed technology concern gas-solid systems ¹⁹.

The two phase model is used in this study to describe reactions in fluidized beds. In this model, the reactant gas enters the bottom of the bed and flows up the reactor in the form of bubbles. As the bubbles rise, mass transfer of the reactant gases takes place as they flow (diffuse) in and out of the bubble to contact the solid particles where the reaction product is formed. The product then flows back into a bubble and finally exits the bed when the bubble reaches the top of the bed. The rate at which the reactants and products transfer in and out of the bubble affects the conversion, as does the time it takes for the bubble to pass through the bed. Consequently, we need to describe the velocity at which the bubbles move through the column and the rate of transport of gases in and out of the bubbles. To calculate these parameters, we need to determine a number of fluid mechanics parameters associated with the fluidization process. Specifically, to determine the velocity of the bubble through the bed we need to first calculate ¹⁶:

1. Porosity at minimum fluidization, ϵ_{mf}
2. Minimum fluidization velocity, u_{mf}
3. Bubble size, d_b

To calculate the mass transport coefficient, we must first calculate

1. Porosity at minimum fluidization, ϵ_{mf}
2. Minimum fluidization velocity, u_{mf}
3. Velocity of bubble rise, u_b
4. Bubble size, d_b

2.2.1 The Mechanics of Fluidized Beds

Consider a vertical bed of solid particles supported by a porous or perforated distributor plate, as in Figure (2.3). The direction of gas flow is upward through this bed

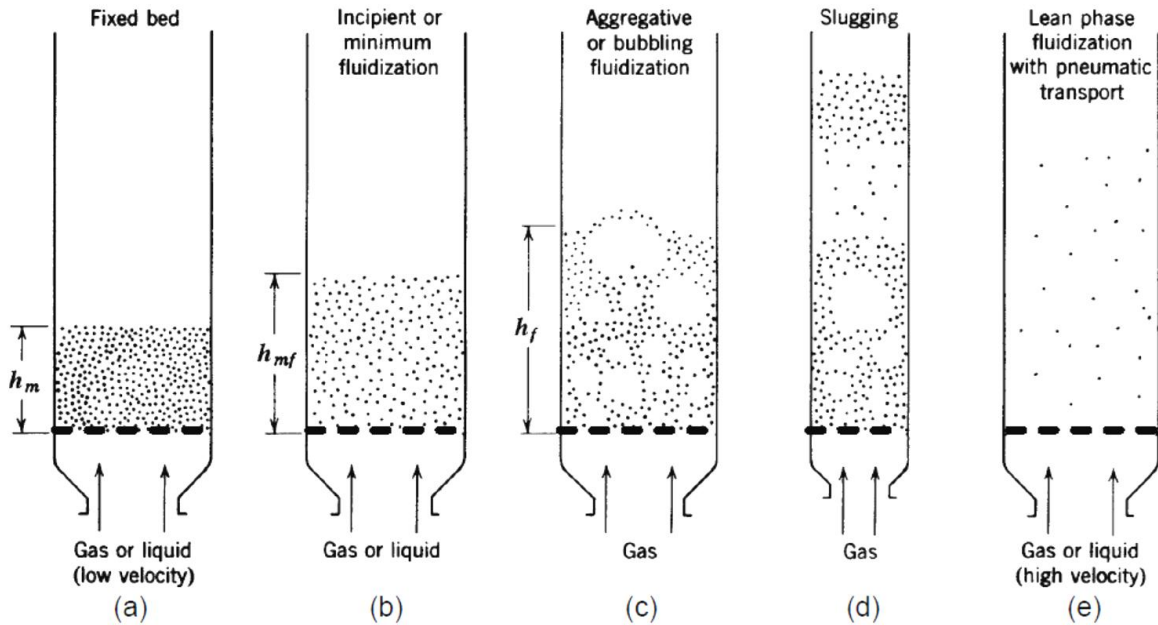


Figure 2.3 Various kinds of contacting of a batch of solids by fluid. ²⁰

There is a drag exerted on the solid particles by the flowing gas, and at low gas velocities the pressure drop resulting from this drag will follow the Ergun equation, when the gas velocity is increased to a certain value however, the total drag on the particles will equal the weight of the bed, and the particles will begin to lift and barely fluidize. If (ρ_c) is density of the solid catalyst particles, (A_c) is the cross sectional area, (h_s) , is the height of the bed settled before the particles start to lift, (h) , is the height of the bed at any time, and (ϵ_s) and (ϵ) are the corresponding porosities, of the settled and expanded bed, respectively; then the mass of solids in the bed, W_s , is ¹⁷

$$W_s = \rho_c A_c h_s (1 - \epsilon_s) = \rho_c A_c h (1 - \epsilon) \quad (2.22)$$

This relationship is a consequence of the fact that the mass of the bed occupied solely by the solid particles is the same no matter what the porosity of the bed.

When the drag force exceeds the gravitational force, the particles begin to lift, and the bed expands (i.e., the height increases) thus increasing the bed porosity, as described by Equation (2.22). This increase in bed porosity decreases the overall drag until it is again balanced by the total gravitational force exerted on the solid particles (Figure 2.3-b).

If the gas velocity is increased still further, expansion of the bed will continue to occur; the solid particles will become somewhat separated from each other and begin to jostle each other and move around in a restless manner. Increasing the velocity just slight amount further causes instabilities, and some of the gas starts bypassing the rest of the bed in the form of bubbles (Figure 3.2-c) ²¹. These bubbles grow in size as they rise up the column. Coincidentally with this, the solids in the bed begin moving upward, downward, and around in a highly agitated fashion appearing as a boiling frothing mixture. With part of the gas bubbling through the bed and the solids being moved around as though they were part of the fluid, the bed of particles is said to be “fluidized.” It is in a state of aggregative, non particulate, or bubbling fluidization.

A further increase in gas velocity will result in slug flow (Figure 3.2-d) and unstable chaotic operation of the bed. Finally at extremely high velocities, the particles are blown or transported out of the bed (Figure 3.2-e).

The range of velocities over which the Ergun equation applies can be fairly large. On the other hand, the difference between the velocities at which the bed starts to expand and the velocity at which the bubbles start to appear can be extremely small and sometimes nonexistent. This observation means that if one steadily increases the gas flow rate, the first evidence of bed expansion may be the appearance of gas bubbles in the bed and the movement of solids. At low gas velocities in the range of fluidization, the rising bubbles contain very few solid

particles. The remainder of the bed has a much higher concentration of solids in it and is known as the emulsion phase of the fluidized bed. The bubbles are shown as the bubble phase. The cloud phase is an intermediate phase between the bubble and emulsion phases.

After the drag exerted on the particles equals the net gravitational force exerted on the particles, that is,

$$\Delta P = g(\rho_c - \rho_g)(1 - \varepsilon)h \quad (2.23)$$

The pressure drop will not increase with an increase in velocity beyond this point. From the point at which the bubbles begin to appear in the bed, the gas velocity can be increased steadily over a quite appreciable range without changing the pressure drop across the bed or flowing the particles out of the bed.

The bubbles become more frequent, and the bed, more highly agitated as the gas velocity is increased (Figure 3.2-c); but the particles remain in the bed. This region is bubbling fluidization. Depending on the physical characteristics of the gas, the solid particles, and the distributor plate; and the internals (e.g., heat exchanger tubes) within the bed, the region of bubbling fluidization can extend over more than an order of magnitude of gas velocities. In other situations, gas velocities in the region of bubbling fluidization may be limited; the point at which the solids begin to be carried out of the bed by the rising gas may be a factor of only three or four times the velocity at incipient fluidization.

Eventually, if the gas velocity is continuously increased, it will become sufficiently rapid to carry the solid particles upward, out of the bed. When this begins to happen, the bubbling and agitation of the solids are still present, and this is known as the region of fast fluidization, and the bed is known as fast-fluidized bed. At velocities beyond this region, the particles are well apart, and the particles are merely carried along with the gas stream. Under these conditions, the reactor is usually referred to as a straight through transport reactor or STTR (Figure 3.2-e).

2.2.2 The Minimum Fluidization Velocity

Fluidization will be considered to begin at the gas velocity at which the weight of the solids gravitational force exerted on the particles equals the drag on the particles from the rising gas. The gravitational force is given by Equation (2.22) and the drag force by the Ergun equation. All parameters at the point where these two forces are equal will be characterized by the subscript “mf,” to denote that this is the value of a particular term when the bed is just beginning to become fluidized. The combination $[g(\rho_c - \rho_g)]$ occurs very frequently, as in Equation (2.23), and this grouping is termed $[\eta]$.

$$\frac{\Delta P}{h} = g\eta(1 - \varepsilon_{mf}) \quad (2.24)$$

The Ergun Equation can be written in the form²²:

$$\frac{\Delta P}{h} = \rho_g U^2 \left[\frac{150(1 - \varepsilon)}{Re_d \psi} + \frac{7}{4} \right] \frac{1 - \varepsilon}{\psi d_p \varepsilon^3} \quad (2.25)$$

Where (ψ) shape factor of catalyst particle, sometimes called the sphericity.

At the point of minimum fluidization, the weight of the bed just equals the pressure drop across the bed

$$W_s = \Delta P A_c \quad (2.26)$$

$$g(1 - \varepsilon)(\rho_c - \rho_g)hA_c = \rho_g U^2 \left[\frac{150(1 - \varepsilon)}{Re_d \psi} + \frac{7}{4} \right] \frac{1 - \varepsilon}{\psi d_p \varepsilon^3} hA_c \quad (2.27)$$

For $Re_p < 10$, ($Re_p = \frac{\rho_g d_p U}{\mu}$), we can solve equation (2.27) for the minimum fluidization velocity to give:

$$U_{mf} = \frac{(\psi d_p)^2}{150\mu} [g(\rho_c - \rho_g)] \frac{\varepsilon_{mf}^3}{1 - \varepsilon_{mf}} \quad (2.28)$$

Reynolds numbers less than 10 represents the usual situation, in which fine particles are fluidized by a gas. Sometimes, higher values of the Reynolds number do exist at the point of incipient fluidization, and then the quadratic Equation (2.28) must be used.

Two dimensionless parameters in these two equations for (U_{mf}) deserve comment. This first is ψ , the sphericity, which is a measure of a particle's nonideality in both shape and roughness. It is calculated by visualizing a sphere whose volume is equal to the particles, and dividing the surface area of this sphere by the actually measured surface area of the particle. Since the volume of a spherical particle is

$$V_p = \frac{\pi d_p^3}{6} \quad (2.29)$$

And its surface area is

$$A_s = \pi d_p^2 = \pi \left[\left(\frac{6V_p}{\pi} \right)^{\frac{1}{3}} \right]^2 \quad (2.30)$$

$$\psi = \frac{A_s}{A_p} = \frac{\left(\pi \left(\frac{6V_p}{\pi} \right)^{\frac{2}{3}} \right)}{A_p} \quad (2.31)$$

Measured values of this parameter range from 0.5 to 1, with 0.6 being a normal value for a typical granular solid.

The second parameter of special interest is the void fraction at the point of minimum fluidization, ε_{mf} . It appears in many of the equations describing fluidized bed characteristics. There is a correlation that apparently gives quite accurate predictions of measured values of ε_{mf} (within 10%) when the particles in the fluidized bed are fairly small

$$\varepsilon_{mf} = 0.586\psi^{-0.72} \left(\frac{\mu^2}{\rho_g \eta d_p^3} \right)^{0.029} \left(\frac{\rho_g}{\rho_c} \right)^{0.021} \quad (2.32)$$

Another correlation commonly used is that of Wen and Yu

$$\varepsilon_{mf} = (0.071/\psi)^{1/3} \quad (2.33)$$

And/ or

$$\varepsilon_{mf} = \frac{0.091(1 - \varepsilon_{mf})}{\psi^2} \quad (2.34)$$

When the particles are large, the predicted ε_{mf} can be much too small. If a value of ε_{mf} below 0.40 is predicted, it should be considered suspect. Kunii and Levenspiel state that ε_{mf} is an easily measurable value. However, if it is not convenient to do so, Equation (2.11) should suffice. Values of ε_{mf} around 0.5 are typical.

2.2.3 Descriptive Behavior of a Fluidized Bed – The Two Phase Model

At gas flow rates above the point of minimum fluidization, a fluidized bed appears much like a vigorously boiling liquid; bubbles of gas rise rapidly and burst on the surface, and the emulsion phase is thoroughly agitated. The bubbles form very near the bottom of the bed, very close to the distributor plate and as a result the design of the distributor plate has a significant effect on fluidized-bed characteristics²³.

Literally hundreds of investigators have contributed to what is now regarded as a fairly practical description of the behavior of a fluidized bed; chief among these is the work of Davidson and Harrison. Early investigators saw that the fluidized bed had to be treated as a two-phase system – an emulsion phase and a bubble phase (often called the dense and lean phases). The bubbles contain very small amounts of solids. They are not spherical; rather they have an approximately hemispherical top and a pushed-in bottom. Each bubble of gas has a wake that contains a significant amount of solids. The two-phase theory of fluidization, states that “Almost all the gas in excess of that necessary for minimum fluidization will appear as gas bubbles” (Figure 2.3)

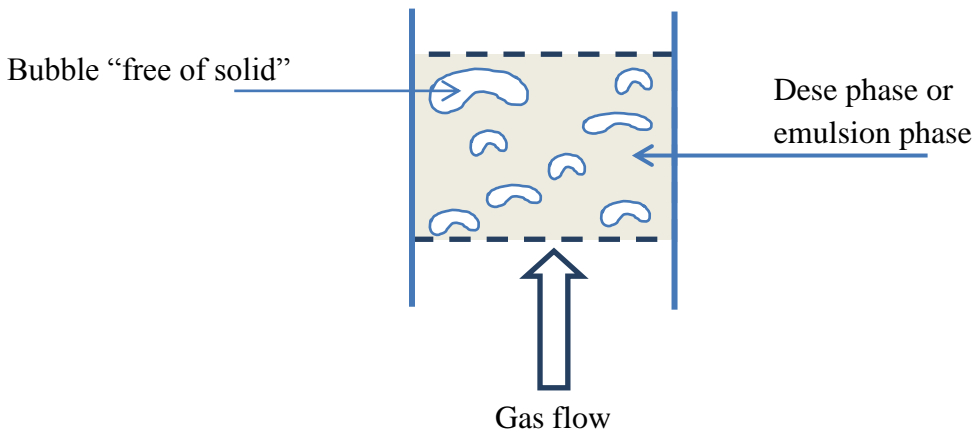


Figure 2.4 Phases of fluidized bed ²⁴

As the bubble rises, it pulls up the wake with its solids behind it. The net flow of the solids in the emulsion phase must therefore be downward.

2.2.4 Model Assumptions

The mathematical model is developed based on the two phase reactor model. The following assumptions are used to simplify the model equations:

1. The system is isothermal and steady state conditions.
2. The lower dense bed assumed to compose of bubble and emulsion phases.
3. The gas in the bubble phase is assumed in plug flow.
4. The dense phase is assumed to be perfectly mixed.
5. Reaction occurs mostly in the dense phase.
6. Negligible mass and heat transfer resistances between the catalyst particles and the emulsion phase gas.
7. Negligible heat of adsorption.

2.2.5 Bubble Velocity and Bubble Size

From experiments with single bubbles, Davidson and Harrison found that the velocity of rise of a single bubble could be related to the bubble size by:

$$U_{br} = 0.71(gd_b)^{1/2} \quad (2.35)$$

When many bubbles are present, this velocity would be affected by other factors. The more bubbles that are present, the less drag there would be on an individual bubble; the bubbles would carry each other up through the bed. The greater number of bubbles would result from larger amounts of gas passing through the bed (i.e., a larger value of U_0). Therefore, the larger the value of U_0 , the faster should be the velocity of a gas bubble as it rises through the bed.

Other factors that should affect this term are the viscosity of the gas and the size and density of the solid particles that make up the bed. Both of these terms also affect the minimum fluidization velocity, and so this term might well appear in any relationship for the velocity of bubble rise; the higher the minimum fluidization velocity, the lower the velocity of the rising bubble.

Adopting an expression used in gas-liquid systems, Davidson and Harrison proposed that the rate of bubble rise in a fluidized bed could be represented by simply adding and subtracting these terms:

$$U_b = U_{br} + (U_0 - U_{mf}) \quad (2.36)$$

$$U_b = U_0 - U_{mf} + 0.71(gd_b)^{1/2} \quad (2.37)$$

2.2.6 Bubble Size

The equations for the velocity of bubble rise, Equations (2.37) and (2.36) are functions of the bubble diameter, an elusive value to obtain.

As might be expected, it has been found to depend on such factors as bed diameter, height above the distributor plate, gas velocity, and the components that affect the fluidization characteristics of the particles. Unfortunately, for predictability, the bubble diameter also depends significantly upon the type and number of baffles,

heat exchangers tubes, and so forth, within the fluidized bed (sometimes called “internals”). The design of the distributor plate, which disperses the inlet gas over the bottom of the bed, can also has a pronounced effect upon the bubble diameter. Studies of bubble diameter carried out thus far have concentrated on fluidized beds with no internals and have involved rather small beds. Under these conditions the bubbles grow as they rise through the bed. The best relationship between bubble diameter and height in the column at this writing seems to be that of Mori and Wen, who correlated the data of studies covering bed diameters of 7 to 130 cm, minimum fluidization velocities of 0.5 to 20 cm/s, and solid particle sizes of 0.006 to 0.045 cm. Their principal equation was

$$\frac{d_{bm} - d_b}{d_{bm} - d_{b0}} = e^{-0.3h/D} \quad (2.38)$$

In this equation, d_b is the bubble diameter in a bed of diameter D , observed at a height h above the distributor plate; d_{b0} is the diameter of the bubble formed initially just above the distributor plate, and d_{bm} is the maximum bubble diameter attained if all the bubbles in any horizontal plane coalesce to form a single bubble (as they will do if the bed is high enough) ¹³.

The maximum bubble diameter, d_{bm} has been observed to follow the Relationship

$$d_{bm} = 0.652[A_c(U_0 - U_{mf})]^{0.4} \quad (2.39)$$

for all beds, while the initial bubble diameter depends upon the type of distributor plate. For porous plates, the relationship

$$d_{b0} = 0.00376(U_0 - U_{mf})^2 \quad (2.40)$$

is observed, and for perforated plates, the relationship

$$d_{b0} = 0.347[A_c(U_0 - U_{mf})/n_d]^{0.4} \quad (2.41)$$

appears to be valid, in which n_d is the number of perforations. For beds with diameters between 30 and 130 cm, these relations appear to predict bubble diameters with an accuracy of about $\pm 50\%$; for beds with diameters between 7 and

30 cm, the accuracy of prediction appears to be approximately + 100%, – 60% of the observed values.

2.2.7 Mass Transfer in Fluidized Beds

There are two types of mass transport important in fluidized-bed operations.

The first is the transport between gas and solid. In some situations this can affect the analysis of fluidized-bed behavior significantly, and in others it might not enter the calculations at all. In the treatment of this type of transfer, it will be seen that this type of transport is quite similar to gas-solid mass transfer in other types of operations.

The second type of mass transfer is unique to fluidized-bed operations. It concerns the transfer of material between the bubbles and the clouds, and between the clouds and the emulsion. In almost every type of fluidized-bed operation, there are significant gas-phase concentration differences between the various elements of the fluidized bed. Consequently, calculations involving this type of mass transfer occur in almost every fluidized-bed analysis²⁵.

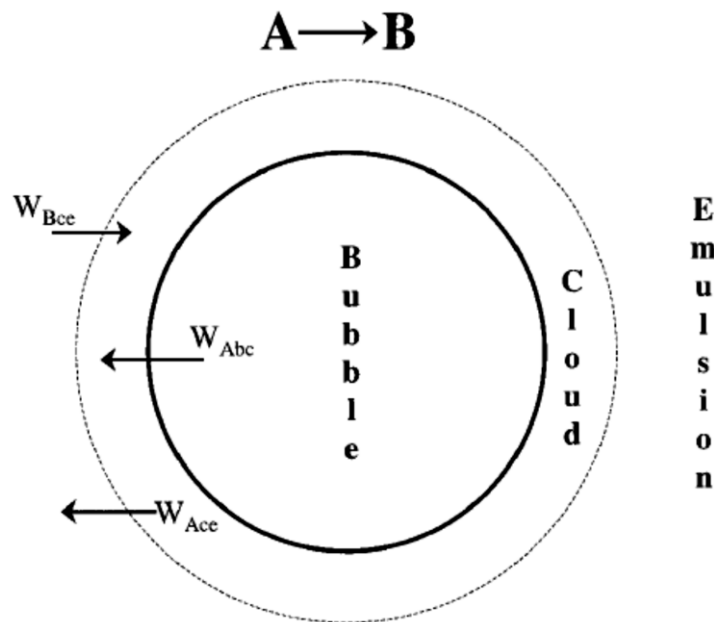


Figure 2.5 Transfer between bubble, cloud, and emulsion¹⁶.

2.2.8 Mass Transfer Between the Fluidized-Bed Phases

For the gas interchange between the bubble and the cloud, Kunii and Levenspiel defined the mass transfer coefficient K_{bc} (s^{-1}) in the following manner:

$$W_{Abc} = K_{bc}(C_{Ab} - C_{Ac}) \quad (2.42)$$

Where C_{Ab} and C_{Ac} are the concentration of A in the bubble and cloud respectively, ($mole/dm^3$) and W_{Abc} represents the number of moles of A transferred from the bubble to the cloud per unit time per unit volume of bubble ($mole/dm^3/s$).

The concept of basing all mass transfer (and later, all reaction) on the bubble volume proves to simplify the calculations markedly. For the products, (e.g., B in $A \rightarrow B$) the rate of transfer into the bubble from the cloud is given by a similar equation ²⁵

$$W_{Bcb} = K_{cb}(C_{Bc} - C_{Bb}) \quad (2.43)$$

The mass transfer coefficient K_{cb} can also be thought of as an exchange volume q between the bubble and the cloud.

$$W_{Bcb} = q_b C_{Ab} - q_c C_{Ac} = q_0(C_{Ab} - C_{Ac}) \quad (2.44)$$

Where

q_b = Volume of gas flowing from the bubble to the cloud per unit time per unit volume of bubble

q_c = Volume of gas flowing from the cloud to the bubble per unit time per unit volume of bubble

q_0 = Exchange volume between the bubble and cloud per unit time per unit volume of bubble (i.e., K_{cb})

$$q_0 = q_b = q_c$$

Using Davidson's expression for gas transfer between the bubble and the cloud, and then basing it on the volume of the bubble, Kunii and Levenspiel obtained this equation for evaluating K_{cb} :

$$K_{cb} = 4.5 \left(\frac{U_{mf}}{d_b} \right) + 5.85 \left(\frac{D_A^2 g^{0.25}}{D^{1.5}} \right) \quad (2.45)$$

where U_{mf} is in cm/s, d_b is in cm, D_A is the diffusivity (cm^2/s) and g is the gravitational constant ($980 cm/s^2$).

We note $K_{cb} = K_{bc}$ and a typical value of K_{bc} is $2 s^{-1}$.

Similarly, these authors defined a mass transfer coefficient for gas interchange between the cloud and the emulsion:

$$W_{Acd} = K_{cd}(C_{Ac} - C_{Ad}) \quad (2.46)$$

$$W_{Bcd} = K_{cd}(C_{Bd} - C_{Bc}) \quad (2.47)$$

where W_{Acd} is the moles of A transferred from the cloud to the emulsion per unit time per unit volume of bubble. Note that even though this mass transfer does not involve the bubble directly, it is still based on the bubble volume.

Using Higbie's penetration theory and his analogy for mass transfer from a bubble to a liquid, Kunii and Levenspiel developed an equation for evaluating K_{cd} ¹⁶:

$$K_{cd} = 6.77 \left(\frac{D_A \epsilon_{mf} U_{br}}{d_b^3} \right)^{0.5} \quad (2.48)$$

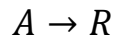
where U_{br} is velocity of bubble rise in cm/s and the other symbols are as defined early. A typical value of K_{cd} is $1 s^{-1}$. K_{cd} can also be thought of as the exchange volume between the cloud and the emulsion.

With knowledge of the mass transfer coefficients, the amount of gas interchange between the phases of a fluidized bed can be calculated and combined to predict the overall mass transfer behavior or reaction behavior of a fluidized-bed process.

2.2.9 General Model Formulation

Based on the two-phase model, a fluidized catalytic bed reactor can be divided into two regions; the dense phase (the emulsion phase), and the bubble phase figure (2.6), with associated mass and heat transfer between the two regions and phases.

Consider the following simple reaction:



Since the dense phase is assumed to be perfectly mixed, the concentration of the reactant (A) C_{Ad} will be constant for all height, while its concentration in the bubble phase which is assumed to be in plug flow C_{Ab} will be a function of the height h .

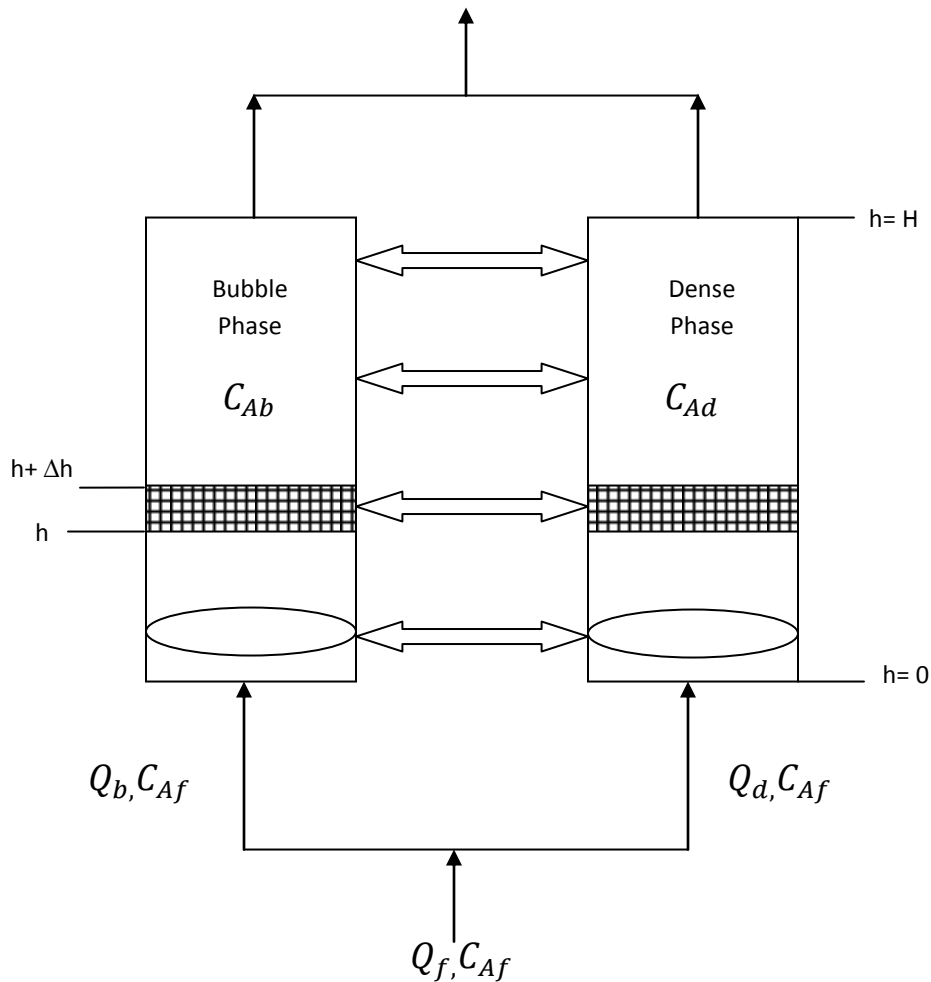


Figure 2.6The two phases of fluidized bed

Where:

C_{Ad} is the concentration of component A in the dense phase

C_{Ab} is the concentration of component A in the bubble phase

2.2.10 Steady-State Modeling of the Bubble Phase

Assuming that there is a negligible rate of reaction for an element in plug flow mode in the bubble phase, the molar balance can be expressed as

$$\frac{dN_{jd}}{dz} = (K_{bd})_j \left(\frac{N_{jd}}{Q_d} - \frac{N_{jb}}{Q_b} \right) A_b \quad (2.49)$$

With the initial conditions $N_{jb} = N_{jbF}$ at $z = 0$. Equation (2.49) can be solved analytically to give:

$$\frac{N_{jb}}{Q_b} - \frac{N_{jd}}{Q_d} = \left(\frac{N_{jbF}}{Q_b} - \frac{N_{jd}}{Q_d} \right) e^{-a_j z} \quad (2.50)$$

$$a_j = \frac{(K_{bd})_j}{U_b} \quad (2.51)$$

An energy balance for the bubble phase is given by ²⁶:

$$\rho_g C_{pg} U_b \frac{dT_b}{dz} = (H_{bd})_b (T_d - T_b) \quad (2.52)$$

With the initial conditions $T_b = T_F$ at $z = 0$. the equation (3.29) can be solved analytically to give:

$$T_b = T_d - (T_d - T_F) e^{-bz} \quad (2.53)$$

$$b = \frac{H_{bd}}{\rho_g C_{pg} U_b} \quad (2.54)$$

2.5.2 Steady-State Modeling of the Dense Phase

The molar balance on the dense phase for component A gives ²⁷:

$$N_{jd} = N_{jdF} + \int_0^H (K_{bd})_j \left(\frac{N_{jb}}{Q_b} - \frac{N_{jd}}{Q_d} \right) A_b dz + V(1 - \delta)(1 - \varepsilon_{mf}) \rho_p r_j \quad (2.55)$$

Using equation (2.50) the integral of equation (2.55) is evaluated and equation (2.55) becomes:

$$(N_j)_d = y_{jF}N_F \frac{Q_{dF}}{Q_F} + U_b A_b \left(\frac{y_{jF}N_F}{Q} - \frac{(N_j)_d}{Q_d} \right) + (1 - e^{-a_j \cdot H}) + V(1 - \delta)(1 - \varepsilon_{mf})\rho_p r_j \quad (2.56)$$

The total moles of component j leaving the reactor are given by:

$$N_j = (N_j)_d + (N_j)_b \quad (2.57)$$

Similarly we obtain the following expression for the energy balance around the dense phase for adiabatic operation:

$$\rho_g C_{pg} Q_{dF} (T_F - 298) - \rho_g C_{pg} Q_d (T_d - 298) + \rho_g C_{pg} U_b A_b (T_F - T_d) (1 - e^{-b \cdot H}) + V(1 - \delta)(1 - \varepsilon_{mf})\rho_p (-\Delta H_r) r_j = 0 \quad (2.58)$$

The fluidized bed exit temperature is given by:

$$T_{exit} = \frac{Q_b T_b + Q_d T_d}{Q_b + Q_d} \quad (2.59)$$

CHAPTER Three

MODELS DEVELOPMENT FOR AMMONIA AND METHANOL PROCESSES

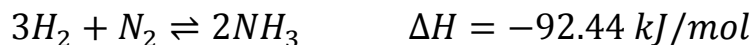
3.1 Modeling of Ammonia Synthesis from Synthesis Gas in Fixed Bed Reactor

The synthesis of ammonia from its elements ranks as one of the most important discoveries in the history of the science of catalysis, not only because of its industrial application in which synthetic fertilizers have contributed enormously to the survival of mankind, but also from the viewpoint of fundamental science.

The present annual production of ammonia is in excess of 120 million tons per year and virtually all of this ammonia is produced from a mixture of hydrogen and nitrogen over a promoted iron catalyst operating at elevated temperature and pressure. Over 90% of ammonia produced is used as a fertilizer, principally in the form of urea or ammonium nitrate ¹.

3.1.2 Kinetics of Ammonia Syntheses

The stoichiometric equation for the ammonia synthesis has the form:



In this model the intrinsic modified form of the Temkin rate expression is used:

$$r_{NH_3} = k_2 \left[k_a^2 f_{N_2} \left(\frac{f_{H_2}^3}{f_{NH_3}^2} \right)^\alpha - \left(\frac{f_{NH_3}^2}{f_{H_2}^3} \right)^{1-\alpha} \right] \quad (3.1)$$

r_{NH_3} is the reaction rate in kmol of NH_3 /(h.m³ of the catalyst bed), k_2 is the velocity constant for the reverse reaction in kmol/(h.m³) and k_a is the equilibrium constant of the reaction ¹³.

The velocity constant is estimated by the Arrhenius relation of the form:

$$K_2 = K_{20} \exp\left(-\frac{E_2}{R.T}\right) \quad (3.2)$$

The respective values for the Montecatini Edison catalyst are:

$$\alpha = 0.55, E_2 = 1.635 \times 10^5 \frac{kJ}{Kmol} \quad \text{and} \quad \log_{10} K_{20} = 14.7102$$

The equilibrium constant is given by Gaines

$$\log K_a = -2.691122 \log T - 5.519265 \times 10^{-5} T + 1.848863 \times 10^{-7} T^2 + \frac{2001.6}{T} + 2.6899 \quad (3.3)$$

the fugacity of component is given by definition as:

$$f_j = \varphi_j x_j P \quad (3.4)$$

Where:

φ_j is the fugacity coefficient of component j

x_j is the mole fraction of component j

P is the total pressure in atm

3.1.3 Ammonia Synthesis

Under the conditions practical for an industrial process ammonia formation is limited by the unfavorable position of the thermodynamic equilibrium, so that only partial conversion of the synthesis gas (25-35%) can be attained on its passage through the catalyst. Ammonia is separated from the un-reacted gas by condensation, which requires relatively low temperatures for reasonable efficiency

28.

The unconverted gas is supplemented with fresh synthesis gas and recycled to the converter. The concentration of the inert gases (methane and argon) in the synthesis loop is controlled by withdrawing a small continuous purge gas stream.

3.1.4 Formation of Ammonia in the Converter

In ammonia production unit, the synthesis loop is located after the syngas production and purification units. Ammonia synthesis process takes place in high pressure and hence high power multi cycle compressors are used to supply the required pressure ²⁹.

The Kellogg synthesis reactor fig. (3.1) incorporated in this loop is of horizontal type with three beds. To control the temperature between first and second beds, an internal heat exchanger has been used in which the input feed to the first bed and the output gas from the same bed have thermal exchange. In addition to the mentioned heat exchanger, the quench gas flow is also used for control of temperature.

The input feed to the reactor, is first divided into two parts, before entrance. One part is considered as feed and the other part as quench gas. The feed, after entering the reactor, passes through the empty spaces of the beds as well as the reactor walls and gets slightly heated. When reaching to the end of the reactor, it passes through the shell of the internal heat exchanger and its temperature reaches 400 °C. Tubes of the heat exchanger contain the output gas from the first bed. Quench gas is used to control the inlet temperature of the first bed. The required temperature for inlet of the first bed is 371 °C. Output gas, after warming up, is then entered to first catalytic bed. Figure (3.1) depicts the schematic diagram of a Kellogg horizontal reactor.

When the gas passes the first bed and the reaction is taken place, its temperature increases and reaches 496 °C. It then enters the tubes of the heat exchanger to cool down. Gas is then entered from top of the second bed. Temperature rises again as the reaction takes place in the second bed. No specific operation is carried out between beds two and three. In fact these two beds act as a single bed whose length is twice the length of each bed. The catalyst of this reactor is magnetic ferro oxide.

In this Chapter the Kellogg horizontal intercooled ammonia converter has been modeled for the purpose of determine the performance of the fixed bed reactors in ammonia synthesis.

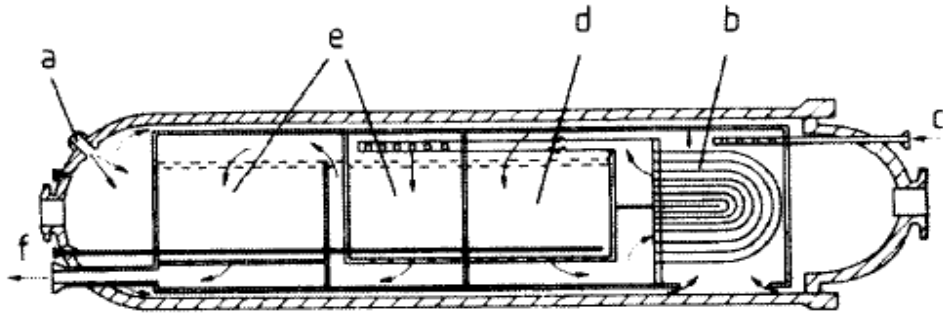


Figure 3.1 Kellogg horizontal intercooled ammonia converter

a) Inlet b) Inter-bed heat exchanger c) Bypass d) Bed 1 e) Bed 2 f) Outlet ¹³

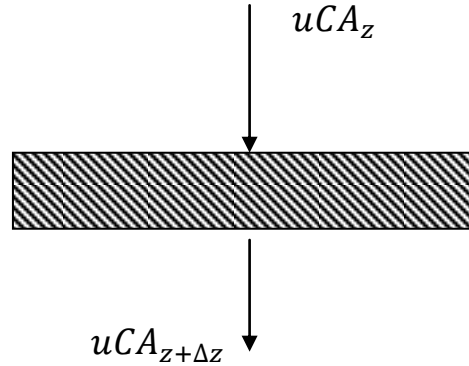
3.1.5 Mathematical Modeling Assumptions

By modeling of the synthesis reactor, temperature, concentrations and pressure profiles are obtained. Of course testing of the model based on the above parameters will be achieved at the end of each bed as industrial data are not usually available along the length of the bed. The following assumptions have been made for this modeling:

1. One-dimensional equations has been considered along with the bulk flow.
2. Negligible axial dispersion:
Usually, dispersion in the axial direction is negligible in industrial reactors. This is because of the high flow rates and long length of the catalyst beds, resulting in Peclet numbers which are high enough to justify the assumption of plug flow
3. The external mass and heat transfer resistances are negligible because of the high gas flow rate that destroys the external resistance
4. Density is constant.
5. Linear velocity profile

3.1.6 Material balance

Considering an element with height of Δz and cross section area equal to that of the bed we'll have:



$$\text{Accumulation} = \text{Consumption} - \text{Production} + \text{Output} - \text{Input} \quad (3.5)$$

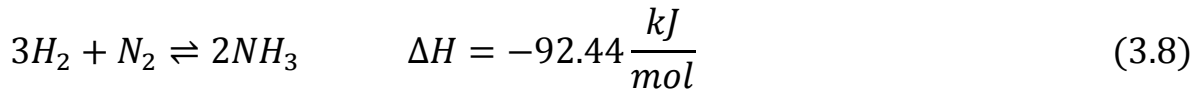
There shall be no accumulation as the system has been considered to be in steady state.

$$uCA_z - uCA_{z+\Delta z} + A\Delta z(-r_{NH_3})\eta = 0 \quad (3.6)$$

Dividing both sides of the equation by $A\Delta z$ and $\Delta z \rightarrow 0$:

$$u \frac{dCA}{dz} + (-r_A)\eta = 0 \quad (3.7)$$

The reaction takes place is:



In this model the intrinsic modified form of the Temkin rate expression is used:

$$r_{NH_3} = k_2 \left[k_a^2 f_{N_2} \left(\frac{f_{H_2}^3}{f_{NH_3}^2} \right)^\alpha - \left(\frac{f_{NH_3}^2}{f_{H_2}^3} \right)^{1-\alpha} \right] \quad (3.9)$$

r_{NH_3} is the reaction rate in kmol of $NH_3/(h.m^3$ of the catalyst bed), K_2 is the velocity constant for the reverse reaction in $kmol/(h.m^3)$ and K_a is the equilibrium constant of the reaction.

The velocity constant is estimated by the Arrhenius relation of the form:

$$K_2 = K_{20} \exp\left(-\frac{E_2}{R.T}\right) \quad (3.10)$$

The respective values for the Montecatini Edison catalyst are ³⁰:

$$\alpha = 0.55, E_2 = 1.635 \times 10^5 \frac{kJ}{Kmol} \quad \text{and} \quad \log_{10} K_{20} = 14.7102$$

The equilibrium constant is given by Gaines

$$\log K_a = -2.691122 \log T - 5.519265 \times 10^{-5} T + 1.848863 \times 10^{-7} T^2 + \frac{2001.6}{T} + 2.6899 \quad (3.11)$$

the fugacity of component is given by definition as²¹:

$$f_j = \varphi_j x_j P \quad (3.12)$$

Where:

φ_j is the fugacity coefficient of component j

x_j is the mole fraction of component j

P is the total pressure in atm

$$\varphi_{H_2} = \exp\left[e^{(-3.8402T^{0.125}+0.541)P} - e^{(-0.1263T^{0.5}-15.98)P^2} + 300(e^{(-0.011901T-5.941)})\left(\frac{P}{e^{300}}\right)\right] \quad (3.13)$$

$$\varphi_{N_2} = 0.93431737 + 0.2028538 \times 10^{-3}T + 0.295896 \times 10^{-3}P - 0.270727 \times 10^{-6}P^2 \quad (3.14)$$

$$\varphi_{NH_3} = 0.1438996 + 0.2028538 \times 10^{-2}T - 0.4487672 \times 10^{-3}P - 0.1142945 \times 10^{-5}T^2 + 0.2761216 \times 10^{-6}P^2 \quad (3.15)$$

$$f_{H_2} = y_{H_2}\varphi_{H_2}P \quad (3.16)$$

$$f_{N_2} = y_{N_2}\varphi_{N_2}P \quad (3.17)$$

$$f_{NH_3} = y_{NH_3}\varphi_{NH_3}P \quad (3.18)$$

3.1.7 Energy balance

Energy balance is investigated on the same element on which mass balance has been considered.

Accumulation = Consumed Energy – Produced Energy + Output Energy – Input Energy

In steady state, the accumulation is zero.

$$A \left[(\rho u C_p T)_z - (\rho u C_p T)_{z+\Delta z} \right] + A \Delta z (-\Delta H_r) (r_{NH_3}) \eta = 0 \quad (3.19)$$

Dividing the above equation by $A \Delta z$ and set $\Delta z \rightarrow 0$:

$$\rho u C_p \frac{dT}{dz} + (-\Delta H_r) (r_{NH_3}) \eta = 0 \quad (3.20)$$

3.1.8 Heat Capacity

The following equation is used to determine the Heat capacity¹⁹:

$$C_{pi} = 4.184(a_i + b_iT + c_iT^2 + d_iT^3) \left(\frac{kJ}{kmol} \right) \quad (3.21)$$

Table (3.1) Coefficients of C_p polynomial for some component³¹

Component	a	b × 10 ²	c × 10 ⁵	d × 10 ⁵
H ₂	6.952	-0.04567	0.09563	-0.2079
N ₂	6.903	-0.03753	0.193	-0.6861
CH ₄	4.75	1.2	0.303	-2.63
Argon	4.9675	----	----	----

In 1967, Shah has developed an equation for determination of ammonia heat capacity which has been used in this model³¹.

$$(C_p)_{NH_3} = 4.184[6.5846 - 0.61251 \times 10^{-2}T + 0.23663 \times 10^{-5}T^2 - 1.5981 \times 10^{-9}T^3 + 96.1678 - 0.067571P + (0.2225 + 1.6847 \times 10^{-4}P)T + (1.289 \times 10^{-4} - 1.009510^{-7}P)T^2] \left(\frac{kJ}{kmol} \right) \quad (3.22)$$

3.1.9 Pressure Drop

To calculate the pressure drop inside beds, Ergun equation has been applied. This relation for a one dimensional flow is as below

$$\Delta P = \frac{150(1 - \varepsilon)^2}{\varepsilon^3} \times \frac{\mu u}{d^2 p} - 1.75 \frac{1 - \varepsilon}{\varepsilon^3} \times \frac{\rho u^2}{dP} \quad (3.23)$$

3.1.10 Model Development

Applying mass, energy and momentum balance on an element, the following mathematical model is obtained using the industrial information in table (3.2) regarding reactor specification, catalyst properties and feed conditions ³².

Table (3.2) Reactor Specification, Catalyst Properties and Feed Conditions

Parameter	Value
Temperature (K)	658
Pressure (<i>bar</i>)	235.8
Molar feed (kmol/h)	10418
Concentration	Mole fraction
H_2	0.6703
N_2	0.2219
CH_4	0.00546
Ar	0.00256
NH_3	0.00276
ρ_c (kg/m^3)	490
ρ_g (kg/m^3)	42.676
d_p (m)	0.035
Reactor length (m)	4
Reactor diameter (m)	1.5

Mathematical Model of Ammonia in Fixed Bed Reactor

$$u \frac{dC_{H_2}}{dz} + (-r_{H_2})\eta = 0 \quad (3.24)$$

$$u \frac{dC_{N_2}}{dz} + (-r_{N_2})\eta = 0 \quad (3.25)$$

$$u \frac{dC_{NH_3}}{dz} + (-r_{NH_3})\eta = 0 \quad (3.26)$$

$$u \frac{dC_{CH_4}}{dz} = 0 \quad (3.27)$$

$$\rho u C_p \frac{dT}{dz} + (-\Delta H_r)(r_{NH_3})\eta = 0 \quad (3.28)$$

3.2 Modeling of Ammonia synthesis from synthesis gas in fluidized bed reactor

The same Reactor Specification, Catalyst Properties and Feed Conditions in table (3.1) used for the modeling of fluidized bed reactor, applying the equations of the two phase model with the assumptions discussed in chapter two the following model is obtained:

$$Q_{bF} = \psi(U_0 - U_{mf})A \quad (3.30)$$

$$Q_{dF} = Q - Q_{bF} \quad (3.31)$$

$$U_{mf} = \frac{\psi d_p}{150\mu} [g(\rho_c - \rho_g)] \frac{\epsilon_{mf}^3}{1 - \epsilon_{mf}} \quad (3.32)$$

$$d_{b0} = \frac{2.78}{g} (U_0 - U_{mf})^2 \quad (3.33)$$

$$d_{bm} = 1.633 \left(\frac{\pi}{4} D^2 (U_0 - U_{mf})^{0.4} \right) \quad (3.34)$$

$$U_{br} = 0.71 (gd_b)^{0.5} \quad (3.35)$$

$$d_b = d_{bm} - (d_{bm} - d_{b0}) \text{Exp} \left(\frac{-0.3h}{D} \right) \quad (3.36)$$

$$U_b = U_0 - U_{mf} + 0.711 (gd_b)^{0.5} \quad (3.37)$$

$$\delta = \frac{U_0 - U_{mf}}{U_b} \quad A_b = \delta A \quad (3.38)$$

$$\Sigma_{V_{H_2}} = 7.07 \quad \Sigma_{V_{N_2}} = 17.9 \quad \Sigma_{V_{NH_3}} = 14.9 \quad \Sigma_{V_{Ar}} = 16.1 \quad \Sigma_{V_{CH_4}} = 24.4$$

$$D_{H_2, N_2} = \frac{T^{1.75} \times 10^{-7} \left(\frac{1}{Mw_{H_2}} + \frac{1}{Mw_{N_2}} \right)^{0.5}}{P \left[(\Sigma_{V_{H_2}})^{\frac{1}{3}} + (\Sigma_{V_{N_2}})^{\frac{1}{3}} \right]^2} \quad (3.39)$$

$$D_{H_2, CH_4} = \frac{T^{1.75} \times 10^{-7} \left(\frac{1}{Mw_{H_2}} + \frac{1}{Mw_{CH_4}} \right)^{0.5}}{P \left[(\Sigma_{V_{H_2}})^{\frac{1}{3}} + (\Sigma_{V_{CH_4}})^{\frac{1}{3}} \right]^2} \quad (3.40)$$

$$D_{H_2, NH_3} = \frac{T^{1.75} \times 10^{-7} \left(\frac{1}{Mw_{H_2}} + \frac{1}{Mw_{NH_3}} \right)^{0.5}}{P \left[(\Sigma_{V_{H_2}})^{\frac{1}{3}} + (\Sigma_{V_{NH_3}})^{\frac{1}{3}} \right]^2} \quad (3.41)$$

$$D_{H_2, Ar} = \frac{T^{1.75} \times 10^{-7} \left(\frac{1}{Mw_{H_2}} + \frac{1}{Mw_{Ar}} \right)^{0.5}}{P \left[(\Sigma_{V_{H_2}})^{\frac{1}{3}} + (\Sigma_{V_{Ar}})^{\frac{1}{3}} \right]^2} \quad (3.42)$$

$$D_{H_2} = \frac{1 - y_{H_2}}{\left[\frac{y_{N_2}}{D_{H_2, N_2}} + \frac{y_{CH_4}}{D_{H_2, CH_4}} + \frac{y_{Ar}}{D_{H_2, Ar}} + \frac{y_{NH_3}}{D_{H_2, NH_3}} \right]} \quad (3.43)$$

$$D_{N_2,CH_4} = \frac{T^{1.75} \times 10^{-7} \left(\frac{1}{MW_{N_2}} + \frac{1}{MW_{CH_4}} \right)^{0.5}}{P[(\Sigma_{V_{N_2}})^{\frac{1}{3}} + (\Sigma_{V_{CH_4}})^{\frac{1}{3}}]^2} \quad (3.44)$$

$$D_{N_2,Ar} = \frac{T^{1.75} \times 10^{-7} \left(\frac{1}{MW_{N_2}} + \frac{1}{MW_{Ar}} \right)^{0.5}}{P[(\Sigma_{V_{N_2}})^{\frac{1}{3}} + (\Sigma_{V_{Ar}})^{\frac{1}{3}}]^2} \quad (3.45)$$

$$D_{N_2,NH_3} = \frac{T^{1.75} \times 10^{-7} \left(\frac{1}{MW_{N_2}} + \frac{1}{MW_{NH_3}} \right)^{0.5}}{P[(\Sigma_{V_{N_2}})^{\frac{1}{3}} + (\Sigma_{V_{NH_3}})^{\frac{1}{3}}]^2} \quad (3.46)$$

$$D_{N_2} = \frac{1 - y_{N_2}}{\left[\frac{y_{H_2}}{D_{N_2,H_2}} + \frac{y_{CH_4}}{D_{N_2,CH_4}} + \frac{y_{NH_3}}{D_{N_2,NH_3}} + \frac{y_{Ar}}{D_{N_2,Ar}} \right]} \quad (3.47)$$

$$D_{CH_4,NH_3} = \frac{T^{1.75} \times 10^{-7} \left(\frac{1}{MW_{CH_4}} + \frac{1}{MW_{NH_3}} \right)^{0.5}}{P[(\Sigma_{V_{CH_4}})^{\frac{1}{3}} + (\Sigma_{V_{NH_3}})^{\frac{1}{3}}]^2} \quad (3.48)$$

$$D_{CH_4,Ar} = \frac{T^{1.75} \times 10^{-7} \left(\frac{1}{MW_{CH_4}} + \frac{1}{MW_{Ar}} \right)^{0.5}}{P[(\Sigma_{V_{CH_4}})^{\frac{1}{3}} + (\Sigma_{V_{Ar}})^{\frac{1}{3}}]^2} \quad (3.49)$$

$$D_{CH_4} = \frac{1 - y_{CH_4}}{\left[\frac{y_{H_2}}{D_{CH_4,H_2}} + \frac{y_{CH_4}}{D_{CH_4,N_2}} + \frac{y_{Ar}}{D_{CH_4,Ar}} + \frac{y_{NH_3}}{D_{CH_4,NH_3}} \right]} \quad (3.50)$$

$$D_{NH_3,Ar} = \frac{T^{1.75} \times 10^{-7} \left(\frac{1}{MW_{NH_3}} + \frac{1}{MW_{Ar}} \right)^{0.5}}{P[(\Sigma_{V_{NH_3}})^{\frac{1}{3}} + (\Sigma_{V_{Ar}})^{\frac{1}{3}}]^2} \quad (3.51)$$

$$D_{NH_3} = \frac{1 - y_{NH_3}}{\left[\frac{y_{H_2}}{D_{NH_3,H_2}} + \frac{y_{CH_4}}{D_{NH_3,CH_4}} + \frac{y_{N_2}}{D_{NH_3,N_2}} + \frac{y_{Ar}}{D_{NH_3,Ar}} \right]} \quad (3.52)$$

$$D_{Ar} = \frac{1 - y_{Ar}}{\left[\frac{y_{H_2}}{D_{Ar,H_2}} + \frac{y_{CH_4}}{D_{Ar,CH_4}} + \frac{y_{N_2}}{D_{Ar,N_2}} + \frac{y_{NH_3}}{D_{Ar,NH_3}} \right]} \quad (3.53)$$

$$(K_{bc})_{H_2} = 4.5 \left(\frac{U_{mf}}{d_b} \right) + 5.85 \left(\frac{D_{H_2}^2 g^{0.25}}{D^{1.5}} \right) \quad (3.54)$$

$$(K_{cd})_{H_2} = 6.77 \left(\frac{D_{H_2} \varepsilon_{mf} U_{br}}{d_b^3} \right)^{0.5} \quad (3.55)$$

$$\frac{1}{(K_{bd})_{H_2}} = \frac{1}{(K_{bc})_{H_2}} + \frac{1}{(K_{cd})_{H_2}} \quad (3.56)$$

$$(K_{bc})_{N_2} = 4.5 \left(\frac{U_{mf}}{d_b} \right) + 5.85 \left(\frac{D_{N_2}^2 g^{0.25}}{D^{1.5}} \right) \quad (3.57)$$

$$(K_{cd})_{N_2} = 6.77 \left(\frac{D_{N_2} \varepsilon_{mf} U_{br}}{d_b^3} \right)^{0.5} \quad (3.58)$$

$$\frac{1}{(K_{bd})_{N_2}} = \frac{1}{(K_{bc})_{N_2}} + \frac{1}{(K_{cd})_{N_2}} \quad (3.59)$$

$$(K_{bc})_{CH_4} = 4.5 \left(\frac{U_{mf}}{d_b} \right) + 5.85 \left(\frac{D_{CH_4}^2 g^{0.25}}{D^{1.5}} \right) \quad (3.60)$$

$$(K_{cd})_{CH_4} = 6.77 \left(\frac{D_{CH_4} \varepsilon_{mf} U_{br}}{d_b^3} \right)^{0.5} \quad (3.61)$$

$$\frac{1}{(K_{bd})_{CH_4}} = \frac{1}{(K_{bc})_{CH_4}} + \frac{1}{(K_{cd})_{CH_4}} \quad (3.62)$$

$$(K_{bc})_{NH_3} = 4.5 \left(\frac{U_{mf}}{d_b} \right) + 5.85 \left(\frac{D_{NH_3}^2 g^{0.25}}{D^{1.5}} \right) \quad (3.63)$$

$$(K_{cd})_{NH_3} = 6.77 \left(\frac{D_{NH_3} \varepsilon_{mf} U_{br}}{d_b^3} \right)^{0.5} \quad (3.64)$$

$$\frac{1}{(K_{bd})_{NH_3}} = \frac{1}{(K_{bc})_{NH_3}} + \frac{1}{(K_{cd})_{NH_3}} \quad (3.65)$$

$$(K_{bc})_{Ar} = 4.5 \left(\frac{U_{mf}}{d_b} \right) + 5.85 \left(\frac{D_{Ar}^2 g^{0.25}}{D^{1.5}} \right) \quad (3.66)$$

$$(K_{cd})_{Ar} = 6.77 \left(\frac{D_{Ar} \varepsilon_{mf} U_{br}}{d_b^3} \right)^{0.5} \quad (3.67)$$

$$\frac{1}{(K_{bd})_{Ar}} = \frac{1}{(K_{bc})_{Ar}} + \frac{1}{(K_{cd})_{Ar}} \quad (3.68)$$

$$a_{H_2} = \frac{(K_{bd})_{H_2}}{U_b} \quad (3.69)$$

$$a_{N_2} = \frac{(K_{bd})_{N_2}}{U_b} \quad (3.70)$$

$$a_{CH_4} = \frac{(K_{bd})_{CH_4}}{U_b} \quad (3.71)$$

$$a_{NH_3} = \frac{(K_{bd})_{NH_3}}{U_b} \quad (3.72)$$

$$a_{Ar} = \frac{(K_{bd})_{Ar}}{U_b} \quad (3.73)$$

The rate of the reaction is calculated from equations (3.8) to (3.18).

3.2.1 Bubble phase material balance

$$\frac{(N_{H_2})_b}{Q_b} + \frac{(N_{H_2})_d}{Q_d} = \left(\frac{(N_{H_2})_{bF}}{Q_b} - \frac{(N_{H_2})_d}{Q_d} \right) e^{-a_{H_2} \cdot z} \quad (3.74)$$

$$\frac{(N_{N_2})_b}{Q_b} + \frac{(N_{N_2})_d}{Q_d} = \left(\frac{(N_{N_2})_{bF}}{Q_b} - \frac{(N_{N_2})_d}{Q_d} \right) e^{-a_{N_2} \cdot z} \quad (3.75)$$

$$\frac{(N_{CH_4})_b}{Q_b} + \frac{(N_{CH_4})_d}{Q_d} = \left(\frac{(N_{CH_4})_{bF}}{Q_b} - \frac{(N_{CH_4})_d}{Q_d} \right) e^{-a_{CH_4} \cdot z} \quad (3.76)$$

$$\frac{(N_{NH_3})_b}{Q_b} + \frac{(N_{NH_3})_d}{Q_d} = \left(\frac{(N_{NH_3})_{bF}}{Q_b} - \frac{(N_{NH_3})_d}{Q_d} \right) e^{-a_{NH_3} \cdot z} \quad (3.77)$$

$$\frac{(N_{Ar})_b}{Q_b} + \frac{(N_{Ar})_d}{Q_d} = \left(\frac{(N_{Ar})_{bF}}{Q_b} - \frac{(N_{Ar})_d}{Q_d} \right) e^{-a_{Ar} \cdot z} \quad (3.78)$$

3.2.2 Dense phase material balance

$$\begin{aligned} (N_{H_2})_d &= y_{H_2} N_F \frac{Q_{dF}}{Q_F} + U_b A_b \left(\frac{y_{H_2} N_F}{Q} - \frac{(N_{H_2})_d}{Q_d} \right) + (1 - e^{-a_{H_2} \cdot H}) \\ &\quad + V(1 - \delta)(1 - \varepsilon_{mf}) \rho_p \alpha_{H_2} r_{NH_3} \end{aligned} \quad (3.79)$$

$$\begin{aligned} (N_{N_2})_d &= y_{N_2} N_F \frac{Q_{dF}}{Q_F} + U_b A_b \left(\frac{y_{N_2} N_F}{Q} - \frac{(N_{N_2})_d}{Q_d} \right) + (1 - e^{-a_{N_2} \cdot H}) \\ &\quad + V(1 - \delta)(1 - \varepsilon_{mf}) \rho_p \alpha_{N_2} r_{NH_3} \end{aligned} \quad (3.80)$$

$$\begin{aligned} (N_{CH_4})_d &= y_{CH_4} N_F \frac{Q_{dF}}{Q_F} + U_b A_b \left(\frac{y_{CH_4} N_F}{Q} - \frac{(N_{CH_4})_d}{Q_d} \right) + (1 - e^{-a_{CH_4} \cdot H}) \\ &\quad + V(1 - \delta)(1 - \varepsilon_{mf}) \rho_p r_{CH_4} \end{aligned} \quad (3.81)$$

$$\begin{aligned} (N_{Ar})_d &= y_{Ar} N_F \frac{Q_{dF}}{Q_F} + U_b A_b \left(\frac{y_{Ar} N_F}{Q} - \frac{(N_{Ar})_d}{Q_d} \right) + (1 - e^{-a_{Ar} \cdot H}) \\ &\quad + V(1 - \delta)(1 - \varepsilon_{mf}) \rho_p r_{Ar} \end{aligned} \quad (3.82)$$

$$\begin{aligned} (N_{NH_3})_d &= y_{NH_3} N_F \frac{Q_{dF}}{Q_F} + U_b A_b \left(\frac{y_{NH_3} N_F}{Q} - \frac{(N_{NH_3})_d}{Q_d} \right) + (1 - e^{-a_{NH_3} \cdot H}) \\ &\quad + V(1 - \delta)(1 - \varepsilon_{mf}) \rho_p \alpha_{NH_3} r_{NH_3} \end{aligned} \quad (3.83)$$

$$N_{H_2} = (N_{H_2})_b + (N_{H_2})_d \quad (3.84)$$

$$N_{N_2} = (N_{N_2})_b + (N_{N_2})_d \quad (3.85)$$

$$N_{CH_4} = (N_{CH_4})_b + (N_{CH_4})_d \quad (3.86)$$

$$N_{NH_3} = (N_{NH_3})_b + (N_{NH_3})_d \quad (3.87)$$

$$N_{Ar} = (N_{Ar})_b + (N_{Ar})_d \quad (3.88)$$

3.2.3 Energy Balance

$$(C_p)_{H_2} = 4.184(6.952 - 0.0457 \times 10^{-2}T + 0.09563 \times 10^5T^2 - 0.2079 \times 10^{-5}T^3) \quad (3.89)$$

$$(C_p)_{N_2} = 4.184(6.903 - 0.0375 \times 10^{-2}T + 0.193 \times 10^{-5}T^2 - 0.6861 \times 10^{-5}T^3) \quad (3.90)$$

$$(C_p)_{NH_3} = 4.184[6.5846 - 0.61251 \times 10^{-2}T + 0.23663 \times 10^{-5}T^2 - 1.5981 \times 10^{-9}T^3 + 96.1678 - 0.067571P + (0.2225 + 1.6847 \times 10^{-4}P)T + (1.289 \times 10^{-4} - 1.009510^{-7}P)T^2] \quad (3.91)$$

$$(C_p)_g = y_{H_2}(C_p)_{H_2} + y_{N_2}(C_p)_{N_2} + y_{NH_3}(C_p)_{NH_3} \quad (3.92)$$

$$k_{H_2} = \mu_{H_2} \left((C_p)_{H_2} + \frac{10.4}{2} \right) \quad (3.93)$$

$$k_{N_2} = \mu_{N_2} \left((C_p)_{N_2} + \frac{10.4}{28} \right) \quad (3.94)$$

$$k_{NH_3} = \mu_{NH_3} \left((C_p)_{NH_3} + \frac{10.4}{17} \right) \quad (3.95)$$

$$k_g = y_{H_2}k_{H_2} + y_{N_2}k_{N_2} + y_{NH_3}k_{NH_3} \quad (3.96)$$

$$H_{bd} = 19.09(U_{mf}\rho_g(C_p)_gd_b) + \frac{5.85(k_g\rho_g(C_p)_g)^{1/2}g^{1/4}}{6d_b^{1/4}} \quad (3.97)$$

3.2.4 Bubble phase heat balance

$$T_b = T_d - (T_d - T_F)e^{-b.z} \quad (3.98)$$

$$b = \frac{H_{bd}}{U_b\rho_g(C_p)_g} \quad (3.99)$$

3.2.5 Dense phase heat balance

$$\rho_g C_{pg} Q_{dF}(T_F - 298) - \rho_g C_{pg} Q_d(T_d - 298) + \rho_g C_{pg} U_b A_b (T_F - T_d)(1 - e^{-b.H}) + V(1 - \delta)(1 - \varepsilon_{mf})\rho_p [(-\Delta H_r)r_{NH_3}] = 0 \quad (3.100)$$

$$T = \frac{Q_b T_b + Q_d T_d}{Q_b + Q_d} \quad (3.101)$$

3.3 Modeling of methanol synthesis from synthesis gas in fluidized bed catalytic reactor

The Khark petrochemical methanol unit will be modeled. This reactor is of shell and tube type. The reactor tubes have synthesis catalysts and water flows in the shell of reactors. Because methanol synthesis reaction is exothermic, released heat is used to produce steam. The characteristics of the industrial reactor are given in Table 3.3. Fresh feed of the unit consists of H_2, CO, CO_2 (that forms the synthesis gas) and also CH_4 and N_2 that participate in methanol synthesis's reactions³³

Table (3.3) Reactor Specification, Catalyst Properties and Feed Conditions

parameter	Value
Temperature (K)	498
Pressure (bar)	82
Molar feed (Kmol/h)	47400
concentration	Mole fraction
H_2	0.8
CO_2	0.0295
N_2	0.0001
CO	0.0476
CH_4	0.1192
H_2O	0.0006
CH_3OH	0.003
ρ_c (kg/m ³)	1063
ρ_g (kg/m ³)	12.12
d_p (m)	0.04
Reactor length (m)	4
Reactor diameter (m)	1.5

$$Q_{bF} = \psi(U_0 - U_{mf})A \quad (3.102)$$

$$Q_{dF} = Q - Q_{bF} \quad (3.103)$$

$$U_{mf} = \frac{\psi d_p}{150\mu} [g(\rho_c - \rho_g)] \frac{\varepsilon_{mf}^3}{1 - \varepsilon_{mf}} \quad (3.104)$$

$$d_{b0} = \frac{2.78}{g} (U_0 - U_{mf})^2 \quad (3.105)$$

$$d_{bm} = 1.633 \left(\frac{\pi}{4} D^2 (U_0 - U_{mf})^{0.4} \right) \quad (3.106)$$

$$U_{br} = 0.71(gd_b)^{0.5} \quad (3.107)$$

$$d_b = d_{bm} - (d_{bm} - d_{b0}) \text{Exp} \left(\frac{-0.3h}{D} \right) \quad (3.108)$$

$$U_b = U_0 - U_{mf} + 0.711(gd_b)^{0.5} \quad (3.109)$$

$$D_{H_2, N_2} = \frac{T^{1.75} \times 10^{-7} \left(\frac{1}{M_{WH_2}} + \frac{1}{M_{WN_2}} \right)^{0.5}}{P \left[(\Sigma_{V_{H_2}})^{\frac{1}{3}} + (\Sigma_{V_{N_2}})^{\frac{1}{3}} \right]^2} \quad (3.111)$$

$$D_{H_2, CH_4} = \frac{T^{1.75} \times 10^{-7} \left(\frac{1}{M_{WH_2}} + \frac{1}{M_{WCH_4}} \right)^{0.5}}{P \left[(\Sigma_{V_{H_2}})^{\frac{1}{3}} + (\Sigma_{V_{CH_4}})^{\frac{1}{3}} \right]^2} \quad (3.112)$$

$$D_{H_2, CO} = \frac{T^{1.75} \times 10^{-7} \left(\frac{1}{M_{WH_2}} + \frac{1}{M_{WCO}} \right)^{0.5}}{P \left[(\Sigma_{V_{H_2}})^{\frac{1}{3}} + (\Sigma_{V_{CO}})^{\frac{1}{3}} \right]^2} \quad (3.113)$$

$$D_{H_2, CO_2} = \frac{T^{1.75} \times 10^{-7} \left(\frac{1}{M_{WH_2}} + \frac{1}{M_{WCO_2}} \right)^{0.5}}{P \left[(\Sigma_{V_{H_2}})^{\frac{1}{3}} + (\Sigma_{V_{CO_2}})^{\frac{1}{3}} \right]^2} \quad (3.114)$$

$$D_{H_2, H_2O} = \frac{T^{1.75} \times 10^{-7} \left(\frac{1}{M_{WH_2}} + \frac{1}{M_{WH_2O}} \right)^{0.5}}{P \left[(\Sigma_{V_{H_2}})^{\frac{1}{3}} + (\Sigma_{V_{H_2O}})^{\frac{1}{3}} \right]^2} \quad (3.115)$$

$$D_{H_2,CH_3OH} = \frac{T^{1.75} \times 10^{-7} \left(\frac{1}{MW_{H_2}} + \frac{1}{MW_{CH_3OH}} \right)^{0.5}}{P[(\Sigma_{V_{H_2}})^{\frac{1}{3}} + (\Sigma_{V_{CH_3OH}})^{\frac{1}{3}}]^2} \quad (3.116)$$

$$D_{H_2} = \frac{1 - y_{H_2}}{\left[\frac{y_{N_2}}{D_{H_2,N_2}} + \frac{y_{CH_4}}{D_{H_2,CH_4}} + \frac{y_{CO}}{D_{H_2,CO}} + \frac{y_{CO_2}}{D_{H_2,CO_2}} + \frac{y_{H_2O}}{D_{H_2,H_2O}} + \frac{y_{CH_3OH}}{D_{H_2,CH_3OH}} \right]} \quad (3.117)$$

$$D_{N_2,CH_4} = \frac{T^{1.75} \times 10^{-7} \left(\frac{1}{MW_{N_2}} + \frac{1}{MW_{CH_4}} \right)^{0.5}}{P[(\Sigma_{V_{N_2}})^{\frac{1}{3}} + (\Sigma_{V_{CH_4}})^{\frac{1}{3}}]^2} \quad (3.118)$$

$$D_{N_2,CO} = \frac{T^{1.75} \times 10^{-7} \left(\frac{1}{MW_{N_2}} + \frac{1}{MW_{CO}} \right)^{0.5}}{P[(\Sigma_{V_{N_2}})^{\frac{1}{3}} + (\Sigma_{V_{CO}})^{\frac{1}{3}}]^2} \quad (3.119)$$

$$D_{N_2,CO_2} = \frac{T^{1.75} \times 10^{-7} \left(\frac{1}{MW_{N_2}} + \frac{1}{MW_{CO_2}} \right)^{0.5}}{P[(\Sigma_{V_{N_2}})^{\frac{1}{3}} + (\Sigma_{V_{CO_2}})^{\frac{1}{3}}]^2} \quad (3.120)$$

$$D_{N_2,H_2O} = \frac{T^{1.75} \times 10^{-7} \left(\frac{1}{MW_{N_2}} + \frac{1}{MW_{H_2O}} \right)^{0.5}}{P[(\Sigma_{V_{N_2}})^{\frac{1}{3}} + (\Sigma_{V_{H_2O}})^{\frac{1}{3}}]^2} \quad (3.121)$$

$$D_{N_2,CH_3OH} = \frac{T^{1.75} \times 10^{-7} \left(\frac{1}{MW_{N_2}} + \frac{1}{MW_{CH_3OH}} \right)^{0.5}}{P[(\Sigma_{V_{N_2}})^{\frac{1}{3}} + (\Sigma_{V_{CH_3OH}})^{\frac{1}{3}}]^2} \quad (3.122)$$

$$D_{N_2} = \frac{1 - y_{N_2}}{\left[\frac{y_{H_2}}{D_{N_2,H_2}} + \frac{y_{CH_4}}{D_{N_2,CH_4}} + \frac{y_{CO}}{D_{N_2,CO}} + \frac{y_{CO_2}}{D_{N_2,CO_2}} + \frac{y_{H_2O}}{D_{N_2,H_2O}} + \frac{y_{CH_3OH}}{D_{N_2,CH_3OH}} \right]} \quad (3.123)$$

$$D_{CH_4,CO} = \frac{T^{1.75} \times 10^{-7} \left(\frac{1}{MW_{CH_4}} + \frac{1}{MW_{CO}} \right)^{0.5}}{P[(\Sigma_{V_{CH_4}})^{\frac{1}{3}} + (\Sigma_{V_{CO}})^{\frac{1}{3}}]^2} \quad (3.124)$$

$$D_{CH_4,CO_2} = \frac{T^{1.75} \times 10^{-7} \left(\frac{1}{Mw_{CH_4}} + \frac{1}{Mw_{CO_2}} \right)^{0.5}}{P \left[(\Sigma_{V_{CH_4}})^{\frac{1}{3}} + (\Sigma_{V_{CO_2}})^{\frac{1}{3}} \right]^2} \quad (3.125)$$

$$D_{CH_4,H_2O} = \frac{T^{1.75} \times 10^{-7} \left(\frac{1}{Mw_{CH_4}} + \frac{1}{Mw_{H_2O}} \right)^{0.5}}{P \left[(\Sigma_{V_{CH_4}})^{\frac{1}{3}} + (\Sigma_{V_{H_2O}})^{\frac{1}{3}} \right]^2} \quad (3.126)$$

$$D_{CH_4,CH_3OH} = \frac{T^{1.75} \times 10^{-7} \left(\frac{1}{Mw_{CH_4}} + \frac{1}{Mw_{CH_3OH}} \right)^{0.5}}{P \left[(\Sigma_{V_{CH_4}})^{\frac{1}{3}} + (\Sigma_{V_{CH_3OH}})^{\frac{1}{3}} \right]^2} \quad (3.127)$$

$$D_{CH_4} = \frac{1 - y_{CH_4}}{\left[\frac{y_{H_2}}{D_{CH_4,H_2}} + \frac{y_{CH_4}}{D_{CH_4,N_2}} + \frac{y_{CO}}{D_{CH_4,CO}} + \frac{y_{CO_2}}{D_{CH_4,CO_2}} + \frac{y_{H_2O}}{D_{CH_4,H_2O}} + \frac{y_{CH_3OH}}{D_{CH_4,CH_3OH}} \right]} \quad (3.128)$$

$$D_{CO,CO_2} = \frac{T^{1.75} \times 10^{-7} \left(\frac{1}{Mw_{CO}} + \frac{1}{Mw_{CO_2}} \right)^{0.5}}{P \left[(\Sigma_{V_{CO}})^{\frac{1}{3}} + (\Sigma_{V_{CO_2}})^{\frac{1}{3}} \right]^2} \quad (3.129)$$

$$D_{CO,H_2O} = \frac{T^{1.75} \times 10^{-7} \left(\frac{1}{Mw_{CO}} + \frac{1}{Mw_{H_2O}} \right)^{0.5}}{P \left[(\Sigma_{V_{CO}})^{\frac{1}{3}} + (\Sigma_{V_{H_2O}})^{\frac{1}{3}} \right]^2} \quad (3.130)$$

$$D_{CO,CH_3OH} = \frac{T^{1.75} \times 10^{-7} \left(\frac{1}{Mw_{CO}} + \frac{1}{Mw_{CH_3OH}} \right)^{0.5}}{P \left[(\Sigma_{V_{CO}})^{\frac{1}{3}} + (\Sigma_{V_{CH_3OH}})^{\frac{1}{3}} \right]^2} \quad (3.131)$$

$$D_{CO} = \frac{1 - y_{CO}}{\left[\frac{y_{H_2}}{D_{CO,H_2}} + \frac{y_{CH_4}}{D_{CO,CH_4}} + \frac{y_{N_2}}{D_{CO,N_2}} + \frac{y_{CO_2}}{D_{CO,CO_2}} + \frac{y_{H_2O}}{D_{CO,H_2O}} + \frac{y_{CH_3OH}}{D_{CO,CH_3OH}} \right]} \quad (3.132)$$

$$D_{CO_2,H_2O} = \frac{T^{1.75} \times 10^{-7} \left(\frac{1}{Mw_{CO_2}} + \frac{1}{Mw_{H_2O}} \right)^{0.5}}{P \left[(\Sigma_{V_{CO_2}})^{\frac{1}{3}} + (\Sigma_{V_{H_2O}})^{\frac{1}{3}} \right]^2} \quad (3.133)$$

$$D_{CO_2,CH_3OH} = \frac{T^{1.75} \times 10^{-7} \left(\frac{1}{MW_{CO_2}} + \frac{1}{MW_{CH_3OH}} \right)^{0.5}}{P \left[(\Sigma_{V_{CO_2}})^{\frac{1}{3}} + (\Sigma_{V_{CH_3OH}})^{\frac{1}{3}} \right]^2} \quad (3.134)$$

$$D_{CO_2} = \frac{1 - y_{CO_2}}{\left[\frac{y_{H_2}}{D_{CO_2,H_2}} + \frac{y_{CH_4}}{D_{CO_2,CH_4}} + \frac{y_{N_2}}{D_{CO_2,N_2}} + \frac{y_{CO}}{D_{CO_2,CO}} + \frac{y_{H_2O}}{D_{CO_2,H_2O}} + \frac{y_{CH_3OH}}{D_{CO_2,CH_3OH}} \right]} \quad (3.135)$$

$$D_{H_2O,CH_3OH} = \frac{T^{1.75} \times 10^{-7} \left(\frac{1}{MW_{H_2O}} + \frac{1}{MW_{CH_3OH}} \right)^{0.5}}{P \left[(\Sigma_{V_{H_2O}})^{\frac{1}{3}} + (\Sigma_{V_{CH_3OH}})^{\frac{1}{3}} \right]^2} \quad (3.136)$$

$$D_{H_2O} = \frac{1 - y_{CO_2}}{\left[\frac{y_{H_2}}{D_{H_2O,H_2}} + \frac{y_{CH_4}}{D_{H_2O,CH_4}} + \frac{y_{N_2}}{D_{H_2O,N_2}} + \frac{y_{CO}}{D_{H_2O,CO}} + \frac{y_{CO_2}}{D_{H_2O,CO_2}} + \frac{y_{CH_3OH}}{D_{H_2O,CH_3OH}} \right]} \quad (3.137)$$

$$D_{CH_3OH} = \frac{1 - y_{CO_2}}{\left[\frac{y_{H_2}}{D_{CH_3OH,H_2}} + \frac{y_{CH_4}}{D_{CH_3OH,CH_4}} + \frac{y_{N_2}}{D_{CH_3OH,N_2}} + \frac{y_{CO}}{D_{CH_3OH,CO}} + \frac{y_{CO_2}}{D_{CH_3OH,CO_2}} + \frac{y_{H_2O}}{D_{CH_3OH,H_2O}} \right]} \quad (3.138)$$

$$(K_{bc})_{H_2} = 4.5 \left(\frac{U_{mf}}{d_b} \right) + 5.85 \left(\frac{D_{H_2}^2 g^{0.25}}{D^{1.5}} \right) \quad (3.139)$$

$$(K_{cd})_{H_2} = 6.77 \left(\frac{D_{H_2} \varepsilon_{mf} U_{br}}{d_b^3} \right)^{0.5} \quad (3.140)$$

$$\frac{1}{(K_{bd})_{H_2}} = \frac{1}{(K_{bc})_{H_2}} + \frac{1}{(K_{cd})_{H_2}} \quad (3.141)$$

$$(K_{bc})_{N_2} = 4.5 \left(\frac{U_{mf}}{d_b} \right) + 5.85 \left(\frac{D_{N_2}^2 g^{0.25}}{D^{1.5}} \right) \quad (3.142)$$

$$(K_{cd})_{N_2} = 6.77 \left(\frac{D_{N_2} \varepsilon_{mf} U_{br}}{d_b^3} \right)^{0.5} \quad (3.143)$$

$$\frac{1}{(K_{bd})_{N_2}} = \frac{1}{(K_{bc})_{N_2}} + \frac{1}{(K_{cd})_{N_2}} \quad (3.144)$$

$$(K_{bc})_{CH_4} = 4.5 \left(\frac{U_{mf}}{d_b} \right) + 5.85 \left(\frac{D_{CH_4}^2 g^{0.25}}{D^{1.5}} \right) \quad (3.145)$$

$$(K_{cd})_{CH_4} = 6.77 \left(\frac{D_{CH_4} \varepsilon_{mf} U_{br}}{d_b^3} \right)^{0.5} \quad (3.146)$$

$$\frac{1}{(K_{bd})_{CH_4}} = \frac{1}{(K_{bc})_{CH_4}} + \frac{1}{(K_{cd})_{CH_4}} \quad (3.147)$$

$$(K_{bc})_{CO} = 4.5 \left(\frac{U_{mf}}{d_b} \right) + 5.85 \left(\frac{D_{CO}^2 g^{0.25}}{D^{1.5}} \right) \quad (3.148)$$

$$(K_{cd})_{CO} = 6.77 \left(\frac{D_{CO} \varepsilon_{mf} U_{br}}{d_b^3} \right)^{0.5} \quad (3.149)$$

$$\frac{1}{(K_{bd})_{CO}} = \frac{1}{(K_{bc})_{CO}} + \frac{1}{(K_{cd})_{CO}} \quad (3.150)$$

$$(K_{bc})_{CO_2} = 4.5 \left(\frac{U_{mf}}{d_b} \right) + 5.85 \left(\frac{D_{CO_2}^2 g^{0.25}}{D^{1.5}} \right) \quad (3.151)$$

$$(K_{cd})_{CO_2} = 6.77 \left(\frac{D_{CO_2} \varepsilon_{mf} U_{br}}{d_b^3} \right)^{0.5} \quad (3.152)$$

$$\frac{1}{(K_{bd})_{CO_2}} = \frac{1}{(K_{bc})_{CO_2}} + \frac{1}{(K_{cd})_{CO_2}} \quad (3.153)$$

$$(K_{bc})_{H_2O} = 4.5 \left(\frac{U_{mf}}{d_b} \right) + 5.85 \left(\frac{D_{H_2O}^2 g^{0.25}}{D^{1.5}} \right) \quad (3.154)$$

$$(K_{cd})_{H_2O} = 6.77 \left(\frac{D_{H_2O} \varepsilon_{mf} U_{br}}{d_b^3} \right)^{0.5} \quad (3.155)$$

$$\frac{1}{(K_{bd})_{H_2O}} = \frac{1}{(K_{bc})_{H_2O}} + \frac{1}{(K_{cd})_{H_2O}} \quad (3.156)$$

$$(K_{bc})_{CH_3OH} = 4.5 \left(\frac{U_{mf}}{d_b} \right) + 5.85 \left(\frac{D_{CH_3OH}^2 g^{0.25}}{D^{1.5}} \right) \quad (3.157)$$

$$(K_{cd})_{CH_3OH} = 6.77 \left(\frac{D_{CH_3OH} \varepsilon_{mf} U_{br}}{d_b^3} \right)^{0.5} \quad (3.158)$$

$$\frac{1}{(K_{bd})_{CH_3OH}} = \frac{1}{(K_{bc})_{CH_3OH}} + \frac{1}{(K_{cd})_{CH_3OH}} \quad (3.159)$$

3.3.1 The Reaction Kinetics

The reactions together with the water-gas shift reaction are:



In this study, the kinetic equation proposed by Vanden Bussche and Froment (1996) is used. The equation is based on equation (2) and (3) and thus the reaction rate r_1 is neglected. The kinetic equation is:

$$r_{CH_3OH} = \frac{k_1 P_{CO_2} P_{H_2} \left(1 - \frac{P_{CH_3OH} P_{H_2O}}{K_2^{eq} P_{CO_2} P_{H_2}^3} \right)}{\left(1 + \frac{k_3 P_{H_2O}}{P_{H_2}} + \sqrt{k_4 P_{H_2}} + k_5 P_{H_2O} \right)^3} \quad (3.160)$$

$$r_{RWGS} = \frac{k_2 P_{CO_2} \left[1 - K_3^{eq} \left(\frac{P_{H_2O} P_{CO}}{P_{CO_2} P_{H_2}} \right) \right]}{\left(1 + \frac{k_3 P_{H_2O}}{P_{H_2}} + \sqrt{k_4 P_{H_2}} + k_5 P_{H_2O} \right)} \quad (3.161)$$

All the constants (k_j) in equations (3.160) and (3.161) follow the general Arrhenius equation and equilibrium constants were obtained from analyses that are listed in table 3.4.

$$k_j = A_j \exp\left(\frac{B_j}{RT}\right) \quad (3.162)$$

Table 3.4 Frequency Factor of Kinetic Equation ³³

k_1	A	1.07
	B	36696
k_3	A	3453.38
	B	-
$\sqrt{k_4}$	A	0.499
	B	17197
k_5	A	6.62×10^{-11}
	B	124119
k_2	A	1.22×10^{10}
	B	-94765
K_2^{eq}	$10^{3066/T-10592}$	
K_3^{eq}	$10^{-2073/T+2029}$	

$$a_{H_2} = \frac{(K_{bd})_{H_2}}{U_b} \quad (3.163)$$

$$a_{N_2} = \frac{(K_{bd})_{N_2}}{U_b} \quad (3.164)$$

$$a_{H_2O} = \frac{(K_{bd})_{H_2O}}{U_b} \quad (3.165)$$

$$a_{CH_4} = \frac{(K_{bd})_{CH_4}}{U_b} \quad (3.166)$$

$$a_{CO} = \frac{(K_{bd})_{CO}}{U_b} \quad (3.167)$$

$$a_{CO_2} = \frac{(K_{bd})_{CO_2}}{U_b} \quad (3.168)$$

$$a_{CH_3OH} = \frac{(K_{bd})_{CH_3OH}}{U_b} \quad (3.169)$$

3.3.2 Bubble phase material balance:

$$\frac{(N_{H_2})_b}{Q_b} + \frac{(N_{H_2})_d}{Q_d} = \left(\frac{(N_{H_2})_{bF}}{Q_b} - \frac{(N_{H_2})_d}{Q_d} \right) e^{-a_{H_2} \cdot z} \quad (3.170)$$

$$\frac{(N_{N_2})_b}{Q_b} + \frac{(N_{N_2})_d}{Q_d} = \left(\frac{(N_{N_2})_{bF}}{Q_b} - \frac{(N_{N_2})_d}{Q_d} \right) e^{-a_{N_2} \cdot z} \quad (3.171)$$

$$\frac{(N_{CH_4})_b}{Q_b} + \frac{(N_{CH_4})_d}{Q_d} = \left(\frac{(N_{CH_4})_{bF}}{Q_b} - \frac{(N_{CH_4})_d}{Q_d} \right) e^{-a_{CH_4} \cdot z} \quad (3.172)$$

$$\frac{(N_{CO})_b}{Q_b} + \frac{(N_{CO})_d}{Q_d} = \left(\frac{(N_{CO})_{bF}}{Q_b} - \frac{(N_{CO})_d}{Q_d} \right) e^{-a_{CO} \cdot z} \quad (3.173)$$

$$\frac{(N_{CO_2})_b}{Q_b} + \frac{(N_{CO_2})_d}{Q_d} = \left(\frac{(N_{CO_2})_{bF}}{Q_b} - \frac{(N_{CO_2})_d}{Q_d} \right) e^{-a_{CO_2} \cdot z} \quad (3.174)$$

$$\frac{(N_{H_2O})_b}{Q_b} + \frac{(N_{H_2O})_d}{Q_d} = \left(\frac{(N_{H_2O})_{bF}}{Q_b} - \frac{(N_{H_2O})_d}{Q_d} \right) e^{-a_{H_2O} \cdot z} \quad (3.175)$$

$$\frac{(N_{CH_3OH})_b}{Q_b} + \frac{(N_{CH_3OH})_d}{Q_d} = \left(\frac{(N_{CH_3OH})_{bF}}{Q_b} - \frac{(N_{CH_3OH})_d}{Q_d} \right) e^{-a_{CH_3OH} \cdot z} \quad (3.176)$$

3.3.3 Dense phase material balance

$$\begin{aligned} (N_{H_2})_d &= y_{H_2} N_F \frac{Q_{dF}}{Q_F} + U_b A_b \left(\frac{y_{H_2} N_F}{Q} - \frac{(N_{H_2})_d}{Q_d} \right) + (1 - e^{-a_{H_2} \cdot H}) \\ &\quad + V(1 - \delta)(1 - \varepsilon_{mf}) \rho_p r_{H_2} \end{aligned} \quad (3.177)$$

$$\begin{aligned} (N_{N_2})_d &= y_{N_2} N_F \frac{Q_{dF}}{Q_F} + U_b A_b \left(\frac{y_{N_2} N_F}{Q} - \frac{(N_{N_2})_d}{Q_d} \right) + (1 - e^{-a_{N_2} \cdot H}) \\ &\quad + V(1 - \delta)(1 - \varepsilon_{mf}) \rho_p r_{N_2} \end{aligned} \quad (3.18)$$

$$(N_{N_2})_d = y_{N_2} N_F \frac{Q_{dF}}{Q_F} + U_b A_b \left(\frac{y_{N_2} N_F}{Q} - \frac{(N_{N_2})_d}{Q_d} \right) + (1 - e^{-a_{N_2} H}) + V(1 - \delta)(1 - \varepsilon_{mf}) \rho_p r_{N_2} \quad (3.179)$$

$$(N_{CH_4})_d = y_{CH_4} N_F \frac{Q_{dF}}{Q_F} + U_b A_b \left(\frac{y_{CH_4} N_F}{Q} - \frac{(N_{CH_4})_d}{Q_d} \right) + (1 - e^{-a_{CH_4} H}) + V(1 - \delta)(1 - \varepsilon_{mf}) \rho_p r_{CH_4} \quad (3.180)$$

$$(N_{CO})_d = y_{CO} N_F \frac{Q_{dF}}{Q_F} + U_b A_b \left(\frac{y_{CO} N_F}{Q} - \frac{(N_{CO})_d}{Q_d} \right) + (1 - e^{-a_{CO} H}) + V(1 - \delta)(1 - \varepsilon_{mf}) \rho_p r_{CO} \quad (3.181)$$

$$(N_{CO_2})_d = y_{CO_2} N_F \frac{Q_{dF}}{Q_F} + U_b A_b \left(\frac{y_{CO_2} N_F}{Q} - \frac{(N_{CO_2})_d}{Q_d} \right) + (1 - e^{-a_{CO_2} H}) + V(1 - \delta)(1 - \varepsilon_{mf}) \rho_p r_{CO_2} \quad (3.182)$$

$$(N_{H_2O})_d = y_{H_2O} N_F \frac{Q_{dF}}{Q_F} + U_b A_b \left(\frac{y_{H_2O} N_F}{Q} - \frac{(N_{H_2O})_d}{Q_d} \right) + (1 - e^{-a_{H_2O} H}) + V(1 - \delta)(1 - \varepsilon_{mf}) \rho_p r_{H_2O} \quad (3.183)$$

$$(N_{CH_3OH})_d = y_{CH_3OH} N_F \frac{Q_{dF}}{Q_F} + U_b A_b \left(\frac{y_{CH_3OH} N_F}{Q} - \frac{(N_{CH_3OH})_d}{Q_d} \right) + (1 - e^{-a_{CH_3OH} H}) + V(1 - \delta)(1 - \varepsilon_{mf}) \rho_p r_{CH_3OH} \quad (3.184)$$

$$N_{H_2} = (N_{H_2})_b + (N_{H_2})_d \quad (3.185)$$

$$N_{N_2} = (N_{N_2})_b + (N_{N_2})_d \quad (3.186)$$

$$N_{CH_4} = (N_{CH_4})_b + (N_{CH_4})_d \quad (3.187)$$

$$N_{CO} = (N_{CO})_b + (N_{CO})_d \quad (3.188)$$

$$N_{CO_2} = (N_{CO_2})_b + (N_{CO_2})_d \quad (3.189)$$

$$N_{H_2O} = (N_{H_2O})_b + (N_{H_2O})_d \quad (3.190)$$

$$N_{CH_3OH} = (N_{CH_3OH})_b + (N_{CH_3OH})_d \quad (3.191)$$

3.3.4 Energy Balance

Molar heat capacity of the components in the reactor is found from the following equation and the information of table (3.5)

$$\frac{C_p}{R} = A_i + B_i T + C_i T^2 + D_i T^{-2} \quad (3.192)$$

Where C_p is molar heat capacity, R gas constant and A_i , B_i , C_i and D_i are constants.

Table 3.5 Frequency Factor for Enthalpy Equation³³

Chemical species	A	$10^3 B$	$10^6 C$	$10^{-5} D$
<i>CH₃OH</i>	2.211	12.216	-3.450	--
<i>H₂O</i>	3.47	1.45	--	0.121
<i>H₂</i>	3.249	0.472	--	0.081
<i>CO₂</i>	5.457	1.045	--	-1.157
<i>CO</i>	3.376	0.557	--	-0.031

$$(C_p)_{H_2} = R(3.249 + 0.472 \times 10^{-3}T + 0.081 \times 10^5 T^{-2}) \quad (3.193)$$

$$(C_p)_{H_2O} = R(3.47 + 1.45 \times 10^{-3}T + 0.121 \times 10^5 T^{-2}) \quad (3.194)$$

$$(C_p)_{CO_2} = R(5.457 + 1.045 \times 10^{-3}T - 1.157 \times 10^5 T^{-2}) \quad (3.195)$$

$$(C_p)_{CO} = R(3.376 + 0.557 \times 10^{-3}T - 0.031 \times 10^5 T^{-2}) \quad (3.195)$$

$$(C_p)_{CH_3OH} = R(2.211 + 12.216 \times 10^{-3}T - 3.450 \times 10^{-6}T^2) \quad (3.196)$$

$$(C_p)_g = y_{H_2}(C_p)_{H_2} + y_{H_2O}(C_p)_{H_2O} + y_{CO_2}(C_p)_{CO_2} + y_{CO}(C_p)_{CO} + y_{CH_3OH}(C_p)_{CH_3OH} \quad (3.197)$$

$$k_{H_2} = \mu_{H_2} \left((C_p)_{H_2} + \frac{10.4}{2} \right) \quad (3.198)$$

$$k_{H_2O} = \mu_{H_2O} \left((C_p)_{H_2O} + \frac{10.4}{18} \right) \quad (3.199)$$

$$k_{CO_2} = \mu_{CO_2} \left((C_p)_{CO_2} + \frac{10.4}{44} \right) \quad (3.200)$$

$$k_{CO} = \mu_{CO} \left((C_p)_{CO} + \frac{10.4}{28} \right) \quad (3.201)$$

$$k_{CH_3OH} = \mu_{CH_3OH} \left((C_p)_{CH_3OH} + \frac{10.4}{32} \right) \quad (3.202)$$

$$k_g = y_{H_2} k_{H_2} + y_{H_2O} k_{H_2O} + y_{CO_2} k_{CO_2} + y_{CO} k_{CO} + y_{CH_3OH} k_{CH_3OH} \quad (3.203)$$

$$H_{bd} = 19.09(U_{mf} \rho_g (C_p)_g d_b) + \frac{5.85(k_g \rho_g (C_p)_g)^{1/2} g^{1/4}}{6d_b^{1/4}} \quad (3.204)$$

3.3.5 Bubble phase heat balance

$$T_b = T_d - (T_d - T_F) e^{-b.z} \quad (3.205)$$

$$b = \frac{H_{bd}}{U_b \rho_g (C_p)_g} \quad (3.206)$$

3.3.6 Dense phase heat balance

$$\begin{aligned} & \rho_g C_{pg} Q_{dF} (T_F - 298) - \rho_g C_{pg} Q_d (T_d - 298) + \rho_g C_{pg} U_b A_b (T_F - T_d) (1 - e^{-b.H}) \\ & \quad + V(1 - \delta)(1 - \varepsilon_{mf}) \rho_p [(-\Delta H_r) r_{CH_3OH} + (-\Delta H_r) r_{RGWS}] \\ & = 0 \end{aligned} \quad (3.207)$$

$$T = \frac{Q_b T_b + Q_d T_d}{Q_b + Q_d} \quad (3.208)$$

3.4 Modeling of methanol synthesis from synthesis gas in fixed bed reactor

The same Reactor Specification, Catalyst Properties and Feed Conditions in table (3.3) used for the modeling of fixed bed reactor, applying the equations of the one dimensional model with the assumptions discussed in chapter two for the fixed bed reactor the following model is obtained:

$$u \frac{dC_{CO_2}}{dz} + (-r_{CH_3OH}) + (-r_{RWGS}) = 0 \quad (3.209)$$

$$u \frac{dC_{H_2}}{dz} + 3(-r_{CH_3OH}) + (-r_{RWGS}) = 0 \quad (3.210)$$

$$u \frac{dC_{CH_3OH}}{dz} + (r_{CH_3OH}) = 0 \quad (3.211)$$

$$u \frac{dC_{CO}}{dz} + (r_{RWGS}) = 0 \quad (3.212)$$

$$u \frac{dC_{H_2O}}{dz} + (r_{CH_3OH}) + (r_{RWGS}) = 0 \quad (3.213)$$

$$\rho u C_p \frac{dT}{dz} + (-\Delta H_{r1})(r_{CH_3OH}) + (-\Delta H_{r2})(r_{RWGS}) = 0 \quad (3.214)$$

CHAPTER Four

RESULTS AND DISCUSSION

In this chapter the four models of ammonia and methanol synthesis in fixed and fluidized bed which has been derived in chapter three are solved. All models are of ordinary differential equations in one variable; the reactor length. MATLAB is used to solve the models and the results are listed in the following sections, also the MATLAB code is used to determine the effect of different operating parameters on the reactor performance.

4.1 Ammonia synthesis in fixed bed reactor

The following results are based on the mathematical model of the Kellogg horizontal intercooled ammonia converter with the industrial feed conditions and reactor specifications. To validate this model the temperature and the conversion at the end of each bed is compared with the industrial data.

Table (4.1) fixed bed reactor industrial data used as a basis for comparison¹⁹

	Fixed bed		
	Bed1	Bed2	Bed3
Feed temperature (K)	658	706	688
Exit temperature (K)	780	775	728
Conversion %	15.78	25.55	28.91

Table (4.2) Comparison between the Results of the Model and Industrial data

	Industrial Fixed bed			Model Values			Difference %		
	Bed1	Bed2	Bed3	Bed1	Bed2	Bed3	Bed1	Bed2	Bed3
Exit Temperature (K)	780	775	728	801	712	748	2.6	5.5	2.7
Conversion %	15.78	25.55	28.91	15.2	24.8	26.79	3.6	2.7	5.2

4.1.1 Conversion Based on N₂ along the Reactor

Figure 4.1 and Table (4.3) illustrate the increase of the nitrogen conversion along the three beds. It is observed that the increase along the first bed is sharper than the increase in the other two beds; as we can notice from Fig. 4.1 that the change along the first bed is 15% while the change in the second and the third bed is only 12% this is because at this early stage the rate of reversible reaction is low and hence low nitrogen production rate³⁰, the conversion then increase gradually till the end of the beds where the maximum conversion achieved is 26.79%.

Table (4.3) Changes of N₂ conversion along the fixed beds

Reactor length (m)	0	0.5	1	1.5	2	2.5	3	3.5	4	4.5
N ₂ Conversion %	0	9.21	13.5	15	17.92	22	24.8	26	26.5	26.79

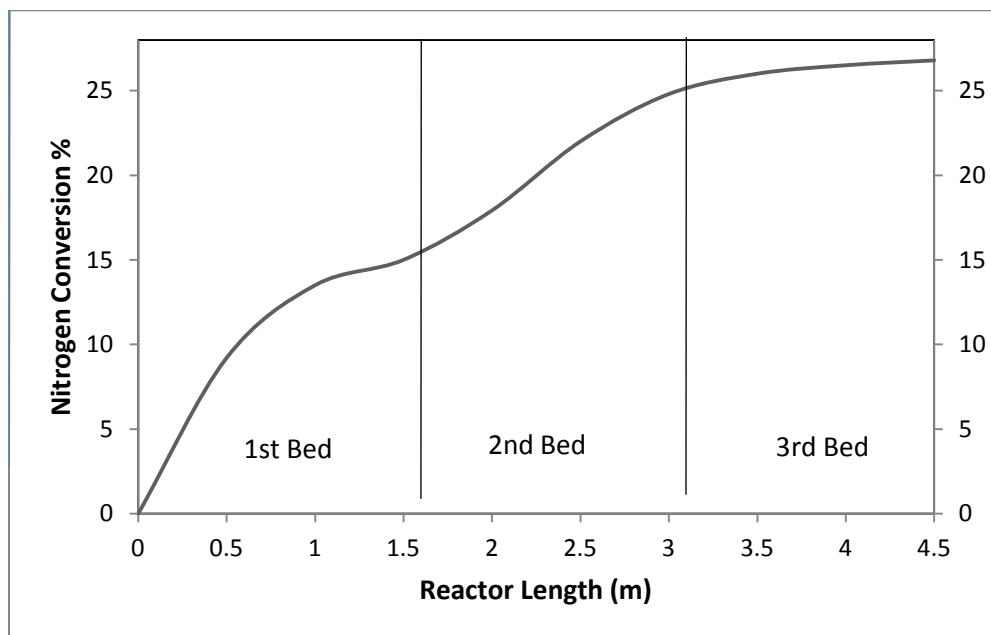


Figure 4.1 Changes of N₂ conversion along the beds

4.1.2 Molar Flow of the components Along the Beds

The three main components in the reaction along the beds are illustrated in Figures (4.2) and (4.3) according to their molar flow rate and mole fractions respectively which can be calculated directly from the conversion rate and the initial amount through the reaction equation, the consumption of hydrogen; 38.1Kmol/hr is three times the conversion of nitrogen; 13.04 Kmol/hr, and the generation of ammonia; 25.66 Kmol/hr is twice the consumption of nitrogen.

Table (4.4) molar flow rate and mole fractions of the main components

Reactor Length (m)	Flow Rate kmol/hr			Mole Fraction%		
	H ₂	N ₂	NH ₃	H ₂	N ₂	NH ₃
0	145.8	52.49	6.32	65.7	23.6	2.7
0.5	136	49.2	12.5	63.12	22.8	5.8
1	129.9	47.2	16.55	61.4	22.32	7.83
1.5	125.15	45.59	19.73	59.9	21.9	9.5
2	121.14	44.26	22.41	58.1	21.5	10.5
2.5	117.64	43.09	24.73	57	21.2	12.2
3	114.53	42.05	26.81	56	20.9	13.3
3.5	111.71	41.12	28.69	55.7	20.63	14.4
4	109.14	40.26	30.41	55.24	20.38	15.39
4.5	107.7	39.46	31.98	54.48	20.18	16.32

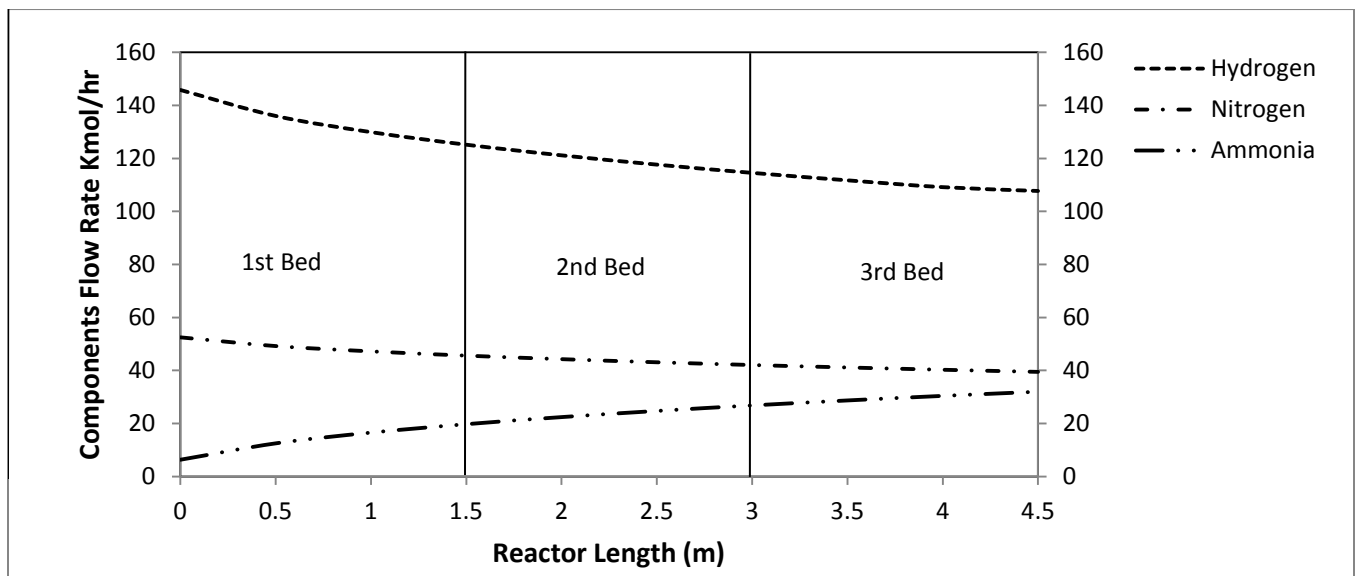


Figure 4.2 Molar Flow of the Components Along The Beds

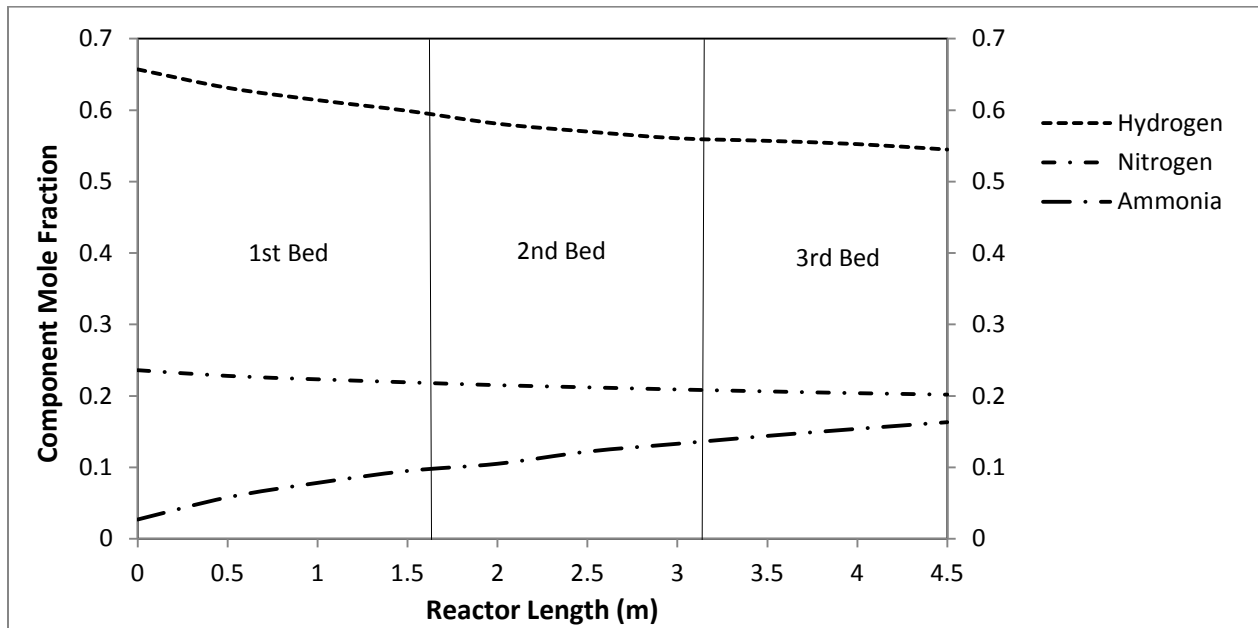


Figure 4.3 Mole Fraction of the Components Along the Beds

4.1.3 Effect of Changes in Flow Rate on Nitrogen Conversion

The performance of the reactor was tested for different values of syngas inlet flow rate and the values of the conversion were reported along the bed. The result of the model run as observed in figures below show that at very high flow rates the conversion of nitrogen is low and as the flow rate decrease the conversion becomes higher; this is because a high flow rate results in higher velocity for the same cross sectional area and hence lower residence time for the component to react over the catalyst bed and vice versa.

Also very low flow rates result in low conversion because the amount of nitrogen and hydrogen available in the reaction space would be least and then lower reaction rate. There must be tradeoff between the velocity and the amount of component contained in the reactor. Also high flow rate contributes in the control of reactor temperature this can be noticed from Figure (4.4) at highest flow rate 27000 kmol/hr the reaction is far from equilibrium.

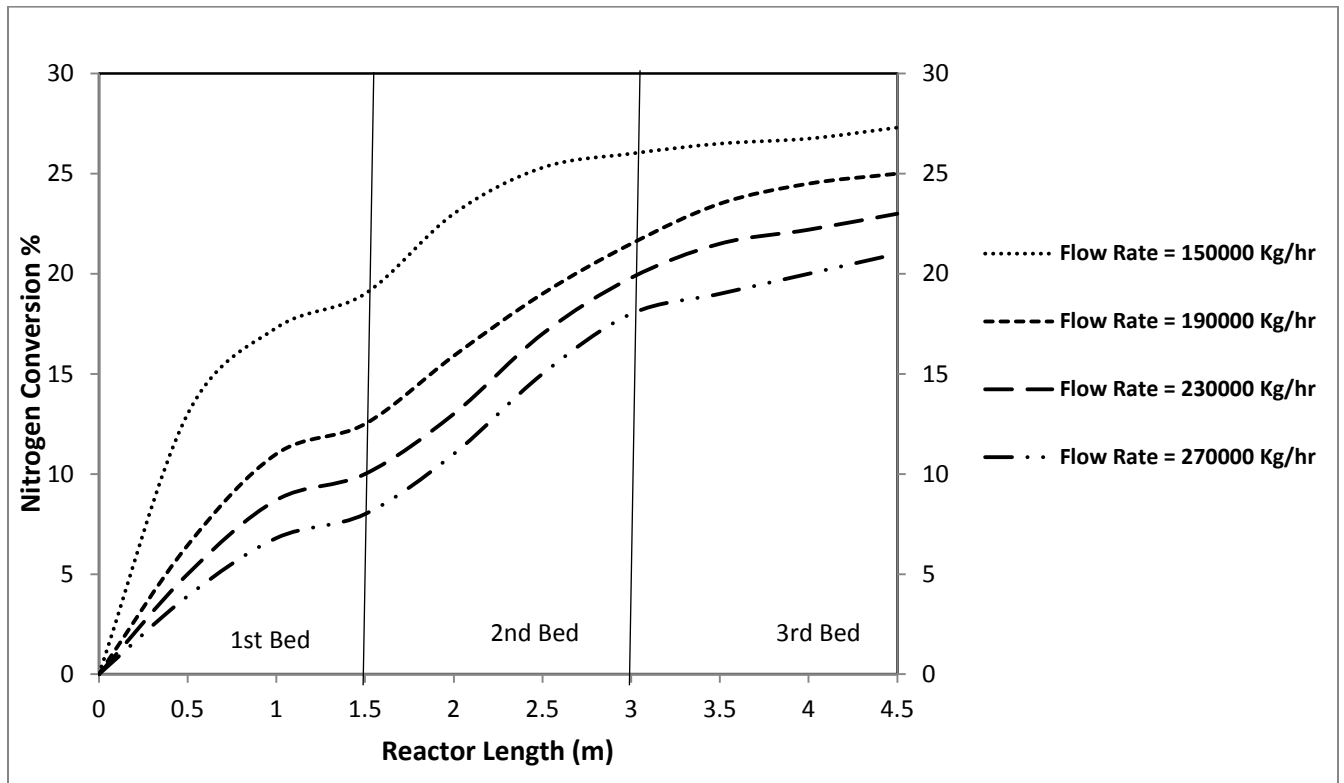


Figure 4.4 The Effect of the Inlet Flow Rate on the Conversion

4.1.4 Effect of Changes in Feed Pressure on Nitrogen Conversion

Different values of pressure were applied to the model which results in a high conversion rate for high pressure value.

The pressure of synthesis gas available is a function of overall ammonia plant load, activity of synthesis catalyst and the inert content in the synthesis loop. There can be constraints on the plant load due to any of the following reasons:

1. Primary reformer limitations.
2. Excessive pressure drop across any catalyst vessel or heat exchangers.
3. Limitation on any of the moving equipments, boiler or exchangers.
4. Highly fouled condition of cooling water exchangers.
5. Feed stock limitation.

Table (4.5) conversion along beds for different values of initial pressure

Reactor Length (m)	N ₂ Conversion%			
	90 bar	110 bar	130 bar	150 bar
0	0	0	0	0
0.5	5	5.59	6.07	6.5
1	8.3	9.15	9.86	10.499
1.5	10	11	12	13
2	13.2	14.34	16	17.5
2.5	16	17	19	20.5
3	18	19	21	22.7
3.5	19	20.6	22	23.4
4	20	21.7	22.98	24.06
4.5	20.5	22	23	24.5

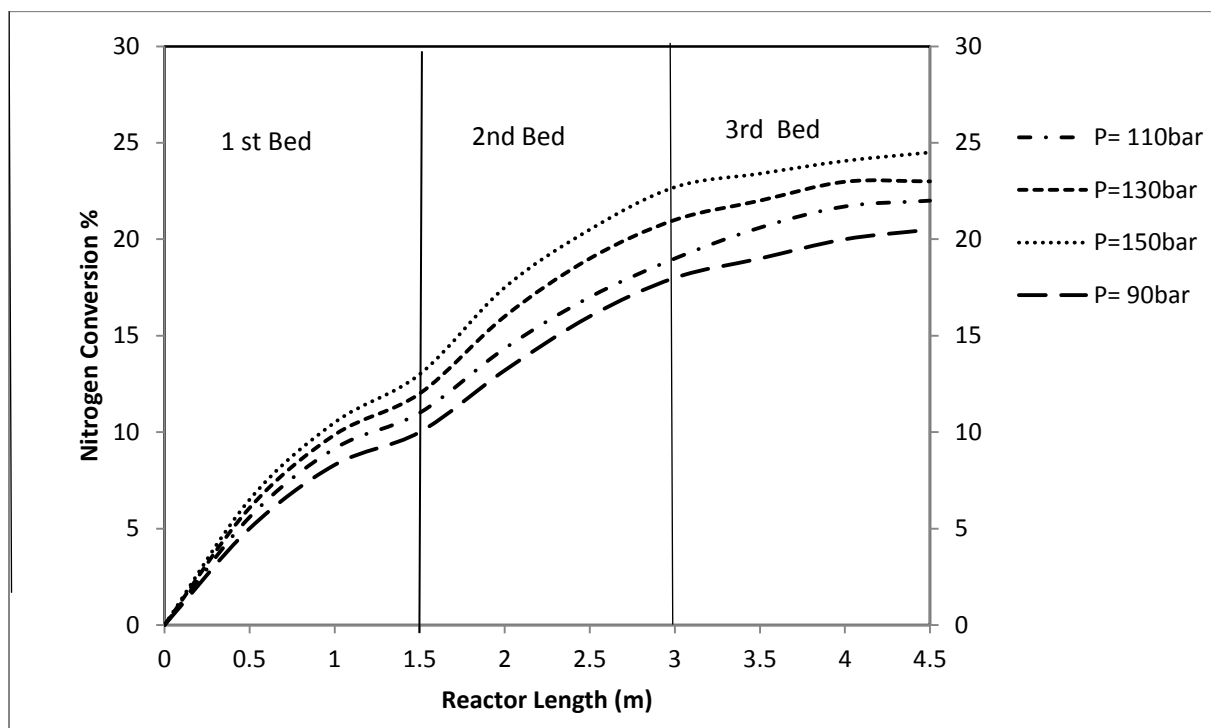


Figure 4.5 The effect of the inlet pressure on the conversion

4.1.5 Effect of Input Ammonia Concentration on the Conversion

As can be observed from next figures the conversion of nitrogen is decrease with the increase of the concentration of ammonia in the feed. It has been discussed earlier that the presence of reasonable amount of ammonia enhances the reversible reaction to produce nitrogen which reduce the conversion rate of nitrogen. The performance of the reactor has been tested for some values of initial concentration of ammonia and the corresponding values of nitrogen conversion were reported

Reactor Length (m)	N ₂ Conversion%			
	NH ₃ = 1%	NH ₃ =2%	NH ₃ =3%	NH ₃ =5%
0	0	0	0	0
0.5	7.19	6.628	6.142	5.5
1	11.17	10.56	10.01	9.28
1.5	13.25	12.5	11.4	10.2
2	17.17	16	15.42	14.37
2.5	20.23	19.1	18.32	17.59
3	23.82	22.64	21.75	20.13
3.5	24.72	23.73	22.8	21.91
4	25.79	24.83	23.87	22.79
4.5	26	25.38	24.21	23.2

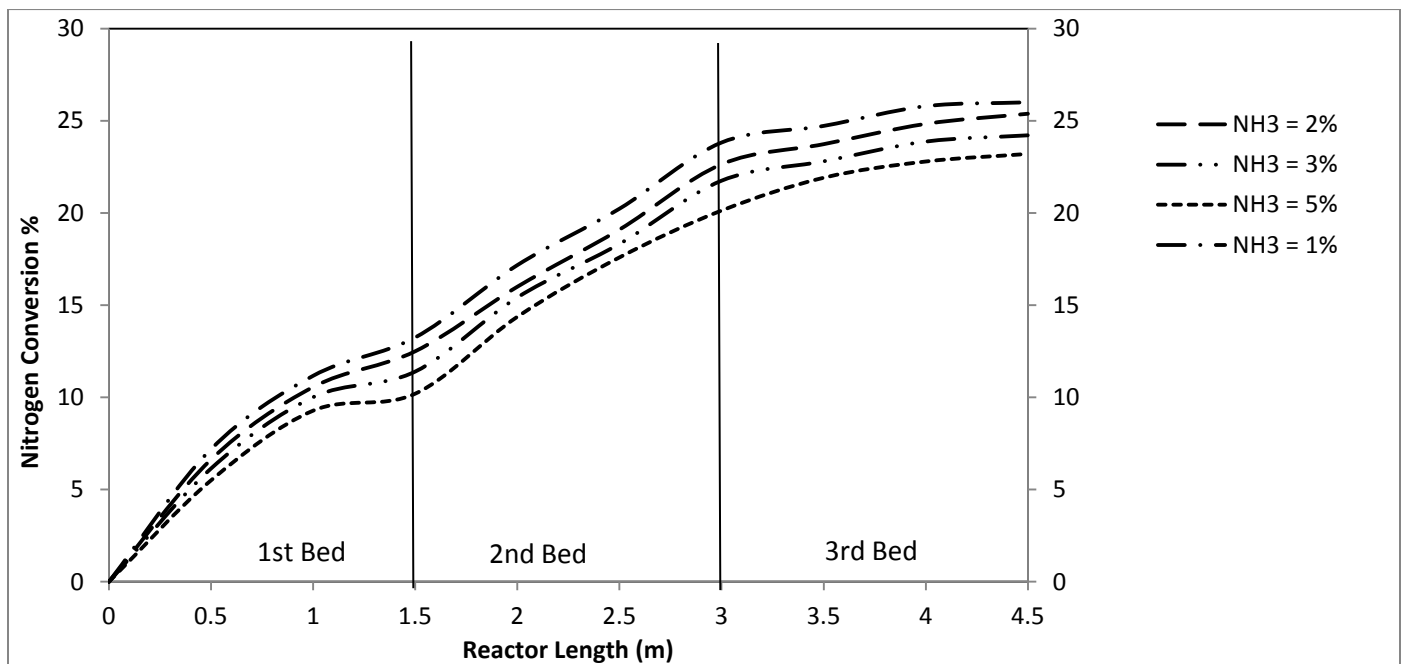


Figure 4.6 The Effect of Initial Ammonia Concentration on the Conversion

4.1.6 Temperature Change Along the Reactor

Figure (4.7) illustrates the temperature changes along the beds. In first bed, as the ammonia concentration is low, the reaction rate is very high and the temperature increases along the bed while approaching equilibrium at its end (the slope of the curve is reduced along the bed). After first bed, gas is cooled down in internal heat exchanger causing that to get far from equilibrium. As it is observed in the Figure 4.7, the gas approaches equilibrium at the end of third bed and the temperature change is low.

Table (4.7) temperature change along beds

Reactor Length (m)	Temperature (K)
0	539
0.5	730
1	793
1.5	801
1.5	560
2	610
2.5	660
3	712
3.5	730
4	745
4.5	748

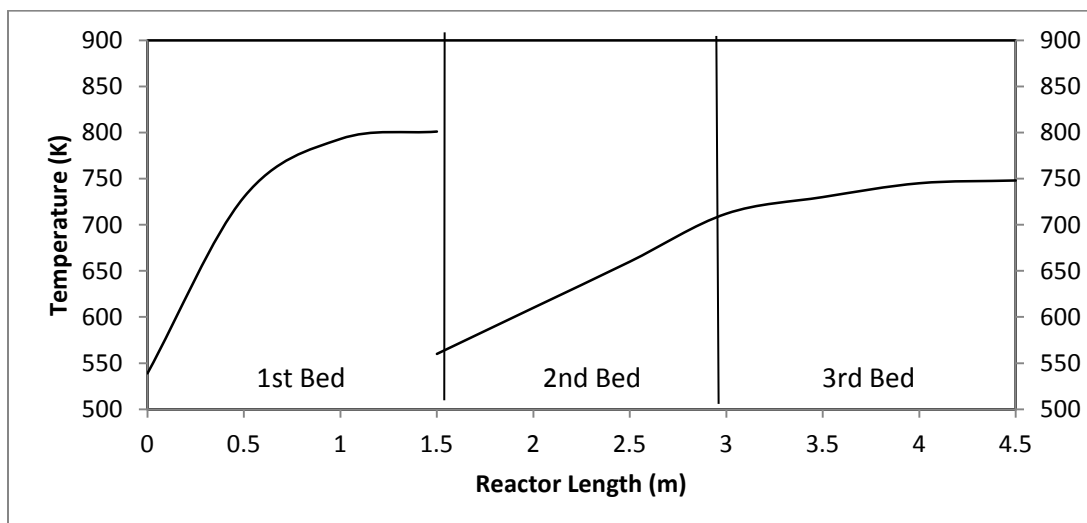


Figure 4.7 Temperature Change Along the Bed

4.2 Fluidized Bed Results

A two phase model of fluidized bed reactor has been generated for ammonia convertor in chapter Three. As can be noticed from Figure (4.8) the conversion is increases gradually by almost constant rate along the bed, the advantage of mass transfer between the bubble and emulsion phase and that the reaction occurs just in the emulsion phase don't allow the concentration of ammonia in the reaction zone to increase and so reduce the rate of the reversible reaction and producing nitrogen. Also the good mixing of the fluidized bed contribute on the temperature control and hence the rate of reaction, so the curve is almost a line

Table (4.8) Nitrogen Conversion Change along the Fluidized Bed Reactor

Reactor Height (M)	N ₂ Conversion%
0	0
0.5	7.78
1	13.66
1.5	18.73
2	22.87
2.5	26.79
3	30.48
3.5	33.96
4	37.22
4.5	40.26

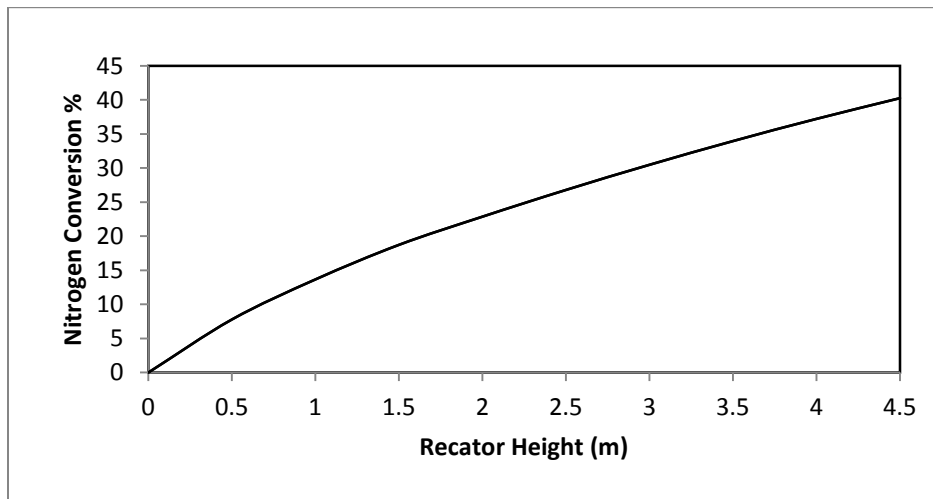


Figure 4.8 Change of Nitrogen Conversion Along the Reactor

4.2.1 Mole Fraction of the Components Along the Reactor

The mole fraction of nitrogen, hydrogen, and ammonia is also calculated from the initial amount of the component and the conversion of nitrogen and illustrated in Figure (4.9) below.

Table (4.9) Change of Mole fractions along the Fluidized Bed Reactor

Reactor Height (m)	Mole Fraction %		
	N ₂	H ₂	NH ₃
0	25.7	74.2	2.45
0.5	24	72.2	3.2
1	23.34	70.26	5.47
1.5	22.7	68.31	8.05
2	22.04	66.37	10.61
2.5	21.4	64.4	13.2
3	20.7	62.55	15.66
3.5	20.14	60.7	18.13
4	19.53	58.86	20.5
4.5	18.9	57.1	22.9

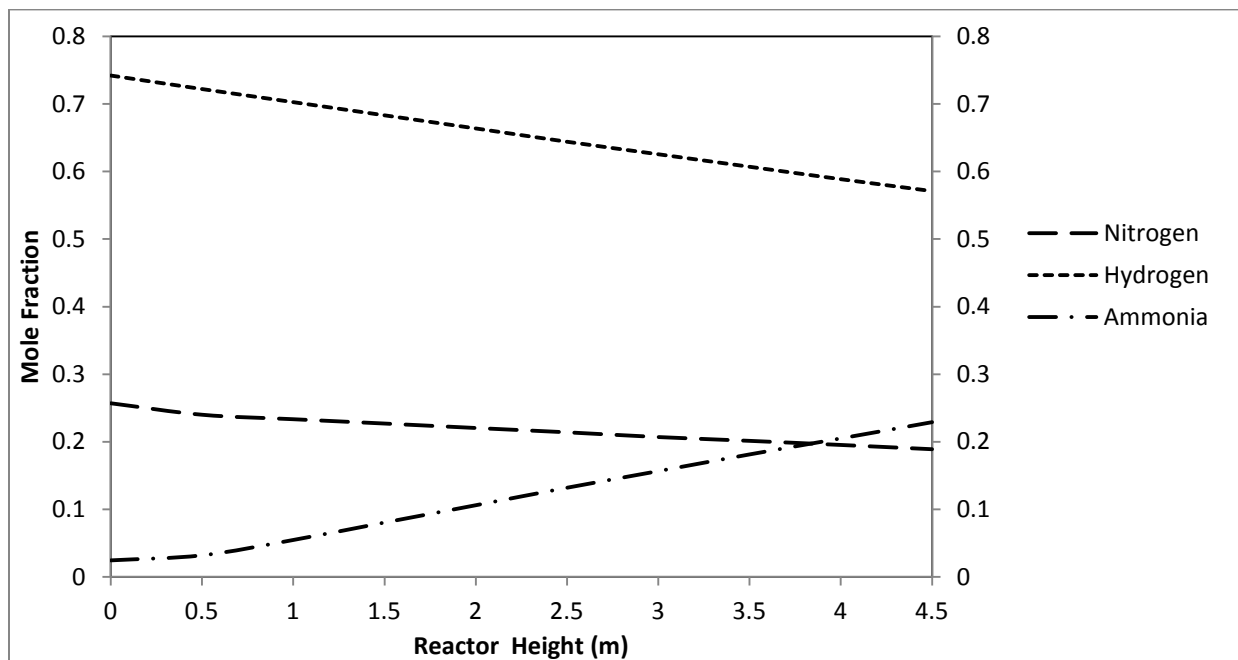


Figure 4.9 Change of Component Mole Fraction Along the Reactor

4.2.2 The Effect of Catalyst Particle Size on the Conversion

Figure (4.10) below conclude the tests done accounting for catalyst particle size. Fixed bed use large sizes of catalyst particles (6 – 12 mm) to avoid excessive pressure drops in the reactor ³⁴. The smaller sizes of particles in fluidized beds eliminate pore diffusion limitations associated with the use of larger particles and hence contribute in increasing the conversion.

Table (4.10) Effect of Particle size on the Conversion

Reactor Height (m)	N2 Conversion %			
	Dp= 0.05mm	Dp= 0.5mm	Dp=1mm	Dp=5mm
0	0	0	0	0
0.5	9.86	7.692	5.45	1.47
1	15.15	13.92	12.359	3.36
1.5	19.814	18.64	17.123	5.29
2	23.95	22.78	21.26	7.64
2.5	27.87	26.69	25.17	10.57
3	31.57	30.39	28.21	13.28
3.5	35.04	33.87	32.35	16.77
4	38.3	37.13	35.64	20.05
4.5	41.35	40.18	38.66	23.122

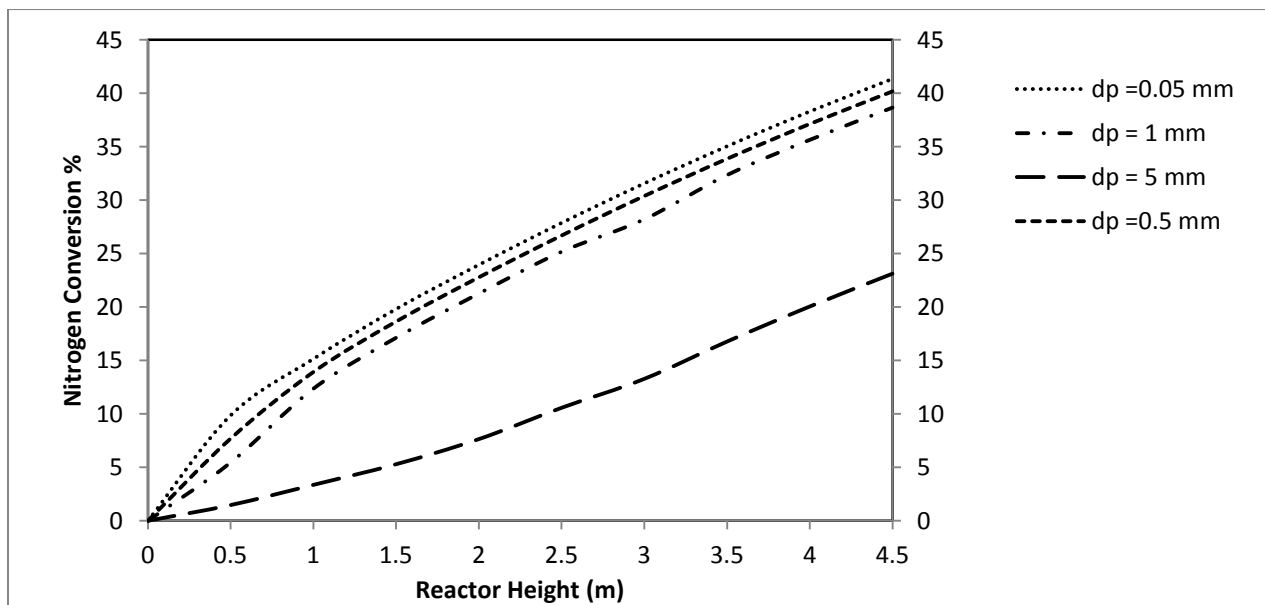


Figure 4.10 The Effect of Particle Diameter on Conversion Along the Reactor

4.2.3 Effect of Mass Transfer Between the Bubble and Dense Phases

It is well known that mixing tends to increase the conversion. Also, the bypass of a certain percentage to reactants through the bubble phase has negative effect on the conversion in fluidized bed reactors. The prediction of the behaviour of the fluidized bed catalytic reactor is quite complex and requires deep understanding of the flow of the gas through the bed, its dispersion and the interchange between the bubble and emulsion phases.

Mass transfer between phases enhances the conversion of the forward reaction for the reversible reactions, the ammonia which transfer to the bubble phase cannot convert to nitrogen because the reaction occurs only in the dense phase. Figure (4.11) shows that the conversion obtained when components allow to transfer between beds ($K_{bd} \neq 0$) the conversion is 40.26% which is high percentage while when the mass transfer coefficient is set to 0 the conversion is only 31.36%. It can be concluded that the net effect of mass transfer between phases results in increasing the conversion.

Table (4.11) The Effect of Mass Transfer Between Phases on the Conversion

Reactor Height (m)	N ₂ Conversion %	
	K _{bd} ≠0	K _{bd} =0
0	0	0
0.5	7.78	2.8735
1	13.66	5.821
1.5	18.73	9.82
2	22.87	13.9
2.5	26.79	17.88
3	30.48	21.57
3.5	33.96	25
4	37.22	28.3
4.5	40.26	31.36

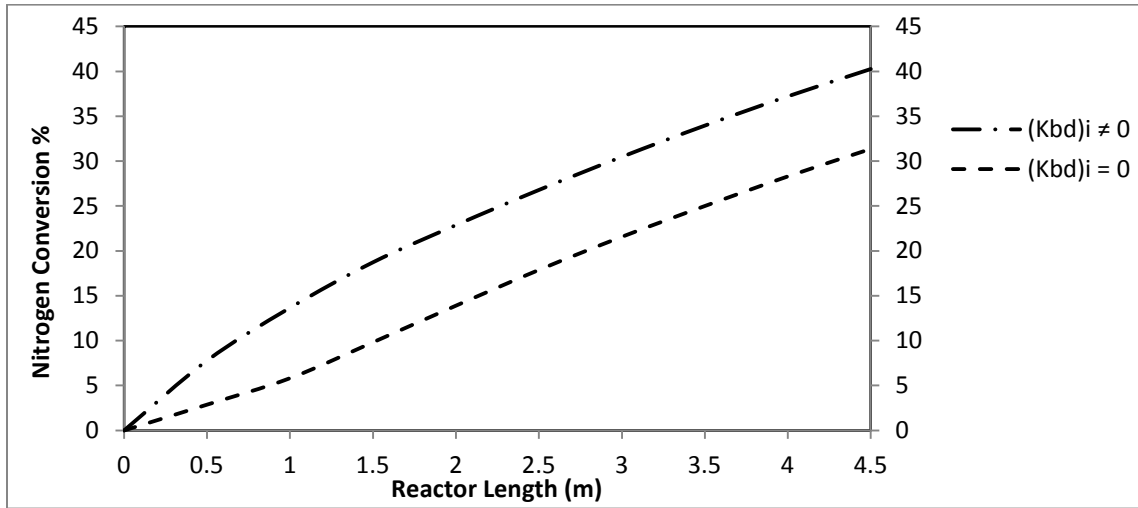


Figure 4.11 The Effect of Components Mass Transfer Between Phases

4.2.4 The Effect of Bed Height to Diameter

Figure (4.12) shows the effect of the height to diameter ratio on the nitrogen conversion. It is clear that this parameter has considerable effect on the conversion. The increase of the height to diameter ratio (by decreasing the bed diameter while keeping the total volume constant) decreases the gas flow in the emulsion phase, thereby increasing the bubble gas flow as shown in Figure (4.13). Since the reaction occurs mostly in the emulsion phase. The decrease of the gas flow has a negative impact on the conversion. Also, the increase of the bubble gas flow affects the conversion negatively:

- By increasing bubble by passing.
- By increasing the bubble size, increase the bubble velocity, decrease the residence time, and decrease the overall coefficient of the gas transfer between the bubble and emulsion phases.

Table (4.12) The Effect of Height to Diameter on the Flow and Conversion

L/D	Qd	Qb	N ₂ Conversion %
	Kmol/hr		
1	823.19	235.3	50.83
2	659.92	513.57	42.65
3	558.9	730.2	40.18
4	489.2	793.5	38.96

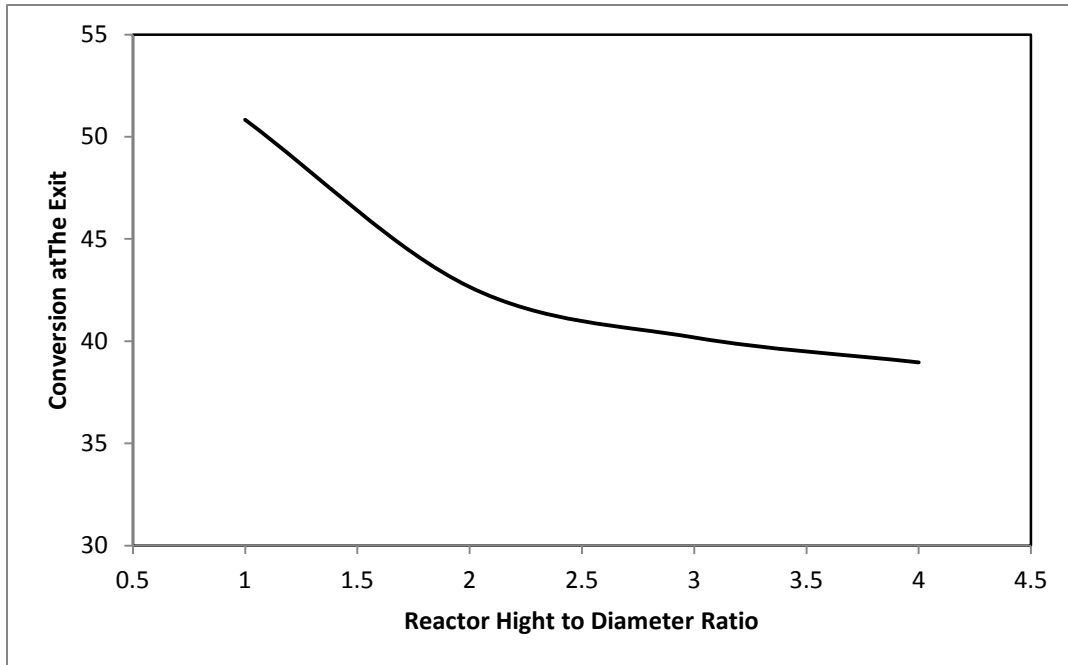


Figure 4.12 Effect of Bed Height to Diameter Ratio on the Conversion

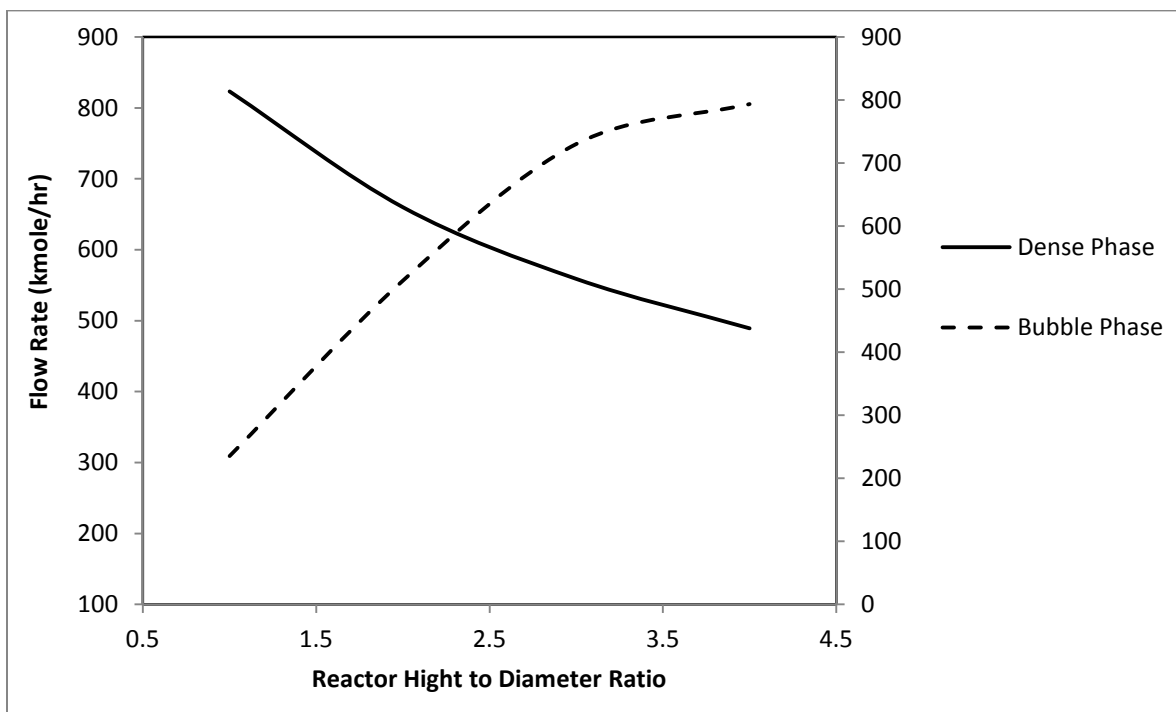


Figure 4.13 Gas Flow in the Bubble and Dense Phases

4.2.5 The Effect of Initial Pressure

Table (4.13) and Figure (4.14) show the effect of the initial pressure on the nitrogen conversion. High value of pressure is needed for breaking the chemical bonds between the reactant atom, it is observed that at low pressure (90 bar) the conversion is 31.2% and it is increases as the pressure increase; the conversion is 44.32% correspond to pressure (150 bar).

Table (4.13) The Effect of Pressure on the Conversion

Reactor Height (m)	N ₂ Conversion %			
	90 bar	110 bar	130 bar	150 bar
0	0	0	0	0
0.5	4.72	6.78	9.32	11.63
1	9.23	12.66	15.12	19.21
1.5	14.23	17.73	20.22	23.83
2	18.62	21.87	24.12	27.73
2.5	21.86	25.79	28.24	31.86
3	25.18	29.48	32.4	35.27
3.5	28.12	32.96	35.932	38.88
4	30.03	35.22	39.28	42.29
4.5	31.2	37.12	41.26	44.32

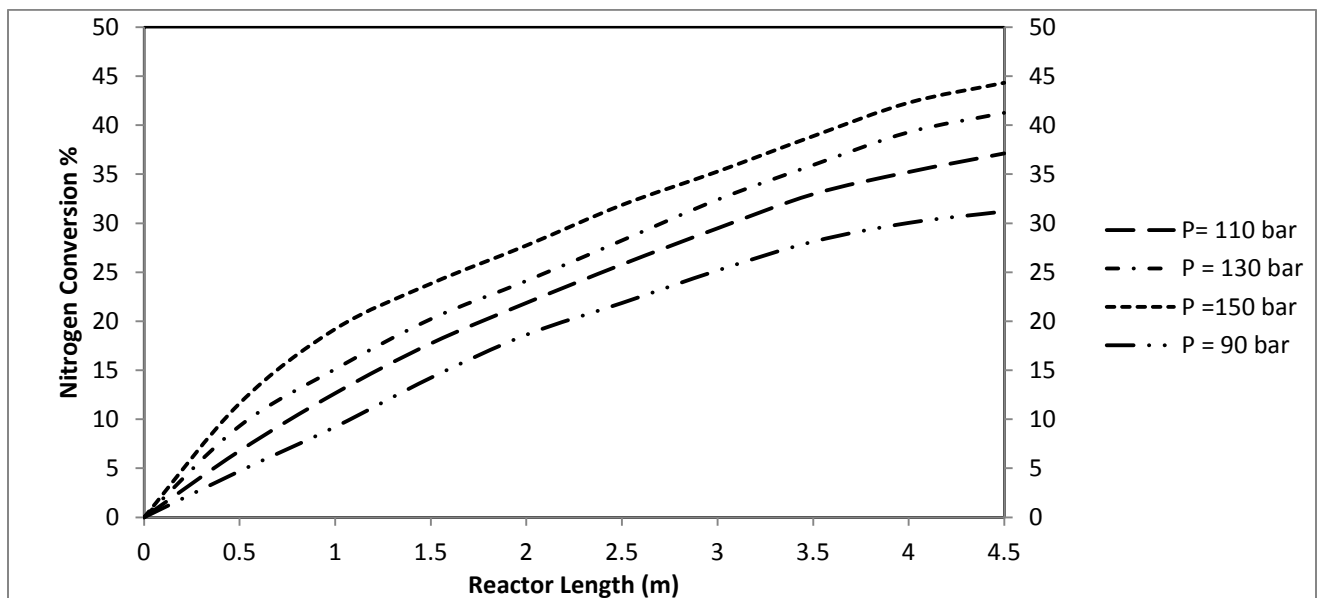


Figure (4.14) The Effect of Pressure on the Conversion

4.3 The Result of Methanol Modeling in Fixed Bed Reactor

The following results are based on the Khark petrochemical methanol unit with the industrial feed conditions and reactor specifications which developed in chapter 3. From the results in the following sections it can be noticed that the behavior of ammonia reaction and methanol reaction are almost same.

To validate this model the temperature and the flow rate of methanol, carbon dioxide, and water at the exit of the reactor are compared with the industrial data.

Table (4.14) Comparison between the Results of the Model and Industrial data

	Industrial Value	Model Calculated Value	Difference %
Exit Temperature (K)	528	524	0.76
Molar Flow Rate (kmol/hr)			
CO ₂	660	705	6.8
CH ₃ OH	900	857	4.8
H ₂ O	713	660	7.4

4.3.1 Conversion of H₂ and CO₂ Along the Reactor

Table (4.15) and figure (4.15) illustrates the change of H₂ and CO₂ along the reactor, the increase of conversion is sharper at the inlet of the reactor compared with the increase at the end of the reactor where the temperature is higher and the reaction is closer to equilibrium.

Table (4.15) Conversion Change Along the Reactor

Reactor Length (m)		0	0.5	1	1.5	2	2.5	3	3.5	4	4.5
Conversion %	CO ₂	0	10.7	18.91	27.61	35.61	40.95	45.12	48.2	49.85	51.08
	H ₂	0	3.38	6.326	8.9	11.12	13.38	15.79	16.93	17.64	17.8

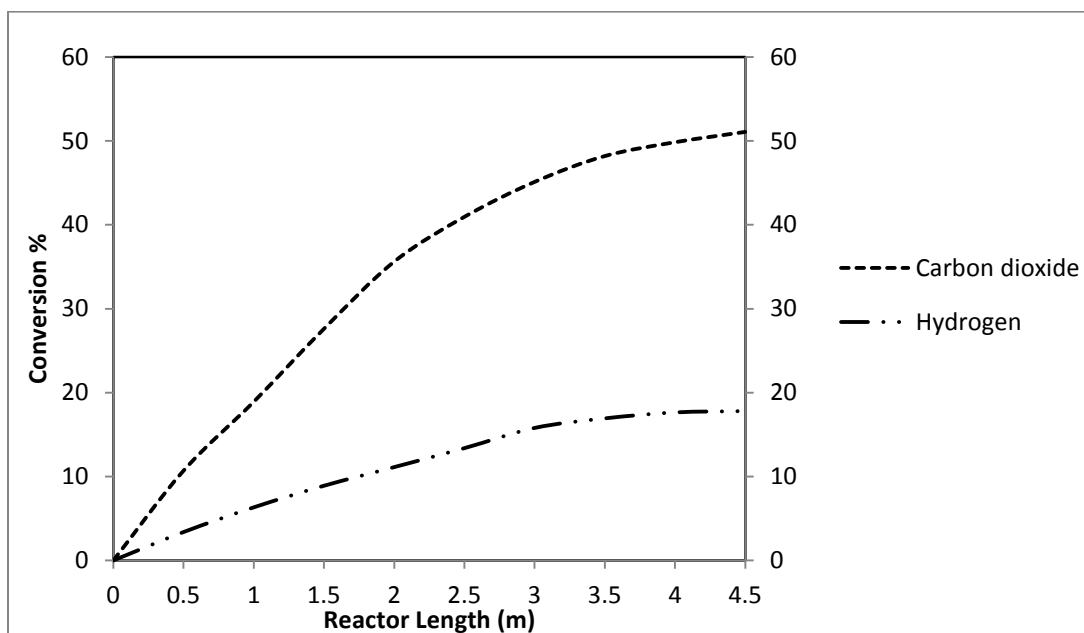


Figure (4.15) conversion change along the reactor

4.3.2 Molar Flow of the Components Along the Beds

The molar flow rate of the main components is illustrated in Figure (4.15) and Table (4.16). It can be easily obtained from the initial flow rate and the conversion calculated in the above section.

Table (4.16) Molar Flow Rate Along the Reactor

Reactor Length (m)	Flow Rate (kmol/hr)		
	CO ₂	CH ₃ OH	H ₂ O
0	1398.3	142.2	0
0.5	1270	270	128
1	1148	382	240
1.5	1011	479	337
2	926	584	422
2.5	840	687	496
3	790	769	580
3.5	740	811	641
4	715	841	654
4.5	705	857	660

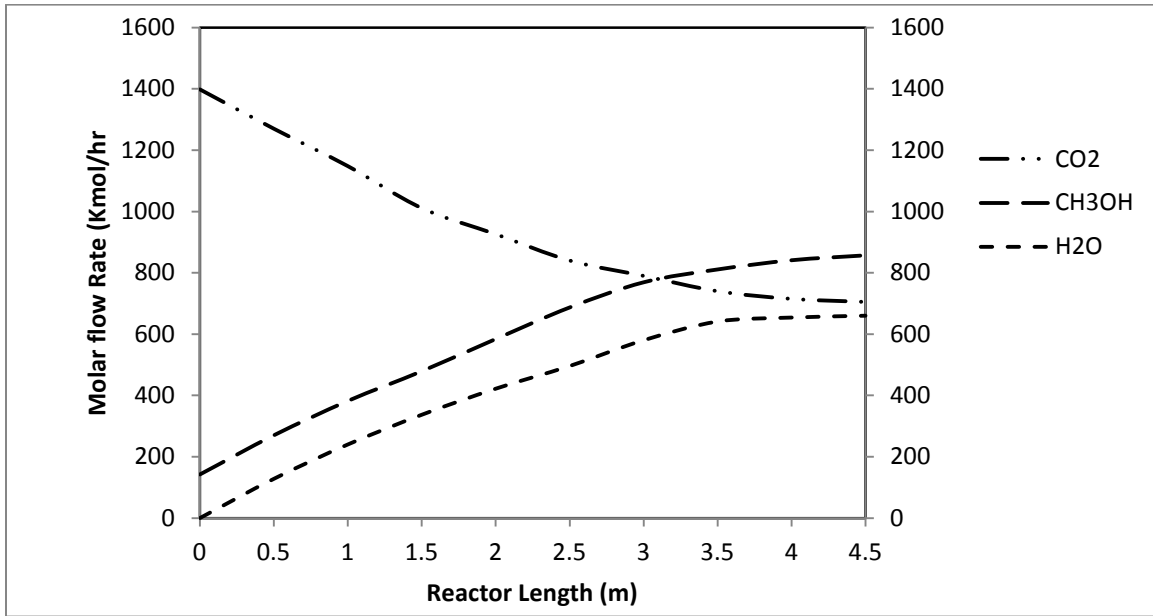


Figure (4.16) Molar Flow Rate Along the Reactor

4.3.3 Temperature Change Along the Reactor

Figure (4.17) and Table (4.17) illustrate the temperature changes along the reactor. At the inlet, as the methanol concentration is low, the reaction rate is very high and the temperature increases while approaching equilibrium at its end of the reactor.

Table (4.7) Temperature Change Along Beds

Reactor Length (m)	Temperature (K)
0	498
0.5	510
1.0	515
1.5	517
2.0	519
2.5	521
3.0	522
3.5	523
4.0	524
4.5	524

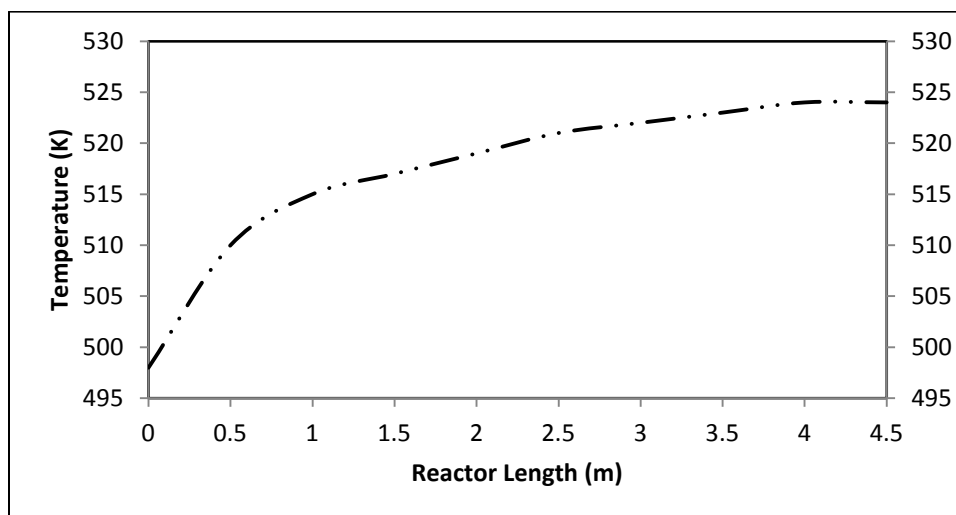


Figure (4.17) Temperature Change Along the Reactor

4.3.4 Effect of Changes in the Feed Pressure

Different values of pressure were applied to the model which results in a high methanol flow rate for high pressure value, however the limitations of applying high pressure which discussed in section 4.1.4 must be considered. Table (4.18) and Figure (4.18) show the flow rate of methanol according to different values of pressure.

Table (4.18) Methanol Flow Rate for Different Values of Pressure

Reactor Length (m)	CH ₃ OH Flow Rate (Kmol/hr)			
	90 bar	110 bar	130 bar	150 bar
0	198	198	198	198
0.5	229	247	265	282
1	308	336	372	398
1.5	380	424	460	506
2	456	505	559	610
2.5	536	586	651	698
3	610	670	727	773
3.5	665	730	791	843
4	687	760	823	878
4.5	699	774	838	893

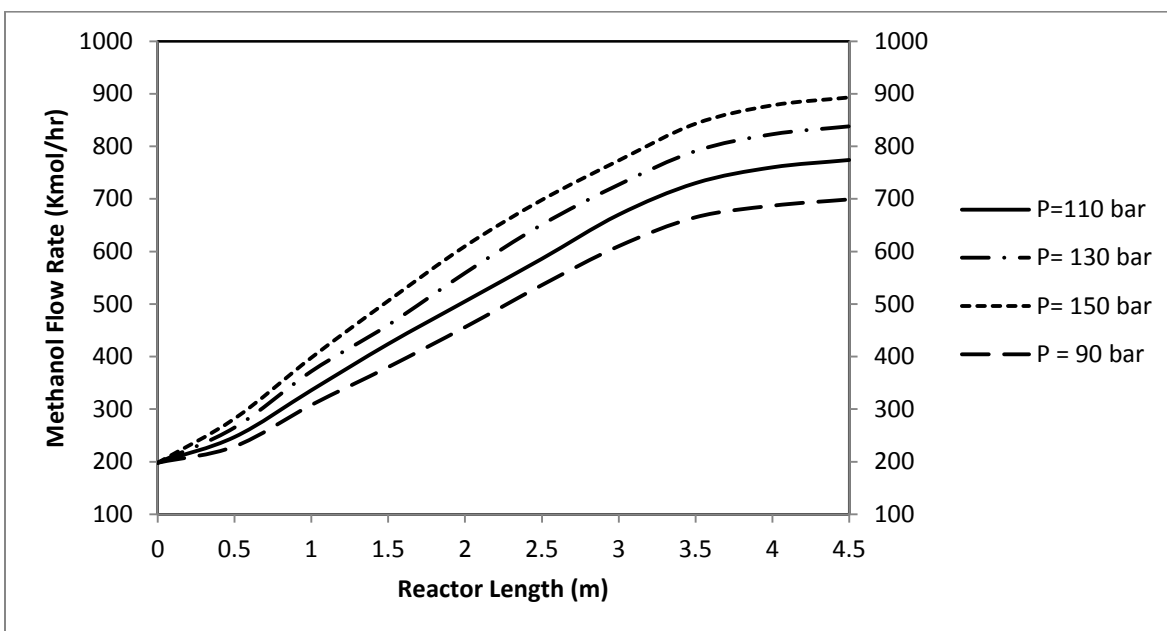


Table (4.18) Methanol Flow Rate For Different Values of Pressure

4.3.5 Effect of Inlet Temperature

The effect of the inlet gas temperature is tested based on the model and the results are shown in Figures (4.19), (4.20) and Table (4.19).

At lower inlet temperature, the reaction is kinetically limited, while at higher temperature the thermodynamic equilibrium set the upper limits for the exit methanol flow rate.

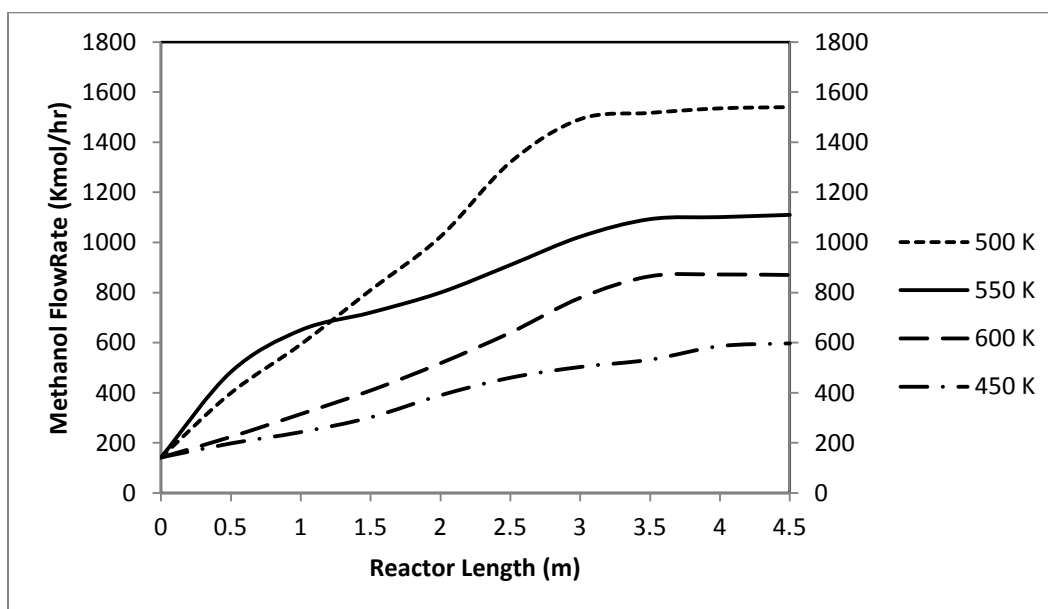


Figure (4.19) The Effect of the Inlet Temperature on The Methanol Flow Rate

Table (4.19) The Effect of the Inlet Temperature on the Methanol Flow Rate

Reactor Length (m)	CH ₃ OH Flow Rate (kmol/hr)			
	450 K	500 K	550 K	600 K
0	142	142	142	142
0.5	198	399	483	224
1	243	593	650	315
1.5	302	810	720	409
2	390	1023	800	518
2.5	460	1320	910	640
3	503	1492	1023	779
3.5	532	1517	1093	865
4	586	1535	1101	872
4.5	597	1540	1110	870

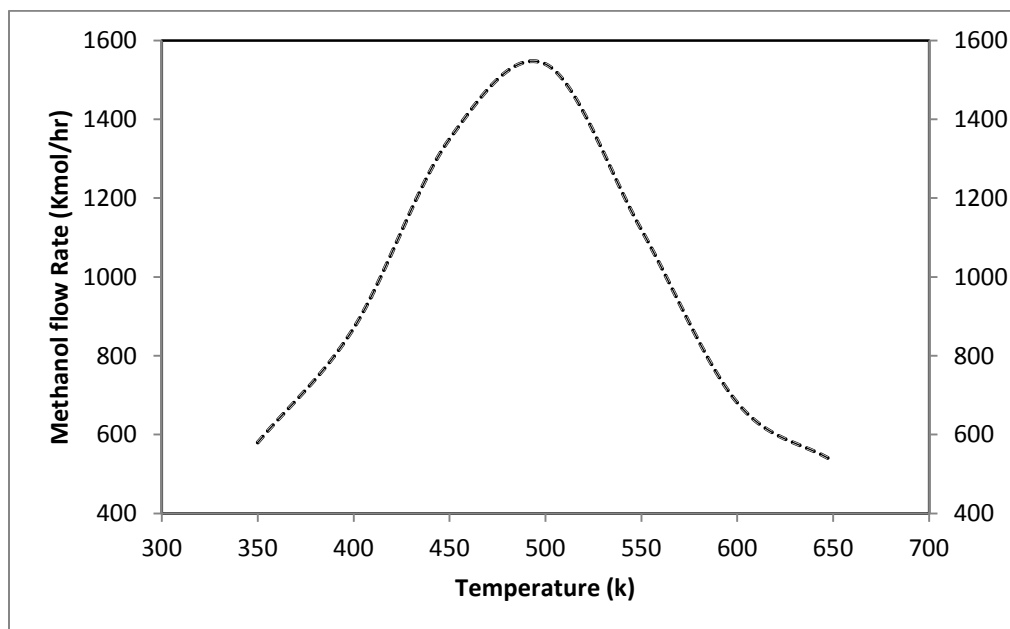


Figure (4.20) Methanol Flow Rate for Different Values of Temperature

4.3.6 The Effect of H₂ to CO₂

Figure (4.21) shows the results of the model for variation of $\left(\frac{H_2}{CO_2}\right)$ in the feed on molar flow rate of methanol. it can be seen from Figure (4.21) that with increase of $\left(\frac{H_2}{CO_2}\right)$ in the feed, molar flow rate of methanol increases at first with sharp slope and finally in the ratio of 3 is maximum then decrease. According to the reaction stoichiometric, it can be observed that the modeling results are consistent with reaction stoichiometric so that the maximum production of methanol in the ratio 3 to 1 of $\left(\frac{H_2}{CO_2}\right)$. Because the reaction is an equilibrium reaction, higher feed concentration goes to the product but it should be noticed that high concentration of H₂ (high molar ratio of $\frac{H_2}{CO_2}$) can reduce CO₂ and subsequently methanol production decrease. In addition, side reaction also takes place. Therefore if $\frac{H_2}{CO_2}$ ratio in synthesis gas was 3, methanol production will be maximum.

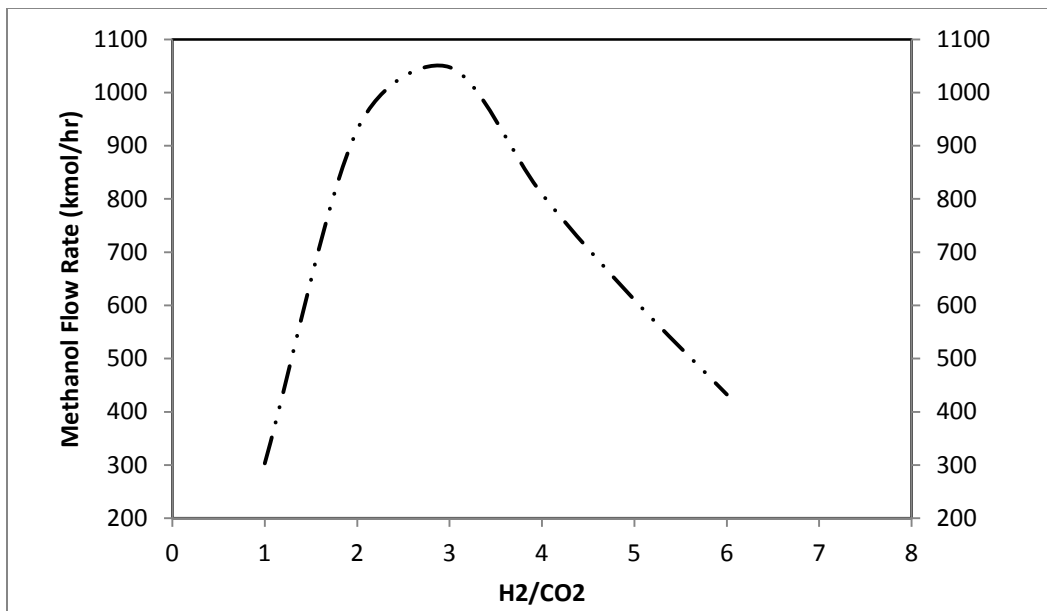


Figure (4.21) CH₃OH flow Rate Against $\frac{H_2}{CO_2}$ Ratio

4.4 The Result of Methanol Modeling in Fluidized Bed Reactor

A two phase model of fluidized bed reactor has been generated for methanol convertor in chapter 3. Figure (4.22) together with Table (4.20) show the flow rate of the main component in the reaction, it will be noticed that the production of methanol is increase by 30% for the same conditions.

Table (4.20) the flow rate of methanol synthesis components along the reactor

Reactor Height (m)	Flow Rate (kmol/hr)		
	CO ₂	CH ₃ OH	H ₂ O
0	1398.3	142.2	0
0.5	1243.2	412.7	243.7
1	1110.4	627.8	419
1.5	952.5	789.9	587.8
2	830.4	897.63	722.5
2.5	678.7	965.4	825.8
3	547	1021.13	900.3
3.5	402.1	1060.21	945.14
4	345	1093.89	968.1
4.5	302.3	1114.1	987.9

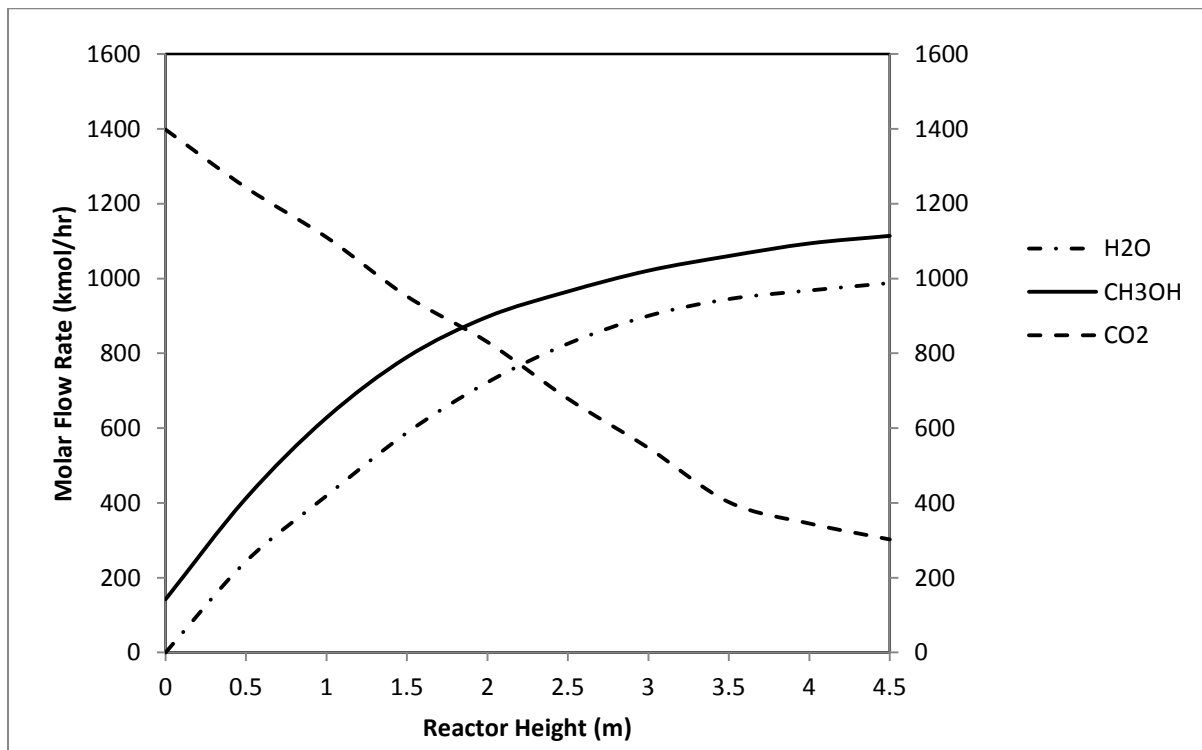


Figure (4.22) Methanol Flow Rate Along Fluidized Bed Reactor

4.4.1 Conversion of CO₂ and H₂ Along the Reactor

The conversion is also improved from the fixed bed; the conversion of carbon dioxide at the exit of the fluidized bed is 75% against 51% for the fixed bed.

Table (4.21) The Change of Conversion Along the Reactor

Reactor Height (m)	Conversion %	
	H ₂	CO ₂
0	0	0
0.5	6.2	15.9
1	10.8	26.7
1.5	15.1	34.98
2	17.47	43.07
2.5	19.1	51.8
3	20.64	59.7
3.5	22.09	67.8
4	23.68	73.3
4.5	25.4	75.1

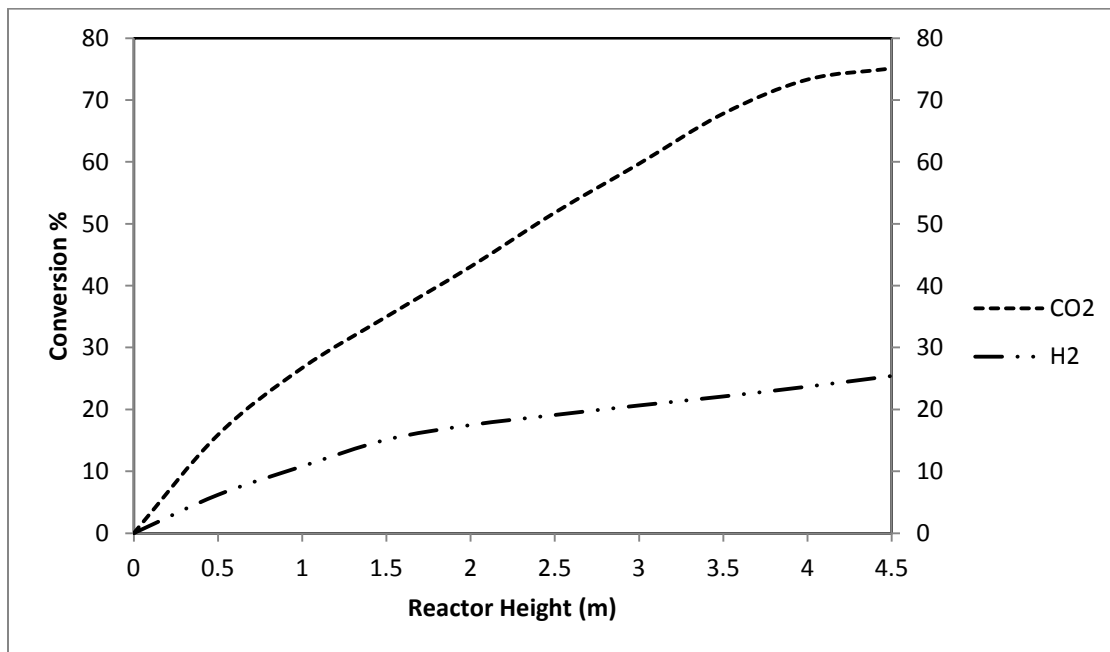


Figure (4.23) The Change of Conversion Along the Reactor

4.4.2 The Effect of Catalyst Particle Size on the Conversion

As discussed in section 4.2.2; the smaller sizes of particles in fluidized beds eliminate pore diffusion limitations associated with the use of larger particles and hence contribute in increasing the methanol production, Figure (4.24) and Table (4.22) show the flow rate of methanol for different particle size.

Table (4.22) Effect of Particle Size on the Methanol Production

Reactor Height (m)	CH ₃ OH Flow Rate (kmol/hr)			
	Dp= 5mm	Dp= 1mm	Dp= 0.5mm	Dp= 0.05mm
0	142.2	142.2	142.2	142.2
0.5	152.2	179.2	250.2	362.2
1	210.9	300.8	390.02	512.7
1.5	295.7	505.32	592.6	711.8
2	412.8	650.02	749.3	875.9
2.5	535.8	785.2	862.9	980.63
3	634.12	879.86	959.6	1050.4
3.5	704.97	925.8	1005.98	1100.13
4	750.7	970.56	1049.67	1140.21
4.5	784.3	995.3	1069.98	1173.89

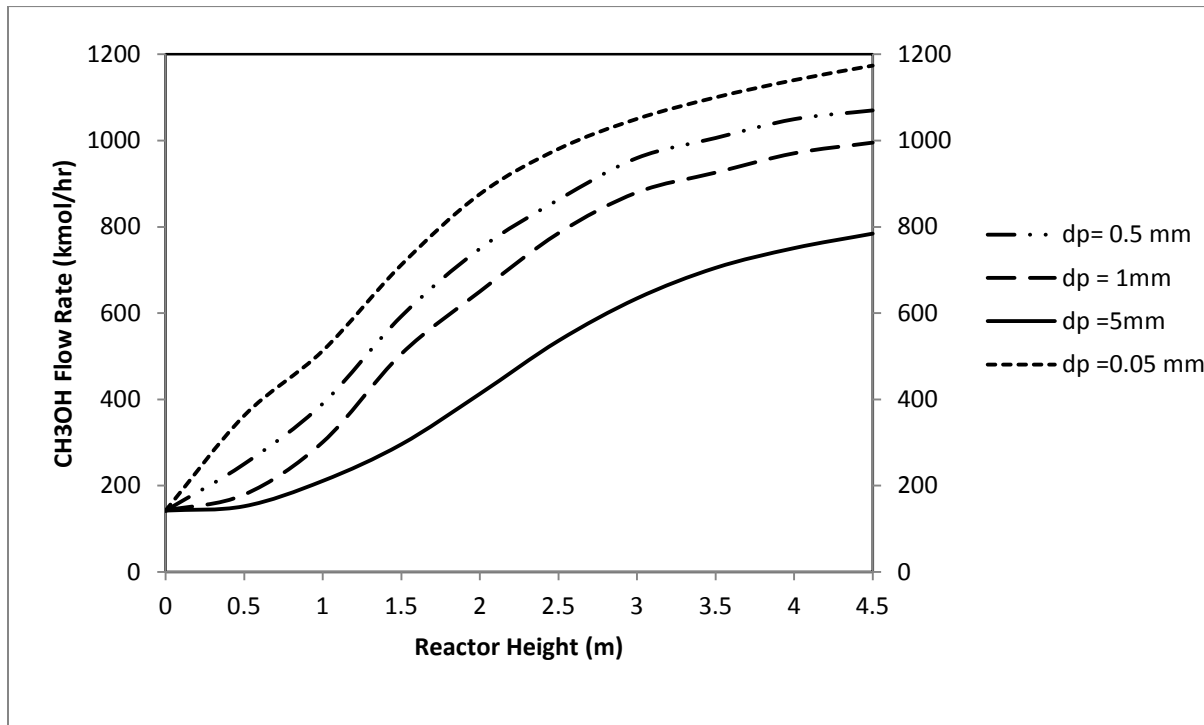


Figure (4.24) Effect of Particle Size on the Methanol Production

4.4.3 Effect of Mass Transfer Between the Bubble and Dense Phases

Mass transfer between phases improves the methanol production flow rate for the reasons discussed in ammonia synthesis in fluidized bed. Table (4.23) and Figure (4.25) show that there is 40% increase in methanol flow rate with mass transfer between phases.

Table (4.23) The Effect of Mass Transfer on Methanol Production

Reactor Height (m)	CH ₃ OH Flow Rate (kmol/hr)	
	(kbd) _i =0	(k bd) _i ≠0
0	142.2	142.2
0.5	212.7	412.7
1	327.8	627.8
1.5	439.9	789.9
2	547.63	897.63
2.5	645.4	965.4
3	721.13	1021.13
3.5	760.21	1060.21
4	773.89	1093.89
4.5	794.1	1114.1

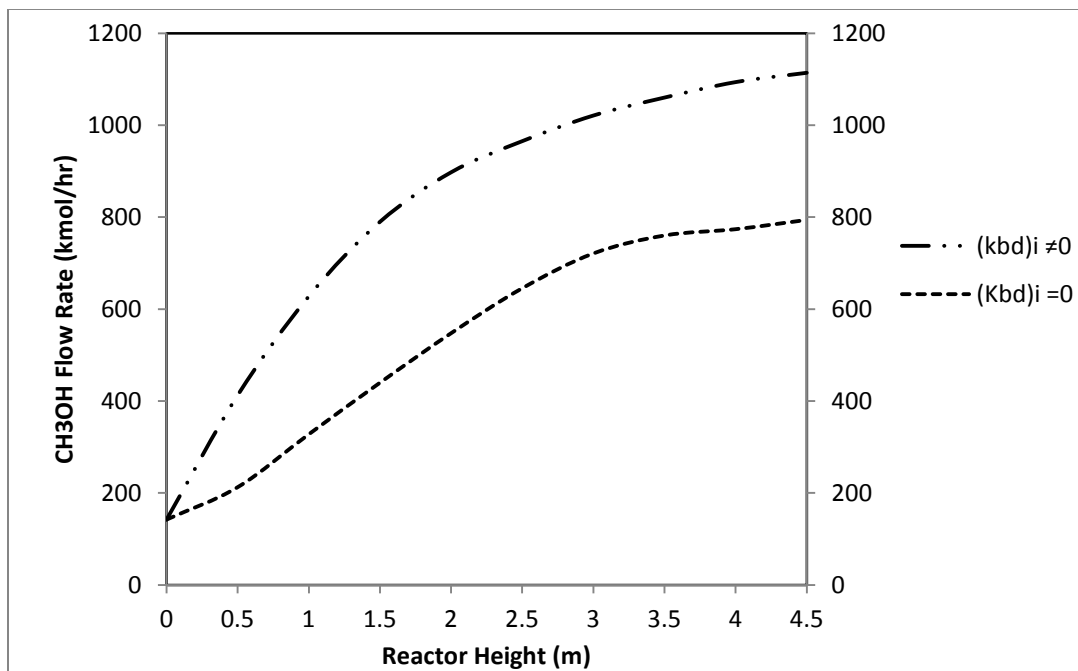


Figure (4.25) The Effect of Mass Transfer on Methanol Production

4.4.4 The Effect of Bed Height to Diameter

The effect of the reactor dimensions is illustrated in Table (4.24) and Figure (4.26) below, as discussed in ammonia fluidized bed the dense phase flow rate is decrease with the increase of L/D ratio while the bubble phase increase which reduce the rate of reaction and hence the methanol production.

Table (4.24) The Effect of Height to Diameter Ratio on Methanol Production.

L/D	Flow Rate (kmol/hr)		
	Dense Phase	Bubble Phase	CH ₃ OH
1	33180	14220	1219.8
2	24885	22898.8	974.7
3	19908	29768.44	857.9
4	17319.96	34256.86	763.48

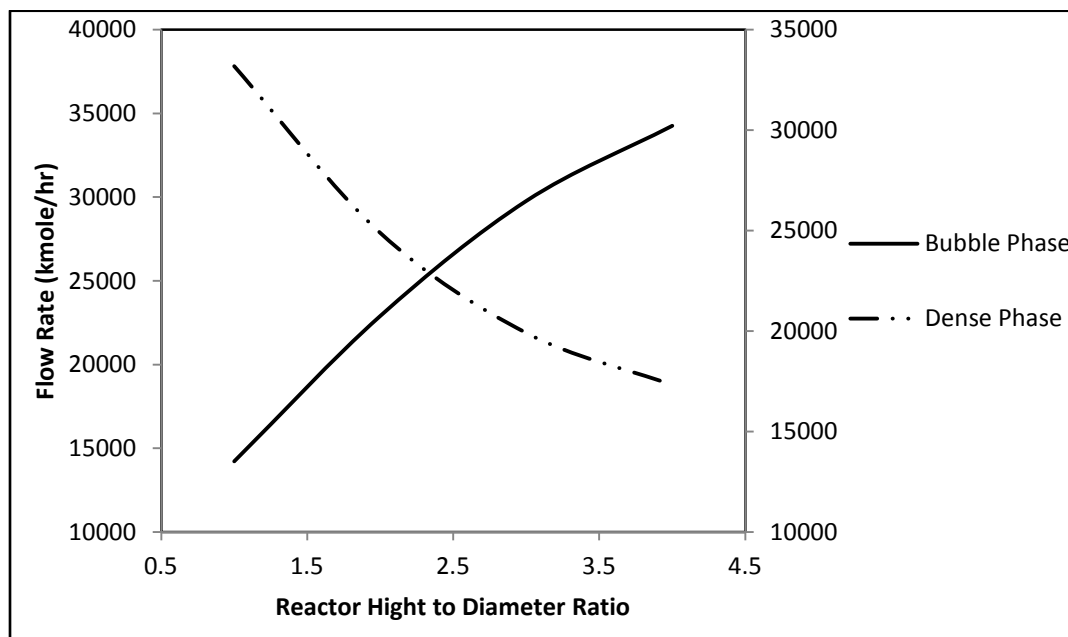


Figure (4.26) The Effect of Height to Diameter Ratio on Phases Flow Rate.

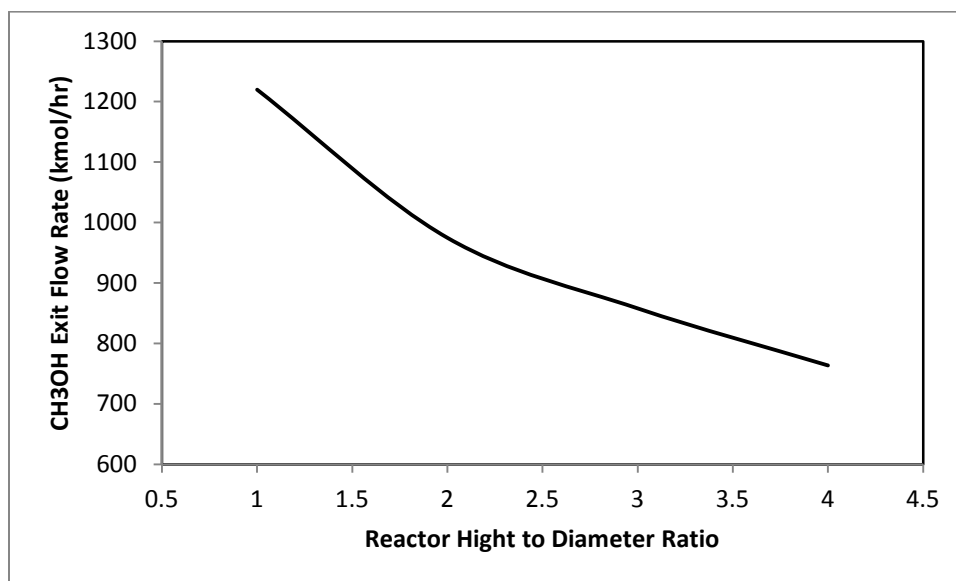


Figure (4.27) The Effect of Height to Diameter Ratio on Methanol Production.

4.4.5 The Effect of Initial Pressure

The flow rate of methanol is tested for different values of initial gas pressure Table (4.25) and Figure (4.28) show that the production is improved by increasing the pressure.

Table (4.25) The Effect of Initial Pressure on Methanol Production

Reactor Height (m)	Methanol Flow Rate (kmol/hr)			
	P= 90 bar	P= 110 bar	P= 130 bar	P= 150 bar
0	142	142	142	142
0.5	536.51	616.9865	678.6852	737.0521
1	816.14	938.561	1032.417	1121.205
1.5	1026.87	1180.901	1298.991	1410.704
2	1166.919	1341.957	1476.153	1603.102
2.5	1255.02	1443.273	1587.6	1724.134
3	1327.469	1526.589	1679.248	1823.664
3.5	1378.273	1585.014	1743.515	1893.458
4	1422.057	1635.366	1798.902	1953.608
4.5	1448.33	1665.58	1832.137	1989.701

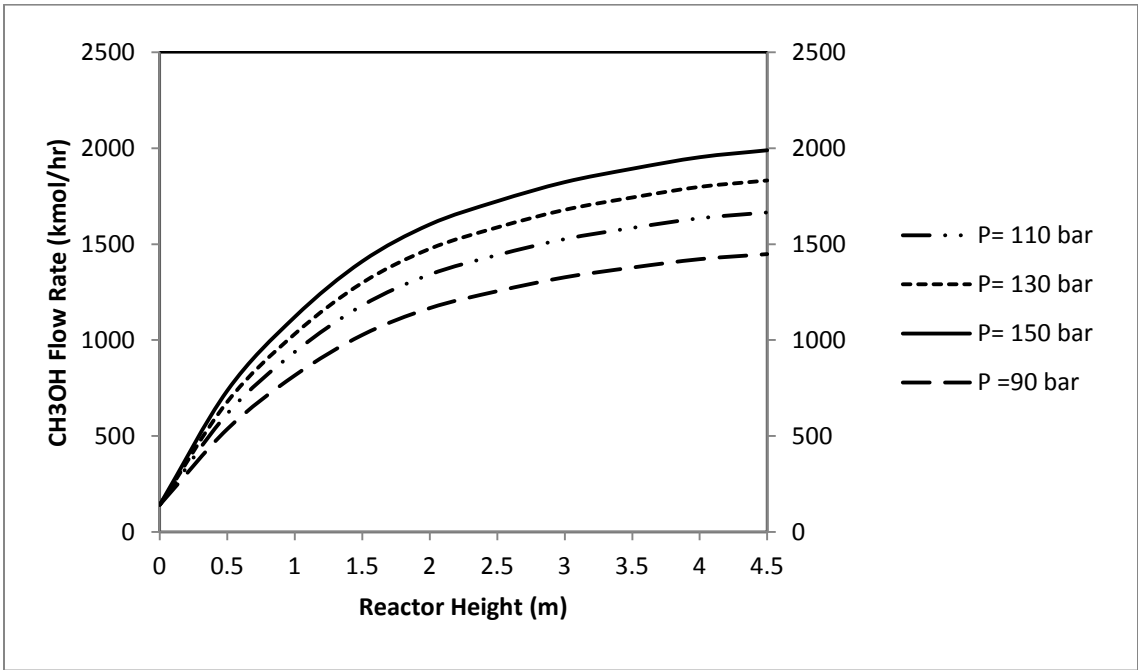


Figure (4.28) The Effect of Initial Pressure on Methanol Flow Rate

CHAPTER FIVE

SIMULATION OF PROCESSES

5.1 Introduction

Simulation of chemical processes involving non ideal reactors is essential for process design, optimization. Control and scale up. Various industrial process simulation programs such as ASPEN PLUS, HYSYS, and CHEMCAD are available for chemical process simulation. Most of these programs are being developed based on the sequential modular approach. They contain only standard ideal reactors but provide no modular for non ideal reactors such as fluidized bed and fixed bed reactors.

In this chapter the processes modeled in chapter three are simulated using HYSYS according to the configuration of the reactor and the results of the simulation are compared to the industrial and model results.

5.2 Simulation of Ammonia Synthesis in Kellogg Reactor

The Kellogg synthesis reactor as described in chapter three with three beds. To control the temperature between first and second beds, Quench gas is used to control the inlet temperature of the second bed. The simulation of this process is illustrated in Figure (5.1) the first bed is simulated as plug flow reactor with the length of the fist bed and the diameter of the reactor and void fraction less than one accenting for the presence of the catalyst, then the properties of the used catalyst are insert and the rate of the reaction is also inserted. The outlet of the first bed is cooled by adding the quench gas in mixture. The second and third bed are considered as one plug flow reactor with the length of two beds, since there is no operation between them.

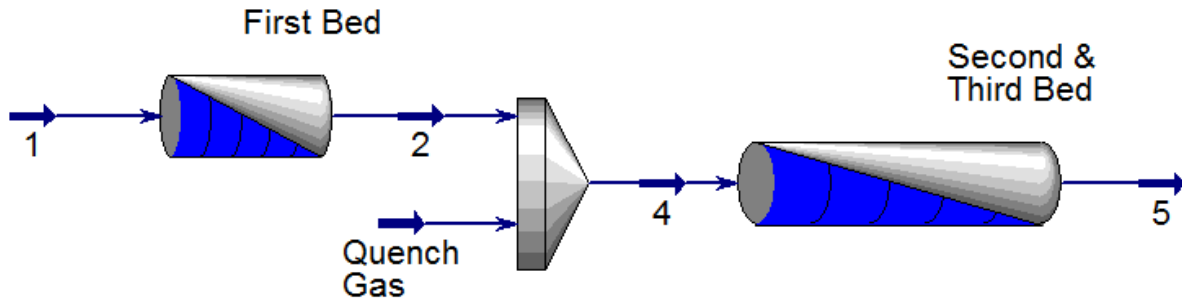


Figure (5.1) Simulation of Kellogg Ammonia Converter

Figures (5.2) through (5.5) represent the result obtained from this simulation which is not far from the industrial and the model results.

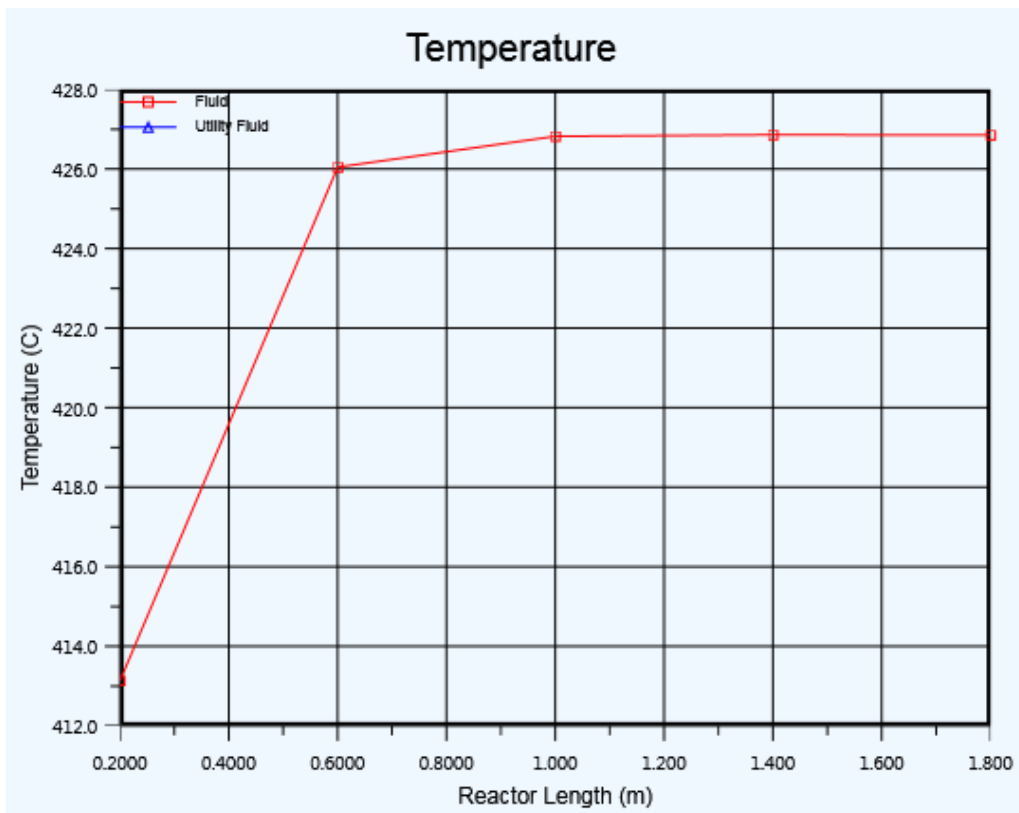


Figure (5.2) Temperature Change Along the First Bed

Figures (5.2) and (5.3) illustrate the temperature profile in the first bed the temperature is increases with the reaction which tends to approach equilibrium at the end of the bed with temperature 430° C, the effluent of the first bed is cooled by adding the quench gas, then the inlet temperature to the second bed is about 300 °C.

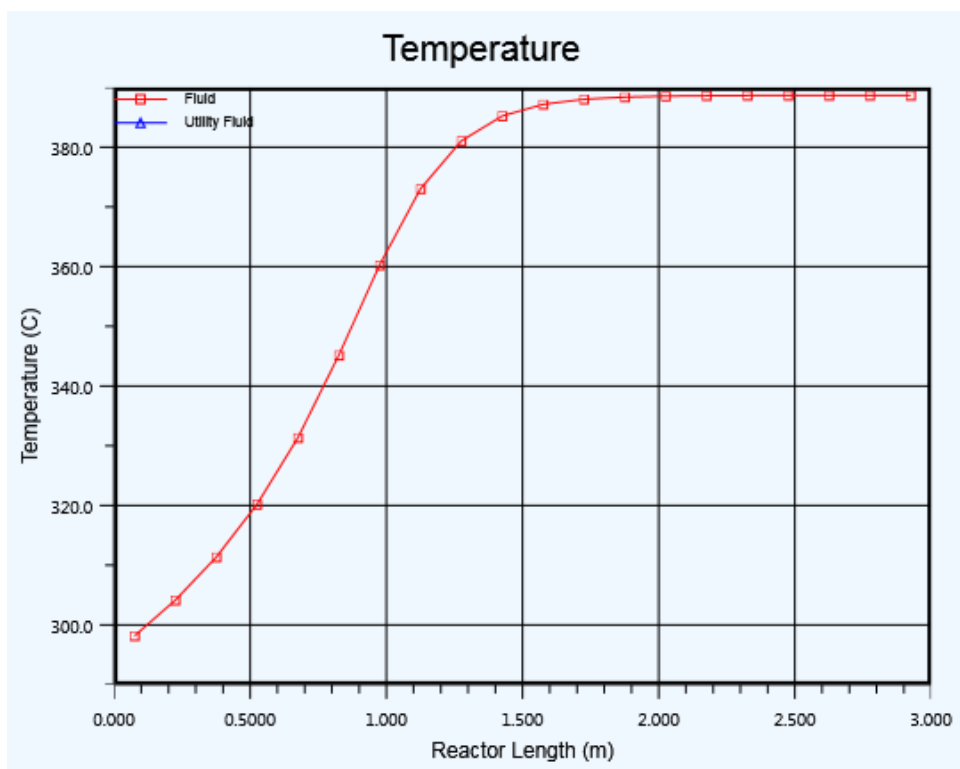


Figure (5.3) Temperature change along the second and third beds

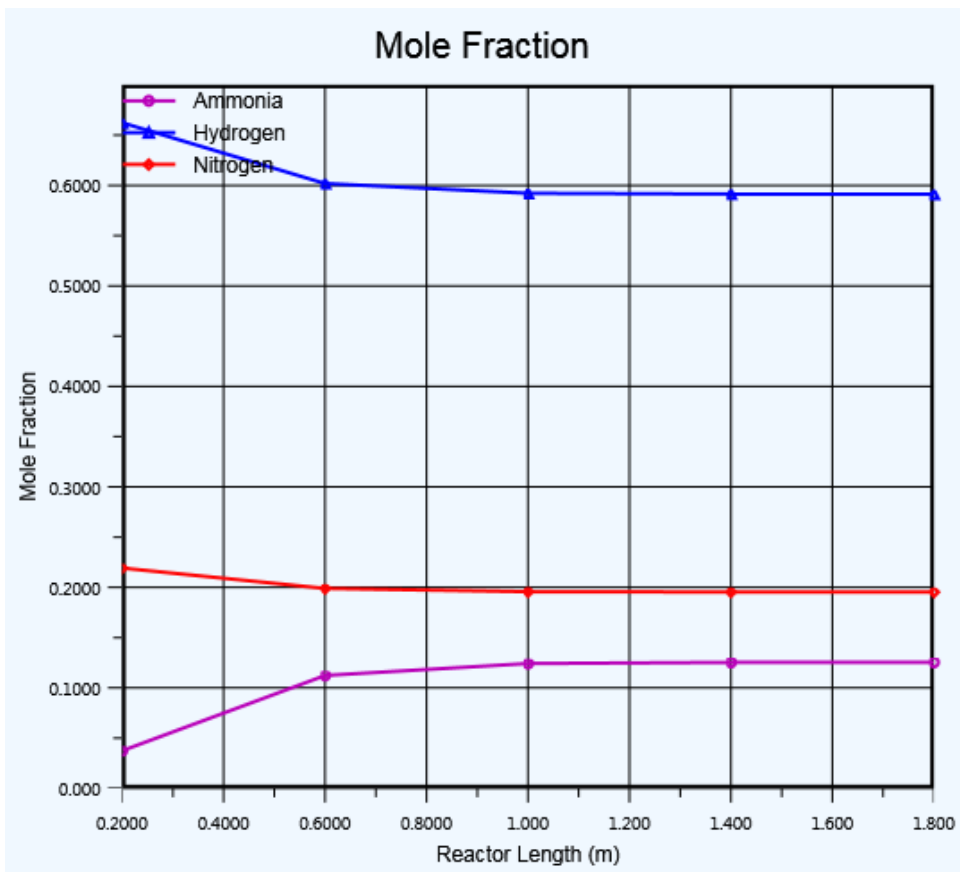


Figure (5.4) Components Mole Fraction Along the First Bed

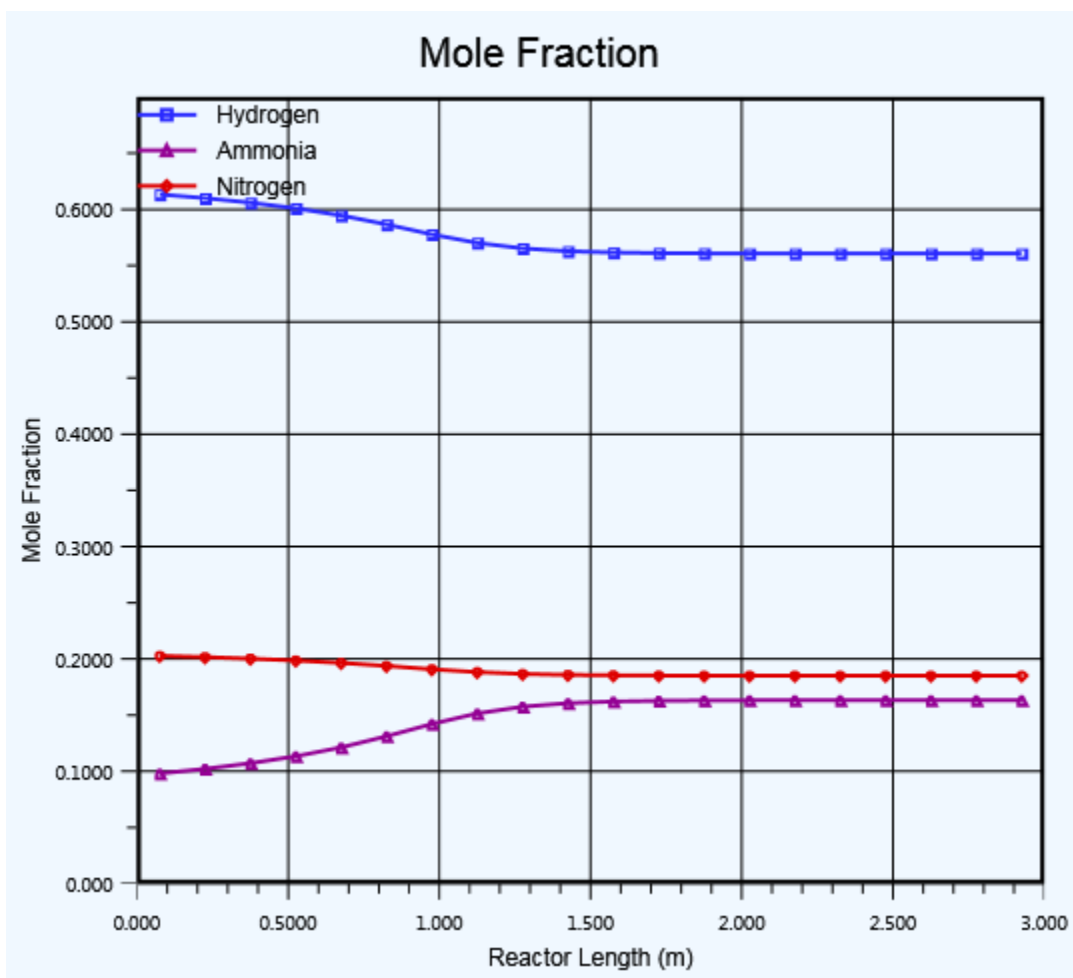


Figure (5.5) Components Mole Fraction Along the Second and Third Beds

Table (5.1) Comparison Between the Industrial, Model and Simulation Values

	Industrial Fixed bed			Model Values			Simulation		
	Bed1	Bed2	Bed3	Bed1	Bed2	Bed3	Bed1	Bed2	Bed3
Exit Temperature (K)	780	775	728	801	712	748	703	673	698
Conversion %	15.78	25.55	28.91	15.2	24.8	26.79	14.4	23.16	26.03

5.3 Simulation of Methanol Synthesis in Khark Reactor

The Khark methanol reactor as described in chapter three is a tubular reactor with ten tubes containing the catalyst. The reacting gas moves through the tubes while the shell contains water to cool the reactor and produce steam. Figure (5.6) represent the simulation of this reactor, a plug flow reactor with the length and the diameter of the reactor and void fraction less than one accounting for the presence of the tubes and catalyst.

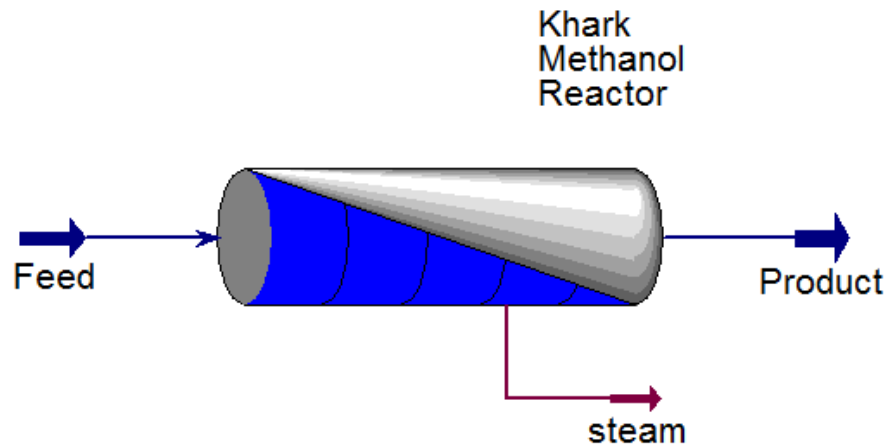


Figure (5.6) Simulation of Methanol Khark Reactor

The temperature profile of methanol synthesis is illustrated in Figure (5.7). Because the reaction is exothermic reaction the temperature is increase with the progress of the reaction as noticed in Figure (5.7), at the end of the reactor the reaction approach equilibrium and there will be no more reaction and hence temperature, the temperature at the reactor outlet is about 251°C.

Figure (5.8) represents the molar flow profile for the main components in the reactor; methanol, carbon dioxide and water, the figure is also shows the thermodynamics limitation at the end of the reactor.

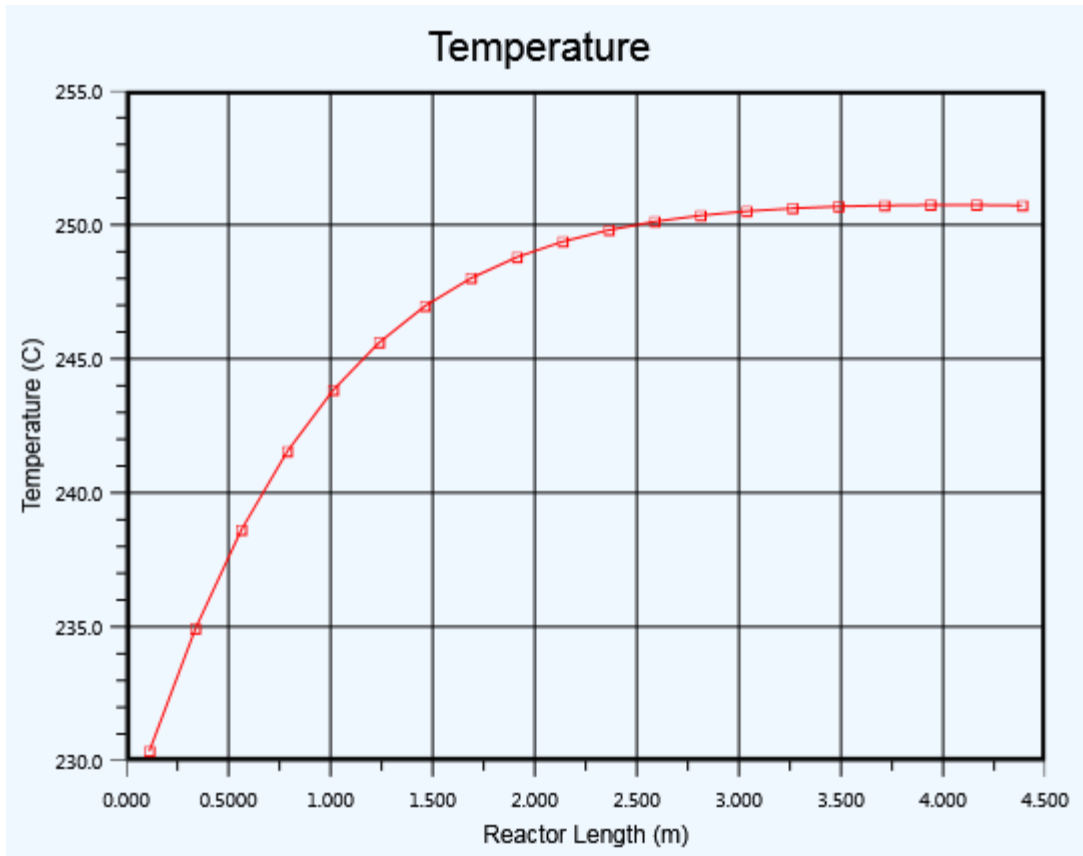


Figure (5.7) Temperature Change Along the Khark Methanol Reactor

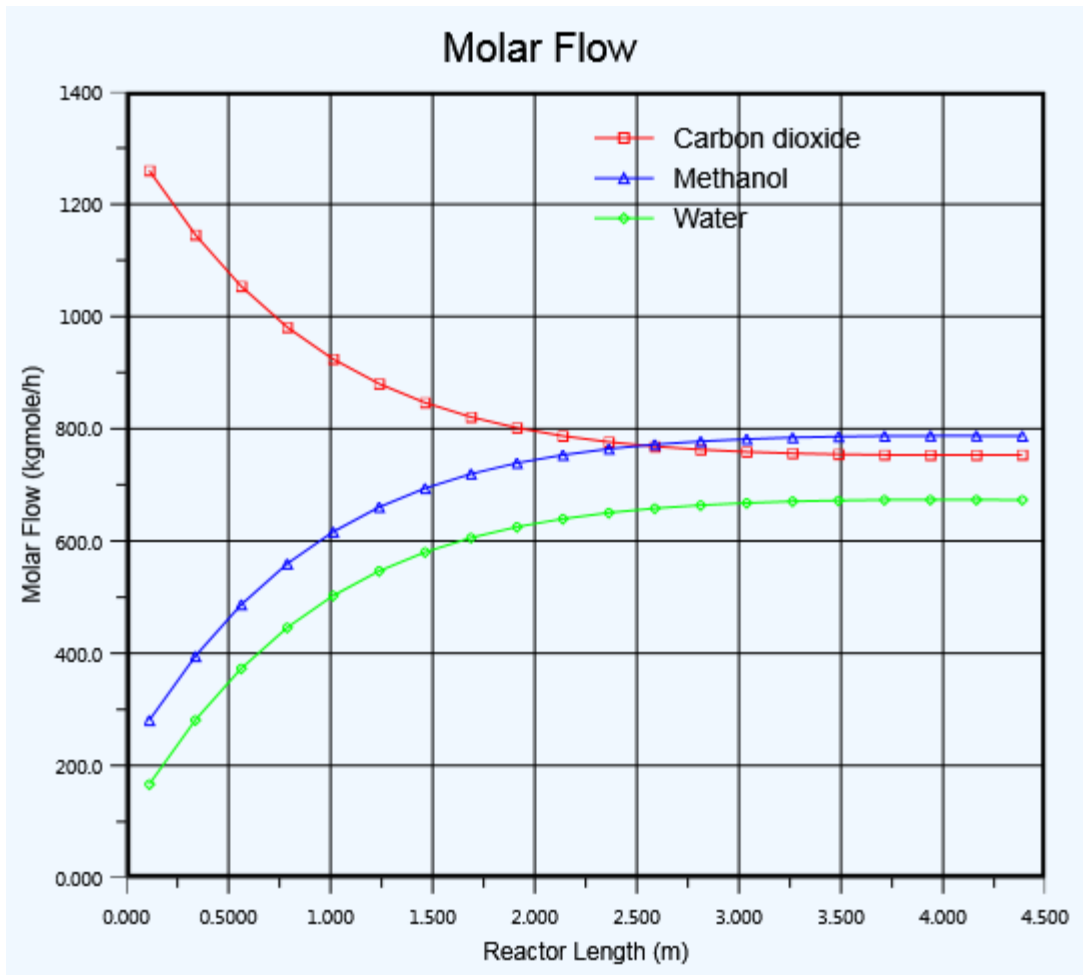


Figure (5.8) Components Molar Flow Rate Along the Reactor

Table (5.2) Comparison Between the Industrial, Model and Simulation Values

	Industrial Value	Model Calculated Value	Simulation
Exit Temperature (K)	528	524	524
Molar Flow Rate (kmol/hr)			
CO ₂	620	705	730
CH ₃ OH	900	857	790
H ₂ O	713	660	630

5.4 Simulation of Ammonia and Methanol Synthesis in Fluidized Bed Reactor

The problem with fluidized bed reactors is that they do not correspond to any of the easily-modeled ideal reactors. While most of the gas flows upward through the suspended particles, some passes through in bubbles with scant contact with any catalyst particles. In addition, there is generally some circulation and turbulent back-mixing. Since process simulators are not set up to model this.

A fluidized bed reactor may be simulated as a plug flow reactor with a non-reacting bypass stream to account for bubbles and circulation.

A tee is used to split the inlet flow into two streams the first is the dense phase flow which is further inter the reactor and contact catalyst, the second stream is the bubble flow which will not react the outlet from the first reactor is also spitted using a tee to account for the mass transfer between the bubble and dense phases, a mixer is used at the of the process to mix the bubble and dense phase to form the output of the reactor.

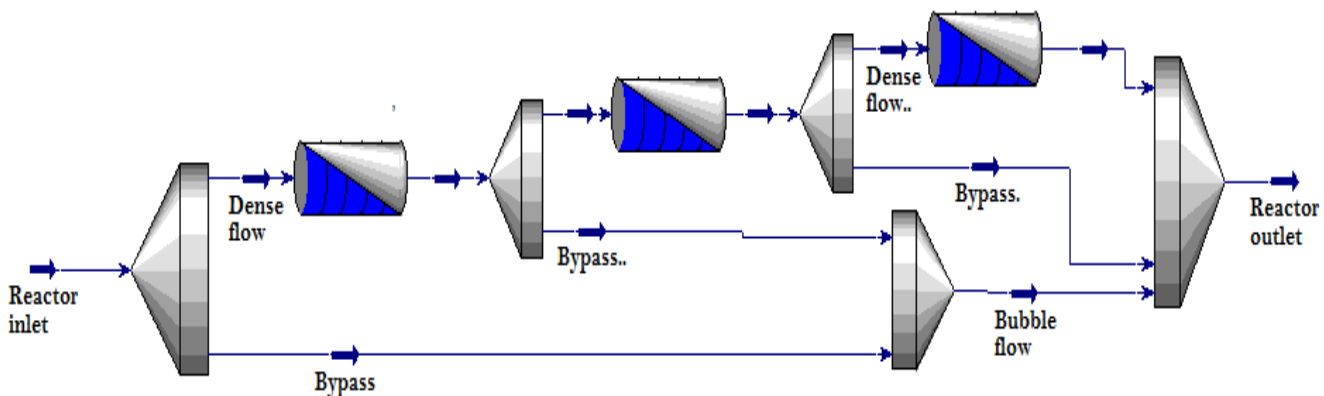


Figure (5.8) Simulation of fluidized bed reactor in HYSYS

Table (5.3) comparison between the model and simulation values of ammonia synthesis in fluidized bed reactor

		Model Values			Simulation		
		1.5 m	3 m	4.5 m	1.5 m	3 m	4.5 m
Exit Temperature (K)		523	561	578	581	602	645
Molar Fraction %	H ₂	68.31	62.55	57.1	75.02	70.7	62.9
	N ₂	22.7	20.7	18.9	23.14	22.98	20.14
	NH ₃	8.05	15.66	22.9	10.03	17.22	24.28

Table (5.4) comparison between the model and simulation values of methanol synthesis in fluidized bed reactor

		Model Values			Simulation		
		1.5 m	3 m	4.5 m	1.5 m	3 m	4.5 m
Exit Temperature (K)		517	522	524	534	562	570
Molar Flow Rate (kmol/hr)	CH ₃ OH	789.9	1021.13	1114.1	817	1103	1189
	CO ₂	952.5	547	302.3	905	512	287
	H ₂ O	587.8	900.3	987.9	610	954	1017

CHAPTER SIX

Conclusions and Recommendations

6.1 Conclusions

In this research, a mathematical model of the fixed bed reactor was developed in the ammonia and methanol industry. The reliability of the models was verified by comparing them with the industrial data. The results obtained from the models were deviated by an acceptable error

The effect of operating factors on the ratio of conversion was tested, including pressure, temperature, flow rate, ammonia ratio in feed, and the optimum values of these factors were proposed.

In another part of the research, models for the ammonia and methanol industry were proposed in fluidized reactors. Comparing their results with the results of the fixed bed reactors considering the same inputs of the flow rate, reactor dimensions, temperature and pressure, it was found that the production of ammonia and methanol in fluidized bed reactors is far higher than their production in fixed bed reactors

In the production of ammonia in the fixed bed reactors, the nitrogen conversion was 26.76% while in the fluidized bed reactors, the conversion increased to 40.26% at the end of the reactor, which reflected positively on the amount of ammonia produced.

The effect of some factors on the performance of the reactor, such as pressure and temperature, the particle size and the ratio of the reactor diameter to high were also investigated. The most important factor affecting the production is the mass transfer between dense and bubble phase. In the presence of mass transfer the conversion of nitrogen was 40.26%. However in the hypothetical case of the absence of mass transfer the conversion declines to 31.36%.

In the production of methanol, the production rate in the fixed bed reactor was 857 kmol /h, while its production in the fluidized bed reactor reached 1114. kmol /h at an increase of 30%.

All the tests conducted in the ammonia industry have been applied to the methanol industry and to determine the optimal values for them

Finally, the four processes were simulated using the HYSYS simulation program and the results were very close to the results of the models.

It can be concluded that the production of ammonia and methanol in fluidized bed reactors yields higher production rates than fixed bed reactors.

6.2 Recommendations

The following recommendations are made for possible future study.

- Study of systems and apply temperature and pressure control system
- Find alternative methods for simulating the fluidized bed reactors in HYSYS and other simulation programs
- Develop two dimensional models for ammonia and methanol in fixed bed reactor and compare its results with the fluidized bed reactors.
- Investigation of the insertion of distributors in fluidized bed reactor.
- Incorporate a simulation package for fluidized bed reactor in HYSYS
- Design and construct a pilot fluidized bed reactor, and compare its results with the results of the mathematical model.

1. MATLAB code for ammonia synthesis in fixed bed reactor

```
Editor - C:\MATLAB7\work\fix.m
File Edit Text Cell Tools Debug Desktop Window Help
[Icons] Stack: Base
1 function y=fix(x)
2 - yH2=0.6303;
3 - yN2=0.2219;
4 - yNH3=0.00276;
5 - ycH4=0.00546;
6 - yAr=0.00256;
7 - P=136.5
8 - NF=2700.19
9 - v=L.A;
10 - j=0.55;
11 - E2=163500;
12 - K20=10^14.7102;
13 %K2=x(5) Ka=x(6) qH2=x(7) qN2=x(8) qNH3=x(9) fH2=x(10) fN2=x(11)
14 %fNH3=x(12) rNH3=x(13)
15 - x(5)=K20*exp(-E2/r.x(15));
16 x(6)=10^(-2.69112*log10(x(4))-0.00005519265*x(4)+.0000001848863*x(4)^2
17 +2001.6/x(15)+2.6899);
18 x(7)=exp(exp(-3.8402*x(4)^0.125+0.541)*P-exp(-0.21263*x(4)^0.5-15.98)*P^2
19 +300*(exp(-0.011901*x(15)-5.941))*(P/exp(300)));
20 - x(8)=0.93431737+0.0002028538*x(4)+0.000295896*P-0.000000270727*x(4)^2
21 - +0.0000004775207*P^2;
22 - x(9)=0.1438996+.0002028538*x(4)-.0004487672*P-0.000001142945*x(4)^2
23 - +0.0000002761216*P^2;
24 - x(10)=x(19)*x(7)*P;
25 - x(11)=x(20)*x(8)*P;
26 - x(12)=x(21)*x(9)*P;
27 - x(13)=x(5)*(x(6)^2*x(11)*(x(10)/x(12))^j-(x(12)^2/x(10)^3)^(1-j));
28 %cpH2=x(14) cpN2=x(15) cpNH3=x(16) cpg=x(17)
29 - x(14)=4.184*(6.952-0.000457*x(4)+0.0000009563*x(4)^2-0.000002079*x(4)^3);
30 - x(15)=4.184*(6.903-0.000375*x(4)+0.00000193*x(4)^2-0.000006861*x(4)^3);
31 - x(16)=4.184*(6.5846-0.0061251*x(4)+0.0000023663*x(4)^2-0.000000015981*x(4)^3
32 +96.1678-0.067571*P+x(4)*(0.0005+0.00016847*P)+x(4)^2*(0.0001289-0.00000010095*P));
33 - x(17)=x(19)*x(14)+x(20)*x(15)+x(21)*x(16);
34 - x(1)=.6703*NF+3*x(13)*z;
35 - x(2)=.2219*NF+x(13)*z;
36 - x(3)=.002219*NF-x(13)*z;
37 %moles=x(18) yH2=x(19) yN2=x(20) yNH3=x(21) yAr=x(22) ycH4=x(23)
38 - x(18)=x(1)+x(2)+x(3)+NF*yCH4+NF*yAr;
39 - x(19)=x(1)/x(18);
40 - x(20)=(x(3))/x(18);
41 - x(21)=(x(5))/x(18);
42 - x(22)=NF*yCH4/x(18);
43 - x(23)=NF*yAr/x(18);
44 - end
45
```

2. MATLAB code for ammonia synthesis in fluidized bed reactor

```

Editor - C:\MATLAB7\work\model.m
File Edit Text Cell Tools Debug Desktop Window Help
[Icons] Stack: Base
1 function y=model(x)
2 - global Q P TF L D M S R E O dp vH2 VN2 VNH3 VAr VcH4 MH2 MN2 MNH3 MAr McH4 NF leng
3 - yH2=0.6303;
4 - yN2=0.2219;
5 - yNH3=0.00276;
6 - ycH4=0.00546;
7 - yAr=0.00256;
8 - A=3.14*D^2/4;
9 - UO=Q/A;
10 - Umf=O*dp*9.8*(R-S)*E^3/(150*M*(1-E));
11 - QbF=O*(UO-Umf)*A;
12 - QdF=Q-QbF;
13 - db0=2.78*(UO-Umf)^2/9.8;
14 - dbm=1.633*(A*(UO-Umf))^0.4;
15 - db=dbm-(dbm-db0)*exp(-0.3*leng/D);
16 - Ubr=0.71*(9.8*db)^.5;
17 - Ub=UO-Umf+0.711*(9.8*db)^.5;
18 - delta=(UO-Umf)/Ub;
19 - Ab=delta*A;
20 % estimation of the diffusion coefficient of H2
21 % DH2N2= x(16) DH2NH3= x(17) DH2Ar=x(18) DH2cH4=x(19) DH2= x(20)
22 - x(17)=x(15)^1.75*10^(-7)*(1/MH2+1/MN2)^0.5/(P*(vH2^(1/3)+VN2^(1/3))^2);
23 - x(17)=x(15)^1.75*10^-7*(1/MH2+1/MNH3)^0.5/(P*(vH2^(1/3)+VNH3^(1/3))^2);
24 - x(18)=x(15)^1.75*10^-7*(1/MH2+1/MAr)^0.5/(P*(vH2^(1/3)+VAr^(1/3))^2);
25 - x(19)=x(15)^1.75*10^-7*(1/MH2+1/McH4)^0.5/(P*(vH2^(1/3)+VcH4^(1/3))^2);
26 - x(20)=1-x(81)/(x(82)/x(16)+x(83)/x(17)+x(84)/x(18)+x(85)/x(19));
27 % estimation of the diffusion coefficient of N2
28 % DN2H2=x(21) DN2NH3=x(22) DN2Ar=x(23) DN2cH4=x(24) DN2=x(25)
29 - x(21)=x(16);
30 - x(22)=x(15)^1.75*10^-7*(1/MN2+1/MNH3)^0.5/(P*(VN2^(1/3)+VNH3^(1/3))^2);
31 - x(23)=x(15)^1.75*10^-7*(1/MN2+1/MAr)^0.5/(P*(VN2^(1/3)+VAr^(1/3))^2);
32 - x(24)=x(15)^1.75*10^-7*(1/MN2+1/McH4)^0.5/(P*(VN2^(1/3)+VcH4^(1/3))^2);
33 - x(25)=1-x(82)/(x(81)/x(21)+x(83)/x(22)+x(84)/x(23)+x(85)/x(24));
34 % estimation of the diffusion coefficient of NH3
35 % DNH3H2=x(26) DNH3N2=x(27) DNH3Ar=x(28) DNH3cH4=x(29) DNH3=x(30)
36 - x(26)=x(17);
37 - x(27)=x(22);
38 - x(28)=x(15)^1.75*10^-7*(1/MNH3+1/MAr)^0.5/(P*(VNH3^(1/3)+VAr^(1/3))^2);
39 - x(29)=x(15)^1.75*10^-7*(1/MNH3+1/McH4)^0.5/(P*(VNH3^(1/3)+VcH4^(1/3))^2);
40 - x(30)=1-x(83)/(x(81)/x(26)+x(82)/x(27)+x(84)/x(28)+x(85)/x(29));
41 % estimation of the diffusion coefficient of Ar
42 % DArH2=x(31) DArN2=x(32) DArNH3=x(33) DArC4=x(34) DAr=x(35)
43 - x(31)=x(18);
44 - x(32)=x(23);
45 - x(33)=x(28);
46 - x(34)=x(15)^1.75*10^-7*(1/MAr+1/McH4)^0.5/(P*(VAr^(1/3)+VcH4^(1/3))^2);
47 - x(35)=1-x(84)/(x(81)/x(31)+x(82)/x(32)+x(83)/x(33)+x(85)/x(34));

```

```

48 % estimation of the diffusion coefficient of cH4
49 %DcH4H2=x(36) DcH4N2=x(37) DcH4NH3=x(38) DcH4Ar=x(39) DcH4=x(40)
50 - x(36)=x(19);
51 - x(37)=x(24);
52 - x(38)=x(29);
53 - x(39)=x(34);
54 - x(40)=1-x(85)/(x(81)/x(36)+x(82)/x(37)+x(83)/x(38)+x(84)/x(39));
55 % estimation of the mass transfer coefficient between phases
56 %kbcH2=x(41) KcdH2=x(42) KbdH2=x(43) kbcN2=x(44) KcdN2=x(45) KbdN2=x(46)
57 %kbcNH3=x(47) KcdNH3=x(48) KbdNH3=x(49) kbcAr=x(50) KcdAr=x(51) KbdAr=x(52)
58 %kbccH4=x(53) KcdcH4=x(54) KbdcH4=x(55)
59 - (4.5*(Umf/db)+5.85*(x(20)^0.5*9.8^0.25/D^1.5))-x(41);
60 - x(42)=6.77*(x(20)*E*Ubr/db^3)^0.5;
61 - x(43)=1/((1/x(41))+(1/x(42)));
62 - x(44)=4.4*(Umf/db)+5.85*(x(25)^0.5*9.8^0.25/D^1.25);
63 - x(45)=6.77*(x(25)*E*Ubr/db^3)^0.5;
64 - x(46)=1/((1/x(44))+(1/x(45)));
65 - x(47)=4.4*(Umf/db)+5.85*(x(30)^0.5*9.8^0.25/D^1.25);
66 - x(48)=6.77*(x(30)*E*Ubr/db^3)^0.5;
67 - x(49)=1/((1/x(47))+(1/x(48)));
68 - x(50)=4.4*(Umf/db)+5.85*(x(35)^0.5*9.8^0.25/D^1.25);
69 - x(51)=6.77*(x(35)*E*Ubr/db^3)^0.5;
70 - x(52)=1/((1/x(50))+(1/x(51)));
71 - x(53)=4.4*(Umf/db)+5.85*(x(40)^0.5*9.8^0.25/D^1.25);
72 - x(54)=6.77*(x(40)*E*Ubr/db^3)^0.5;
73 - x(55)=1/((1/x(53))+(1/x(54)));
74 %aH2=x(56) aN2=x(57) aNH3=x(58) aAr=x(59) acH4=x(60)
75 - x(56)=x(43)/Ub;
76 - x(57)=x(46)/Ub;
77 - x(58)=x(49)/Ub;
78 - x(59)=x(52)/Ub;
79 - x(60)=x(55)/Ub;
80 - v=L.A;
81 - j=0.55;
82 - E2=163500;
83 - K20=10^14.7102;
84 %K2=x(61) Ka=x(62) qH2=x(63) qN2=x(64) qNH3=x(65) fH2=x(66) fN2=x(67)
85 %fNH3=x(68) rNH3=x(69)
86 - x(61)=K20*exp(-E2/r.x(15));
87 - x(62)=10^(-2.69112*log10(x(15))-0.00005519265*x(15)+.0000001848863*x(15)^2
88 - +2001.6/x(15)+2.6899);
89 - x(63)=exp(exp(-3.8402*x(15)^0.125+0.541)*P-exp(-0.21263*x(15)^0.5-15.98)*P^2
90 - +300*(exp(-0.011901*x(15)-5.941))*(P/exp(300)));
91 - x(64)=0.93431737+0.0002028538*x(15)+0.000295896*P-0.000000270727*x(15)^2
92 - +0.0000004775207*P^2;
93 - x(65)=0.1438996+.002028538*x(15)-.0004487672*P-0.000001142945*x(15)^2
94 - +0.0000002761216*P^2;
95 - x(66)=x(81)*x(63)*P;
96 - x(67)=x(82)*x(64)*P;
97 - x(68)=x(83)*x(65)*P;
98 - x(69)=x(61)*(x(62)^2*x(67)*(x(66)/x(68))^j-(x(68)^2/x(66)^3)^(1-j));
99 - jH2=-3;
100 - jN2=-1;

```

```

102 - x(1)/x(14)-x(2)/x(13)-(NF/x(14)-x(2)/x(13))*exp(-x(56)*leng);
103 - x(3)/x(14)-x(4)/x(13)-(NF/x(14)-x(4)/x(13))*exp(-x(57)*leng);
104 - x(5)/x(14)-x(6)/x(13)-(NF/x(14)-x(6)/x(13))*exp(-x(58)*leng);
105 - x(7)/x(14)-x(8)/x(13)-(NF/x(14)-x(8)/x(13))*exp(-x(59)*leng);
106 - x(9)/x(14)-x(10)/x(13)-(NF/x(14)-x(10)/x(13))*exp(-x(60)*leng);
107 - x(2)=x(81)*NF*(QdF/Q)+Ub*Ab*(x(81)*NF/Q-x(2)/x(13))+(1-exp(-x(56)*L))
108 - +v*(1-delta)*(1-E)*R*jH2*x(69);
109 - x(4)=x(82)*NF*(QdF/Q)+Ub*Ab*(x(82)*NF/Q-x(4)/x(13))+(1-exp(-x(57)*L))
110 - +v*(1-delta)*(1-E)*R*jN2*x(69);
111 - x(6)=x(83)*NF*(QdF/Q)+Ub*Ab*(x(83)*NF/Q-x(6)/x(13))+(1-exp(-x(58)*L))
112 - +v*(1-delta)*(1-E)*R*jNH3*x(69);
113 - x(8)=x(84)*NF*(QdF/Q)+Ub*Ab*(x(84)*NF/Q-x(8)/x(13))+(1-exp(-x(59)*L));
114 - x(10)=x(85)*NF*(QdF/Q)+Ub*Ab*(x(85)*NF/Q-x(10)/x(13))+(1-exp(-x(60)*L));
115 - %cpH2=x(70) cpN2=x(71) cpNH3=x(72) cpg=x(73)
116 - x(70)=4.184*(6.952-0.000457*x(15)+0.0000009563*x(15)^2-0.000002079*x(15)^3);
117 - x(71)=4.184*(6.903-0.000375*x(15)+0.00000193*x(15)^2-0.000006861*x(15)^3);
118 - x(72)=4.184*(6.5846-0.0061251*x(15)+0.0000023663*x(15)^2-0.000000015981*x(15)^3
119 - +96.1678-0.067571*P+x(15)*(0.0005+0.00016847*P)+x(15)^2*(0.0001289-0.00000010095*P));
120 - x(73)=x(81)*x(70)+x(82)*x(71)+x(83)*x(72);
121 - mH2=0.02;
122 - mN2=0.004;
123 - mNH3=0.03;
124 - %kH2=x(74) kN2=x(75) kNH3=x(76) kg=x(77) Hbd=x(78) b=x(79)
125 - x(74)=mH2*(x(70)+10.4/2);
126 - x(75)=mN2*(x(71)+10.4/28);
127 - x(76)=mNH3*(x(72)+10.4/17);
128 - x(77)=x(81)*x(74)+x(82)*x(75)+x(83)*x(76);
129 - x(78)=19.09*(Umf*S*x(73)*db)+(5.85*(x(77)*S*x(73))^0.5*9.8^0.25)/(6*db^0.25);
130 - x(79)=x(78)/(Ub*S*x(73));
131 - x(11)=x(12)-(x(12)-TF)*exp(-x(79)*length);
132 - S*x(73)*QdF*(TF-298)-S*x(73)*x(13)*(x(12)-298)+Ub*S*x(73)*Ab*(TF-x(12))
133 - *(1-exp(-x(79)*L))-v*(1-delta)*(1-E)*S*92.44*x(69);
134 - x(13)=r*x(12)*(x(2)+x(4)+x(6)+x(8)+x(10))/(x(66)+x(67)+x(68));
135 - x(14)=Q-x(13);
136 - x(15)=(x(14)*x(11)+x(13)*x(12))/(x(14)+x(13));
137 - %moles=x(80) yH2=x(81) yN2=x(82) yNH3=x(83) yAr=x(84) yCH4=x(85)
138 - x(80)=x(1)+x(2)+x(3)+x(4)+x(5)+x(6)+x(7)+x(8)+x(9)+x(10);
139 - x(81)=(x(1)+x(2))/x(80);
140 - x(82)=(x(3)+x(4))/x(80);
141 - x(83)=(x(5)+x(6))/x(80);
142 - x(84)=(x(7)+x(8))/x(80);
143 - x(85)=(x(9)+x(10))/x(80);
144 - end

```

3. MATLAB code for methanol synthesis in fluidized bed reactor

```

Editor - C:\MATLAB7\work\methfluid.m*
File Edit Text Cell Tools Debug Desktop Window Help
[Icons] Stack: Base
1 function y=methfluid(x)
2 - global Q P TF L D M S R E O dp vH2 VN2 VNCH4 VCO VCO2 VH2O VCH3OH MH2 MN2 MCO
3 - MCO2 McH4 MH2O McH3OH NF len
4 - yH2=0.8;|
5 - yN2=0.0001;
6 - yCO=0.0476;
7 - ycH4=0.1192;
8 - yCO2=0.02956;
9 - yCH3OH=0.003;
10 - yH2O= 0.0006;
11 - A=3.14*D^2/4;
12 - UO=Q/A;
13 - Umf=0*dp*9.8*(R-S)*E^3/(150*M*(1-E));
14 - QbF=0*(UO-Umf)*A;
15 - QdF=Q-QbF;
16 - db0=2.78*(UO-Umf)^2/9.8;
17 - dbm=1.633*(A*(UO-Umf))^0.4;
18 - db=dbm-(dbm-db0)*exp(-0.3*leng/D);
19 - Ubr=0.71*(9.8*db)^.5;
20 - Ub=UO-Umf+0.711*(9.8*db)^.5;
21 - delta=(UO-Umf)/Ub;
22 - Ab=delta*A;
23 % estimation of the diffusion coefficient of H2
24 % DH2N2= x(1) DH2CO= x(2) DH2CO2=x(3) DH2cH4=x(4) DH2H2o=x(5) DH2cH3OH=x(6)
25 %DH2= x(7)
26 - x(1)=x(15)^1.75*10^(-7)*(1/MH2+1/MN2)^0.5/(P*(vH2^(1/3)+VN2^(1/3))^2);
27 - x(2)=x(15)^1.75*10^-7*(1/MH2+1/MCO)^0.5/(P*(vH2^(1/3)+VCO^(1/3))^2);
28 - x(3)=x(15)^1.75*10^-7*(1/MH2+1/MCO2)^0.5/(P*(vH2^(1/3)+VCO2^(1/3))^2);
29 - x(4)=x(15)^1.75*10^-7*(1/MH2+1/MH2O)^0.5/(P*(vH2^(1/3)+VH2O^(1/3))^2);
30 - x(5)=x(15)^1.75*10^-7*(1/MH2+1/McH3OH)^0.5/(P*(vH2^(1/3)+VcH3OH^(1/3))^2);
31 - x(6)=x(15)^1.75*10^-7*(1/MH2+1/McH4)^0.5/(P*(vH2^(1/3)+VcH4^(1/3))^2);
32 - x(7)=1-x(81)/(x(82)/x(1)+x(83)/x(2)+x(84)/x(3)+x(85)/x(5)+x(85)/x(6)+x(85)/x(7));

```

```

33 % estimation of the diffusion coefficient of N2
34 % DN2H2=x(8) DN2CO= x(9) DN2CO2=x(10) DN2cH4=x(11) DN2H2o=x(12) DN2cH3OH=x(13)
35 % DN2= x(14)
36 - x(8)=x(1);
37 - x(9)=x(15)^1.75*10^-7*(1/MN2+1/MCO)^0.5/(P*(VN2^(1/3)+VCO^(1/3))^2);
38 - x(10)=x(15)^1.75*10^-7*(1/MN2+1/MCO2)^0.5/(P*(VN2^(1/3)+VCO2^(1/3))^2);
39 - x(11)=x(15)^1.75*10^-7*(1/MN2+1/McH4)^0.5/(P*(VN2^(1/3)+VcH4^(1/3))^2);
40 x(14)=1-x(82)/(x(81)/x(8)+x(83)/x(9)+x(84)/x(10)+x(85)/x(11)+x(85)/x(12)
41 +x(85)/x(13));
42 - x(13)=x(15)^1.75*10^-7*(1/MN2+1/McH3OH)^0.5/(P*(VN2^(1/3)+VcH3OH^(1/3))^2);
43 - x(12)=x(15)^1.75*10^-7*(1/MN2+1/MH2O)^0.5/(P*(VN2^(1/3)+VH2O^(1/3))^2);
44 % estimation of the diffusion coefficient of CO2
45 %DCO2H2=x(16) DCO2N2=x(17) DCO2CO=x(18) DCO2cH4=x(19) DCO2cH3OH=x(20)
46 %DCO2H2O=x(21) DCO2=x(22)
47 - x(16)=x(3);
48 - x(17)=x(10);
49 - x(18)=x(15)^1.75*10^-7*(1/MCO2+1/MCO)^0.5/(P*(VCO2^(1/3)+VCO^(1/3))^2);
50 - x(19)=x(15)^1.75*10^-7*(1/MCO2+1/McH4)^0.5/(P*(VCO2^(1/3)+VcH4^(1/3))^2);
51 - x(20)=x(15)^1.75*10^-7*(1/MCO2+1/McH3OH)^0.5/(P*(VCO2^(1/3)+VcH3OH^(1/3))^2);
52 - x(21)=x(15)^1.75*10^-7*(1/MCO2+1/MH2O)^0.5/(P*(VCO2^(1/3)+VH2O^(1/3))^2);
53 x(22)=1-x(83)/(x(81)/x(16)+x(82)/x(17)+x(84)/x(18)+x(85)/x(19)+x(85)/x(20)
54 +x(85)/x(21));
55 % estimation of the diffusion coefficient of CO
56 %DCOcH4=x(23) DCOcH3OH=x(24) DCOH2O=x(25) DCO=x(29)
57 - x(26)=x(2);
58 - x(27)=x(9);
59 - x(28)=x(18);
60 - x(23)=x(15)^1.75*10^-7*(1/MCO+1/McH4)^0.5/(P*(VCO^(1/3)+VcH4^(1/3))^2);
61 - x(24)=x(15)^1.75*10^-7*(1/MCO+1/McH3OH)^0.5/(P*(VCO^(1/3)+VcH3OH^(1/3))^2);
62 - x(25)=x(15)^1.75*10^-7*(1/MCO+1/MH2O)^0.5/(P*(VCO^(1/3)+VH2O^(1/3))^2);
63 x(29)=1-x(84)/(x(81)/x(26)+x(82)/x(27)+x(83)/x(28)+x(85)/x(23)+x(85)/x(24)
64 +x(85)/x(25));
65 % estimation of the diffusion coefficient of cH4
66 %DcH4H2=x(30) DcH4N2=x(31) DcH4CO2=x(32) DcH4CO=x(33) DcH4cH3OH=x(34)
67 %DcH4H2O=x(35) DcH4=x(36)
68 - x(30)=x(4);
69 - x(31)=x(11);
70 - x(32)=x(19);
71 - x(33)=x(23);
72 - x(34)=x(15)^1.75*10^-7*(1/McH4+1/McH3OH)^0.5/(P*(VcH4^(1/3)+VcH3OH^(1/3))^2);
73 - x(35)=x(15)^1.75*10^-7*(1/McH4+1/MH2O)^0.5/(P*(VcH4^(1/3)+VH2O^(1/3))^2);
74 x(36)=1-x(85)/(x(81)/x(30)+x(82)/x(31)+x(83)/x(32)+x(84)/x(33)+x(84)/x(34)
75 +x(84)/x(35));
76 % estimation of the diffusion coefficient of cH3OH
77 %DcH3OHH2=x(37) DcH3OHN2=x(38) DcH3OHCO2=x(39) DcH3OHCO=x(40) DcH3OHcH4=x(41)
78 %DcH3OHH2O=x(42) DcH3OH=x(43)
79 - x(37)=x(6);
80 - x(38)=x(13);
81 - x(39)=x(20);
82 - x(40)=x(24);
83 - x(41)=x(23);
84 - x(42)=x(15)^1.75*10^-7*(1/MH2O+1/McH3OH)^0.5/(P*(VH2O^(1/3)+VcH3OH^(1/3))^2);
85 x(33)=1-x(85)/(x(81)/x(37)+x(82)/x(38)+x(83)/x(39)+x(84)/x(40)+x(84)/x(41)
86 +x(84)/x(42));

```

```

87 % estimation of the diffusion coefficient of H2O
88 %DH2OH2=x(43) DH2ON2=x(44) DH2OCO2=x(45) DH2OCO=x(46) DH2OCH3OH=x(47)
89 %DcH4H2O=x(48) DH2O=x(49)
90 - x(43)=x(5);
91 - x(44)=x(12);
92 - x(45)=x(21);
93 - x(46)=x(25);
94 - x(47)=x(35);
95 - x(48)=x(42);
96 x(49)=1-x(85)/(x(81)/x(43)+x(82)/x(44)+x(83)/x(45)+x(84)/x(46)+x(84)/x(47)
97 +x(84)/x(48));
98 % estimation of the mass transfer coefficient between phases
99 %kbcH2=x(49) KcdH2=x(50) KbdH2=x(51) kbcN2=x(52) KcdN2=x(53) KbdN2=x(54)
100 %kbcO2=x(47) KcdCO2=x(48) KbdCO2=x(49) kbcCO=x(50) KcdCO=x(51) KbdCO=x(52)
101 %kbcH4=x(53) KcdcH4=x(54) KbdH4=x(55)%kbcH3OH=x(56) KcdcH3OH=x(57) KbdH3OH=x(58)
102 %kbcH2O=x(59) KcdH2O=x(60) KbdH2O=x(61)
103 - (4.5*(Umf/db)+5.85*(x(20)^0.5*9.8^0.25/D^1.5))-x(49);
104 - x(50)=6.77*(x(20)*E*Ubr/db^3)^0.5;
105 - x(43)=1/((1/x(41))+1/x(42));
106 - x(44)=4.4*(Umf/db)+5.85*(x(25)^0.5*9.8^0.25/D^1.25);
107 - x(45)=6.77*(x(25)*E*Ubr/db^3)^0.5;
108 - x(46)=1/((1/x(44))+1/x(45));
109 - x(47)=4.4*(Umf/db)+5.85*(x(30)^0.5*9.8^0.25/D^1.25);
110 - x(48)=6.77*(x(30)*E*Ubr/db^3)^0.5;
111 - x(49)=1/((1/x(47))+1/x(48));
112 - x(50)=4.4*(Umf/db)+5.85*(x(35)^0.5*9.8^0.25/D^1.25);
113 - x(51)=6.77*(x(35)*E*Ubr/db^3)^0.5;
114 - x(52)=1/((1/x(50))+1/x(51));
115 - x(53)=4.4*(Umf/db)+5.85*(x(40)^0.5*9.8^0.25/D^1.25);
116 - x(54)=6.77*(x(40)*E*Ubr/db^3)^0.5;
117 - x(55)=1/((1/x(53))+1/x(54));
118 - x(56)=4.4*(Umf/db)+5.85*(x(40)^0.5*9.8^0.25/D^1.25);
119 - x(57)=6.77*(x(40)*E*Ubr/db^3)^0.5;
120 - x(58)=1/((1/x(56))+1/x(57));
121 - x(59)=4.4*(Umf/db)+5.85*(x(40)^0.5*9.8^0.25/D^1.25);
122 - x(60)=6.77*(x(40)*E*Ubr/db^3)^0.5;
123 - x(61)=1/((1/x(59))+1/x(60));
124 %aH2=x(62) aN2=x(63) aCO2=x(64) aCO=x(65) acH4=x(66) aCH3OH=x(67) aH2O=x(68)
125 - x(62)=x(43)/Ub;
126 - x(63)=x(46)/Ub;
127 - x(64)=x(49)/Ub;
128 - x(65)=x(52)/Ub;
129 - x(66)=x(55)/Ub;
130 - x(67)=x(58)/Ub;
131 - x(68)=x(61)/Ub;
132 - A1=1.07
133 - B1=36696
134 - A3=3453.38
135 - B3=0
136 - A4=0.499
137 - B4=17197
138 - A5=6.62*10^11
139 - B5= 124119
140 - A2=1.22*10^10
141 - B2=-94765

```

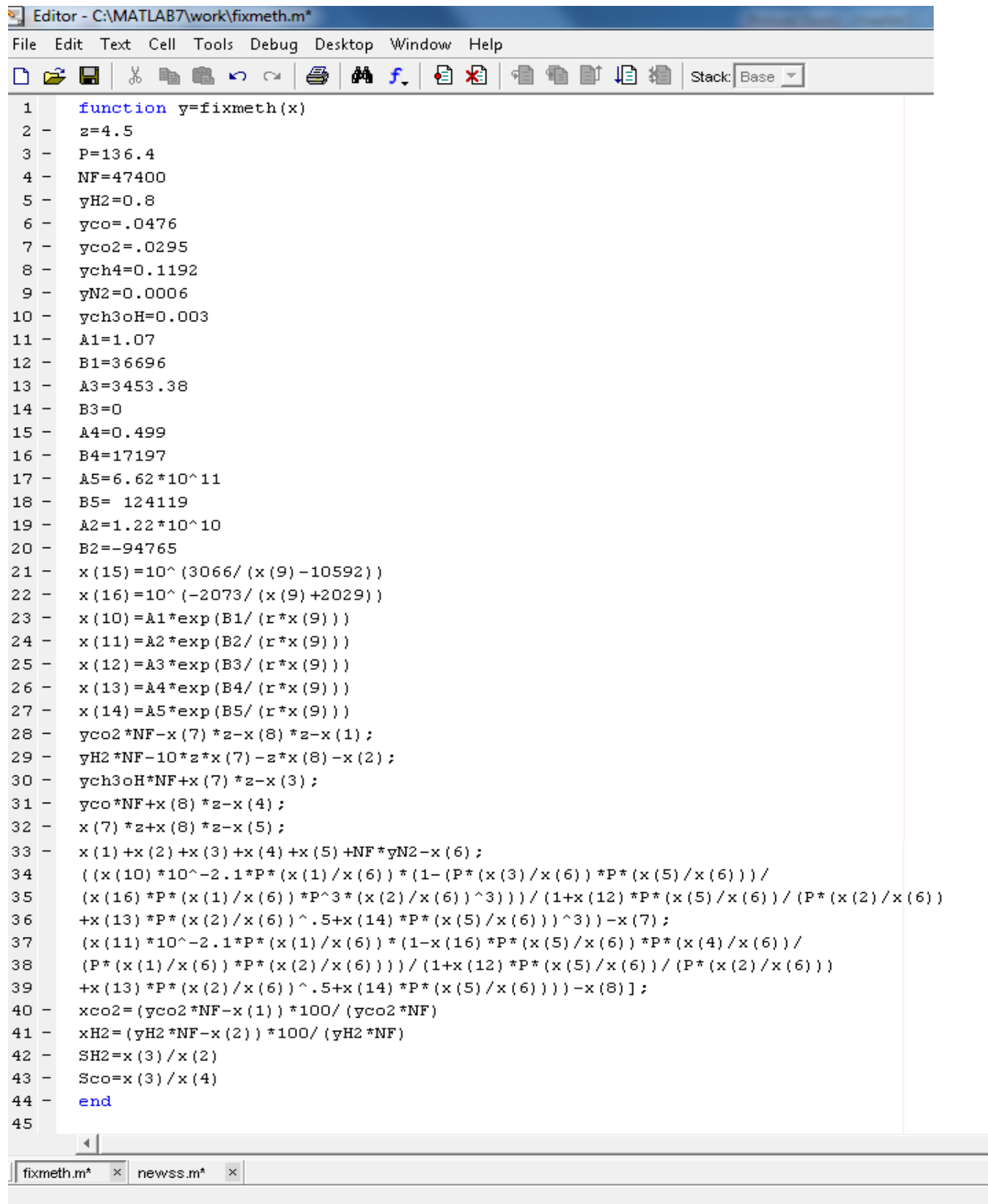
```

142 - K2eq=10^(3066/(x(15)-10592))
143 - K3eq=10^(-2073/(x(15)+2029))
144 - k1=A1*exp(B1/(r*x(15)))
145 - k2=A2*exp(B2/(r*x(15)))
146 - k3=A3*exp(B3/(r*x(15)))
147 - k4=A4*exp(B4/(r*x(15)))
148 - k5=A5*exp(B5/(r*x(15)))
149 - ((k1*10^-2.1*P*(x(1)/x(6))* (1-(P*(x(3)/x(6))*P*(x(5)/x(6)))/
150 - (K2eq*P*(x(1)/x(6))*P^3*(x(2)/x(6))^3))/ (1+k3*P*(x(5)/x(6))/(P*(x(2)/x(6))
151 - +k4*P*(x(2)/x(6))^5+k5*P*(x(5)/x(6))^3))-x(7);
152 - (k2*10^-2.1*P*(x(1)/x(6))* (1-K3eq*P*(x(5)/x(6))*P*(x(4)/x(6)))/
153 - (P*(x(1)/x(6))*P*(x(2)/x(6)))/ (1+k3*P*(x(5)/x(6))/(P*(x(2)/x(6))
154 - +k4*P*(x(2)/x(6))^5+k5*P*(x(5)/x(6)))-x(8)];
155 - x(68)/x(14)-x(69)/x(13)-(NF/x(14)-x(69)/x(13))*exp(-x(56)*leng);
156 - x(70)/x(14)-x(4)/x(13)-(NF/x(14)-x(71)/x(13))*exp(-x(57)*leng);
157 - x(72)/x(14)-x(6)/x(13)-(NF/x(14)-x(73)/x(13))*exp(-x(58)*leng);
158 - x(74)/x(14)-x(8)/x(13)-(NF/x(14)-x(75)/x(13))*exp(-x(59)*leng);
159 - x(76)/x(14)-x(10)/x(13)-(NF/x(14)-x(77)/x(13))*exp(-x(60)*leng);
160 - x(69)=x(81)*NF*(QdF/Q)+Ub*Ab*(x(81)*NF/Q-x(2)/x(13))+(1-exp(-x(62)*L))
161 - +v*(1-delta)*(1-E)*R*jH2*x(69);
162 - x(71)=x(82)*NF*(QdF/Q)+Ub*Ab*(x(82)*NF/Q-x(4)/x(13))+(1-exp(-x(63)*L))
163 - +v*(1-delta)*(1-E)*R*jN2*x(69);
164 - x(73)=x(83)*NF*(QdF/Q)+Ub*Ab*(x(83)*NF/Q-x(6)/x(13))+(1-exp(-x(64)*L))
165 - +v*(1-delta)*(1-E)*R*jNH3*x(69);
166 - x(75)=x(84)*NF*(QdF/Q)+Ub*Ab*(x(84)*NF/Q-x(8)/x(13))+(1-exp(-x(65)*L));
167 - x(77)=x(85)*NF*(QdF/Q)+Ub*Ab*(x(85)*NF/Q-x(10)/x(13))+(1-exp(-x(66)*L))
168 - x(70)=4.184*(6.952-0.000457*x(15)+0.0000009563*x(15)^2-0.000002079*x(15)^3);
169 - x(71)=4.184*(6.903-0.000375*x(15)+0.00000193*x(15)^2-0.000006861*x(15)^3);
170 - x(72)=4.184*(6.5846-0.0061251*x(15)+0.0000023663*x(15)^2-0.0000000015981*x(15)^3
171 - +96.1678-0.067571*P+x(15)*(0.0005+0.00016847*P)+x(15)^2*(0.0001289-0.00000010095*P));
172 - x(73)=x(81)*x(70)+x(82)*x(71)+x(83)*x(72);
173 - x(74)=mH2*(x(70)+10.4/2);
174 - x(75)=mN2*(x(71)+10.4/28);
175 - x(76)=mCH3OH*(x(72)+10.4/17);
176 - x(77)=x(81)*x(74)+x(82)*x(75)+x(83)*x(76);
177 - x(78)=19.09*(Umf*S*x(73)*db)+(5.85*(x(77)*S*x(73))^0.5*9.8^0.25)/(6*db^0.25);
178 - x(79)=x(78)/(Ub*S*x(73));
179 - x(11)=x(12)-(x(12)-TF)*exp(-x(79)*length);
180 - S*x(73)*QdF*(TF-298)-S*x(73)*x(13)*(x(12)-298)+Ub*S*x(73)*Ab*(TF-x(12))
181 - *(1-exp(-x(79)*L))-v*(1-delta)*(1-E)*S*92.44*x(69);
182 - x(13)=r*x(12)*(x(2)+x(4)+x(6)+x(8)+x(10))/(x(66)+x(67)+x(68));
183 - x(14)=Q-x(13);
184 - x(15)=(x(14)*x(11)+x(13)*x(12))/(x(14)+x(13));
185 - x(82)=x(1)+x(2)+x(3)+x(4)+x(5)+x(6)+x(7)+x(8)+x(9)+x(10);
186 - x(83)=(x(68)+x(69))/x(82);
187 - x(84)=(x(70)+x(71))/x(82);
188 - x(85)=(x(72)+x(73))/x(82);
189 - x(86)=(x(74)+x(75))/x(82);
190 - x(87)=(x(76)+x(77))/x(82);
191 - x(88)=(x(78)+x(79))/x(82);
192 - x(89)=(x(80)+x(81))/x(82);
193 - end

```

model.m × methfluid.m* × fixmeth.m ×

4. MATLAB code for methanol synthesis in fixed bed reactor



```
Editor - C:\MATLAB7\work\fixmeth.m*
File Edit Text Cell Tools Debug Desktop Window Help
Stack: Base
1 function y=fixmeth(x)
2 z=4.5
3 P=136.4
4 NF=47400
5 yH2=0.8
6 yco=.0476
7 yco2=.0295
8 ych4=0.1192
9 yN2=0.0006
10 ych3oH=0.003
11 A1=1.07
12 B1=36696
13 A3=3453.38
14 B3=0
15 A4=0.499
16 B4=17197
17 A5=6.62*10^11
18 B5= 124119
19 A2=1.22*10^10
20 B2=-94765
21 x(15)=10^(3066/(x(9)-10592))
22 x(16)=10^(-2073/(x(9)+2029))
23 x(10)=A1*exp(B1/(r*x(9)))
24 x(11)=A2*exp(B2/(r*x(9)))
25 x(12)=A3*exp(B3/(r*x(9)))
26 x(13)=A4*exp(B4/(r*x(9)))
27 x(14)=A5*exp(B5/(r*x(9)))
28 yco2*Nf-x(7)*z-x(8)*z-x(1);
29 yH2*Nf-10*z*x(7)-z*x(8)-x(2);
30 ych3oH*Nf+x(7)*z-x(3);
31 yco*Nf+x(8)*z-x(4);
32 x(7)*z+x(8)*z-x(5);
33 x(1)+x(2)+x(3)+x(4)+x(5)+Nf*yN2-x(6);
34 ((x(10)*10^-2.1*P*(x(1)/x(6))*(1-(P*(x(3)/x(6))*P*(x(5)/x(6))))/
35 (x(16)*P*(x(1)/x(6))*P^3*(x(2)/x(6))^3))/(1+x(12)*P*(x(5)/x(6))/(P*(x(2)/x(6))
36 +x(13)*P*(x(2)/x(6))^0.5+x(14)*P*(x(5)/x(6))^3))-x(7);
37 (x(11)*10^-2.1*P*(x(1)/x(6))*(1-x(16)*P*(x(5)/x(6))*P*(x(4)/x(6)))/
38 (P*(x(1)/x(6))*P*(x(2)/x(6)))/(1+x(12)*P*(x(5)/x(6))/(P*(x(2)/x(6))
39 +x(13)*P*(x(2)/x(6))^0.5+x(14)*P*(x(5)/x(6)))-x(8)];
40 xco2=(yco2*Nf-x(1))*100/(yco2*Nf)
41 xH2=(yH2*Nf-x(2))*100/(yH2*Nf)
42 SH2=x(3)/x(2)
43 Sco=x(3)/x(4)
44 end
45
```

fixmeth.m* x newss.m* x

References:

1. Twigg, M. V, Samon. M. S. *Catalytic Ammonia Synthesis*. (Plenum Press, New York, 1991).
2. Nielsen, C. S., Dybkjær, I. and Perregaard, J. Large Scale Methanol Production from Natural Gas. *International Journal of Science & Engineering Research* 1–14 (2007).
3. Bertau, M., Offermanns, H., Plass, L. & Schmidt, F. *Methanol : The Basic Chemical and Energy Feedstock of the Future*. (Springer-VSpringer-Verlag Berlin Heidelberg, 2014).
4. Elnashaie, S. S. E. M. *Conservation Equations and Modeling of Chemical and Biochemical Processes*. (Marcel Dekker, Inc., 2003).
5. Knop, F. C. *modeling, analysis and optimization of process and energy system*. (John Wiley & Sons, Inc., 2011).
6. Froment, G. F. Analysis and Design of Fixed Bed Catalytic Reactors. *Advances in Chemistry; American Chemical Society* **23**, (1974).
7. Iordanidis, A. A. *Mathematical Modeling of Catalytic Fixed Bed Reactors*. (Twente University Press, 2002).
8. Azarpour, A., Zahedi, G., Sin, G., Gani, R. & Engineering, B. Generic Modeling of Fixed-bed Catalytic Reactors. in *Proceedings of the 6th International Conference on Process Systems Engineering (PSE ASIA)* 25–27 (Process System Engineering Center, 2013).
9. M. Chocron., N. E. Amadeo', and M. A. L. Heterogeneous Modeling of an Adiabatic Packed Bed Reactor. *chemical engineering processes* **8250**, 2–6 (1998).
10. Said Elnashaie, Frank Uhlig, C. A. *Numerical Techniques for Chemical and Biological Engineers Using MATLAB*. (Springer Science+Business Media, LLC, 2007).

11. A. Kayode Coker. *Modeling of Chemical Kinetics and Reactor Design*. (Gulf Publishing Company, 2009).
12. Aishah, N., Amin, S. & Yee, N. P. Mathematical Modelling of Catalytic Fixed-Bed Reactor for Carbon Dioxide Reforming of Methane over Rh / Al₂O₃ Catalyst. *Bulletin of Chemical Reaction Engineering & Catalysis* **3**, 21–29 (2008).
13. Dashti, A., Khorsand, K., Marvast, M. A. & Kakavand, M. Modeling and Simulation of Ammonia Synthesis Reactor. *Petroleum & Coal* 15–23 (2006).
14. Kuczynski, M. & Westerterp, W. I. B. H. J. F. Reaction Kinetics for the Synthesis of Methanol from CO and H₂ on a Copper Catalyst. *chemical engineering processes* **21**, 179–191 (1987).
15. Stanisław Ledakowicz¹, Lech Nowicki¹, Jerzy Petera¹, Jarosław Nizioł¹, Paweł Kowalik², A. G. Kinetics Characterisation of Catalysts for Methanol Synthesis. *Chemical and Process Engineering* **34**, 497–506 (2013).
16. Silva, G. G., Jiménez, N. P. & Salazar, O. F. Fluid Dynamics of Gas – Solid Fluidized Beds. *Advanced Fluid Dynamics* 1–21 (2010).
17. Gunter Wozny, Reinhard Schomacker, G. B. *Modeling and Design of the Fluidized Bed Reactor for the Oxidative Coupling of Methane*. (Springer Science+Business Media, LLC, 2012).
18. Newton, H. W. in *Chemical Reaction Engineering* **168**, 1–44 (John Wiley & Sons Ltd, 1969).
19. Appl, M. *Ammonia: Principles and Industrial Practice*. (WILEY-VCH Verlag GmbH, D-69469 Weinheim, 1999).
20. Jafari, B. R., Sotudeh-gharebagh, R. & Mostoufi, N. Modular Simulation of Fluidized Bed Reactors. *Chemical Engineering Technology* 123–129 (2004). doi:10.1002/ceat.200401908

21. Kishor G. Gudekar, B. S. Modeling, Control, and Optimization of Fixed Bed Reactors. (Texas Tech University, 2002).
22. Yang, W.C. *Handbook of Fluidization and Fluid-Particle Systems edited by Wen-Ching Yang*. (Marcel Dekker, Inc., 2003).
23. Quina, M. M. J. & Ferreira, R. M. Q. Model comparison and sensitivity analysis for a fixed bed reactor with two catalytic zones. *Chem. Eng. J.* **75**, 149–159 (1999).
24. Fogler, H. S. *Elements of Chemical Reaction Engineering*. (Pearson Education, Inc., 2004).
25. Panahi, P. N., Mousavi, S. M., Niaei, A., Farzi, A. & Salari, D. Simulation of methanol synthesis from synthesis gas in fixed bed catalytic reactor using mathematical modeling and neural networks. *Int. J. Sci. Eng. Res.* **3**, 1–7 (2012).
26. Zagona, E. A. Effect of operation of Ammonia Plants on The Performance of Heavy Water Plants *Heavy. Sci. Technol.* **4**, 1–25 (2000).
27. Abasheer, M. implementation of mathematical and computer modelling to investigate the characteristics of isothermal ammonia fluidized bed catalytic reactors. *mathematical and computer modelling* **37**, 439–456 (2003).
28. J. F. Richardson, J. H. Harker, and J. R. B. U. *Chemical engineering volume 2 Particle Technology and Separation Processes.* **2**, (J. F. Richardson and J. H. Harker., 2002).
29. White, R. E. *Computational Mathematics*. (Chapman & Hall/CRC No, 2004).
30. S.S.E.H. Elnashaia , K.M. Wagialla, and M. E. E. A. The Use of Mathematical and Computer Models to Explore the Advantages of Fluidized Bed Technology for Catalytic Reactions with Equilibrium Diffusional Limitations. *Math. Comput. Model.* **3**, 27–70 (1991).

31. Octave Levenspiel. *Chemical Reaction Engineering*. (John Wiley & Sons, Inc., 1999).
32. Heijden, F. Van Der & Ridder, D. De. *Classification , Parameter Estimation and State Estimation*. (John Wiley & Sons Ltd, 2004).
33. Mäyrä, O. & Leiviskä, K. *Modelling in methanol synthesis*. (2008).
34. Carl R. Branan. *Rules of Thumb for Chemical Engineers*. (Elsevier Inc, 2005).